Development and Testing of A Low Cost Linear Slot Impulse Turbine

A Thesis By

Michael T. Brennison

M.S. Aerospace Engineering, University of Kansas, 2010

B.S. Aerospace Engineering, Auburn University, 2006

Submitted to the graduate degree program in the Department of Aerospace Engineering and the Graduate Faculty of the University of Kansas in partial fulfillment of the requirements for the degree of Master of Science

_____
Dr. Ronald M Barrett-Gonzalez
Associate Professor of Aerospace Engineering
(Chairperson)

_____
Dr. Ray Taghavi
Professor of Aerospace Engineering
(Committee Member)

_____
Dr. Craig McLaughlin
Assistant Professor of Aerospace Engineering
(Committee Member)

Date Defended: _____

The Thesis Committee for Michael T. Brennison

certifies that this is the approved version of the following thesis:

Development and Testing of A Low Cost Linear Slot Impulse Turbine

_____

Dr. Ronald M Barrett-Gonzalez
Associate Professor of Aerospace Engineering
(Chairperson)

_____

Dr. Ray Taghavi
Professor of Aerospace Engineering
(Committee Member)

_____

Dr. Craig McLaughlin
Assistant Professor of Aerospace Engineering
(Committee Member)

Date Defended: _____

Abstract

In this thesis, an impulse turbine with geometric characteristics aimed to have significantly lower manufacturing costs than other turbines of the similar scale was investigated. Experiments were performed to ascertain rotational speeds, torque, and power the turbine was capable. The turbine was of the impulse type with the channels between the buckets forming linear slots, milled with 0.125” (3.18 mm) bore.

The thesis begins with a summary chronicling the development of the turbomachinery that led to the design of the turbine investigated. The characteristics of the turbine design are then discussed, emphasizing the geometric characteristics used to reduce the cost of manufacture. The thesis then covers the calculations used in the development of the dynamometer and the analysis. Details of the dynamometer structure are then expressed, beginning with a computer aided design model and then delving into the dynamometer built. Then the hardware that the dynamometer is comprised is discussed with details as to how each subassembly operates. The procedures followed to test the turbine in the dynamometer are then described.

The results showed the turbine operated at speeds between 29,500 and 33,100 RPM. The average blade Mach numbers for that range of speeds was 0.287-0.322. The average torque measured during the tests ranged from 0.0451-0.0798 in*lbf (0.00510-0.00902 N*m). During the tests, the turbine was capable of producing 0.0230-0.0404 hp (17.2-30.1 W). The resulting efficiencies from the power produced ranged from 2.68% to 4.77%.

Acknowledgements

The author would like to thank his advisor Dr. Ron Barrett for all of his support and guidance throughout the course of this project. Thanks are also due to the University of Kansas Transportation Research Institute and the Department of Aerospace Engineering for funding this work. I would also like to thank Dr. Ray Taghavi and Dr. Craig McLaughlin for serving as members of my Master's committee as well as for their support and guidance offered throughout my education at the University of Kansas.

I would also like to thank the staff of the University of Kansas Adaptive Aerostructures Laboratory for their assistance manufacturing components used in this project. I would like to thank Mr. Richard Bramlette for his advice and support which proved invaluable. I also want to thank Lauren Kerth and the Kerth family for their machining assistance.

Finally, I would like to thank my family for supporting me throughout my education and their unwavering support in my ambitions in Aerospace since I was a child. They have always been behind me and without them I would not have made it this far.

Table of Contents

List of Symbols

Symbol	Definition	Units
a	Speed of Sound	ft/s, (m/s)
A	Area	in^2, (mm^2)
c	Radius of the shaft	in, (mm)
d	diameter	in., (mm)
I	Moment of Inertia	in^4, ($mm^{4)}$
L	Length	in., (mm)
M	Mach Number	-
M	Moment	(ft*lb_f), (N*m)
p	Pressure	lb_f/in^2, (kPa)
P	Power	hp, (W)
Q	Volumetric Flow Rate	in^3/s, (m^3/s)
R	Specific Gas Constant	ft*lb_f/(slug*°R), J/(kg*K)
t	Time	s
T	Temperature	°F, °R, (°C), (K)
V	Velocity	ft / s, (m/s)

Greek Symbol	Definition	Units
α	Nozzle Divergent Section Half-Angle	Degrees
β	Angle of injection	Degrees
γ	Ratio of Specific Heat	-
η	Efficiency	-

List of Symbols (Cont.)

σ	Stress	lb_f/in^2, (kPa)
τ	Torque	in*lb_f, (N*m)
μ	Viscosity	lb_f*s/ft^2, (Pa*s)
ω	Radial Velocity	rad/sec

Acronym	**Definition**	**Units**
CAD	Computer Aided Design	-
CD	Converging-Diverging	-
ID	Internal Diameter	in. (mm)
MAV	Micro Aerial Vehicle	-
OD	Outer Diameter	in. (mm)
OWC	Oscillating Water Column	-
RPM	Revolution Per Minute	-
UAV	Unmanned Aerial Vehicle	-

List of Figures

List of Tables

1.0 Introduction

Neilson defines a turbine as “a machine in which a rotary motion is obtained by the gradual change of momentum of a fluid.” The turbine is a device often used to produce or recover energy in a fluid by method using a series of vanes known as “blades” or “buckets”.[1] Turbines extract kinetic energy from a moving fluid and convert that energy into power.[2] Turbines can be broken down into two main categories: axial and radial (centrifugal). In an axial flow turbine, the majority of the flow remains parallel to the shaft of the turbine. Conversely in a centrifugal flow turbine, the flow travels the hub to the tip of the turbine.[1]

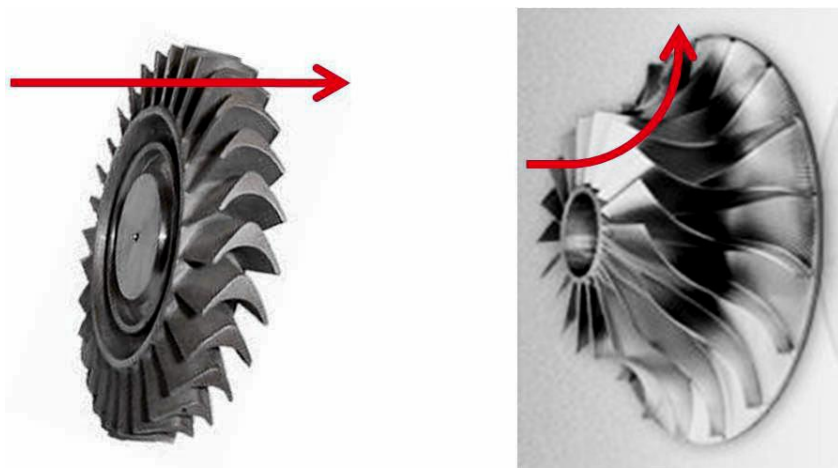

Figure 1: Axial Flow (Left) & Centrifugal Flow (Right) Turbines [3-4]

Each of these types of turbines can be further broken down into two groups: impulse turbines and reaction turbines. [5]

In an impulse turbine, the flow does not expand as it passes through the buckets. This means the turbine exit velocity is equal to the intake velocity. Furthermore, for an impulse turbine, if a compressible fluid is the primary constituent of the flow, it would be necessary for the fluid to be fully expanded prior to entering the buckets. Alternatively, a reaction turbine is one in which the flow expands as it passes along the buckets. The gas injected into the turbine

continues to accelerate until it exits from the other side.[2] Comparing geometry, the buckets of an impulse turbine are symmetric about the turbine's centerline, with a constant cross sectional area between the buckets; often requiring the center of the bucket to be significantly thicker than the tips.[6] The buckets of a reaction turbine possess an airfoil shape and do not require a constant cross sectional area between the buckets.

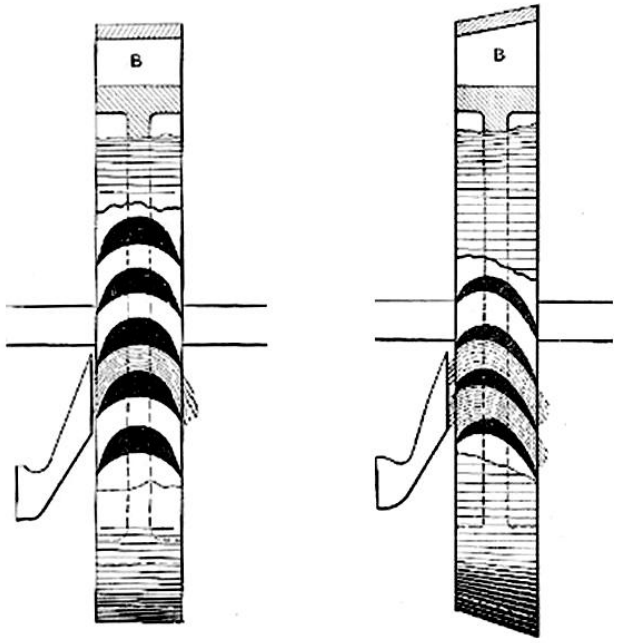

Figure 2: Typical Buckets of an Impulse Turbine (Left) and Reaction Turbine (Right)[7]

With an impulse turbine the fluid is fully expanded before entering the buckets, negating the need for tight seals between the nozzle and the turbine; however, in a reaction turbine, prevention of any leaks is critical in the turbine's performance.[7] Turbines of the impulse type are driven first by the pressure from the impulse of the fluid on the buckets and then by the reaction of the fluid after the buckets have reversed the direction of the flow.[6] For both turbine types, the turbine operates at peak efficiency when the speed of the buckets is approximately equal to half the speed of the fluid exiting the nozzle.[7] In modern days, the design process for

turbines has evolved from empirical tests to the method of characteristics, and then to fully unsteady Navier-Stokes solutions with imposed body forces and structural dynamics.[5]

As development of steam turbines continued into the 20th century, advances in attempting to further increase the rotational speed and power output came to a halt due to the limitations of the materials of the day; existing alloys were at their physical limits of stress, temperature, and availability. Advances since the early 1900's has largely been due to alloys and engineering tools that have emerged since.[2]

Throughout much of the 1900's, the impulse turbine largely lost favor to the reaction turbine because of the superior efficiencies of the latter. However, impulse turbines have found their place in a variety of applications. In both Europe and Asia, impulse turbines are being examined for use in Oscillating Water Column (OWC) tidal energy power plants. Impulse turbines have proven ideal in OWC plants due to their ability to operate unidirectionally while exposed to bidirectional flow.[8] Impulse turbines have also made their way into aerospace applications. In a liquid fueled rocket turbopump it may be undesirable to decrease a fluid's total pressure because this could lead to cavitation, which occurs when a fluid's pressure decreases below its vapor pressure. Cavitation causes bubbles to form which can lower efficiency and cause damage to the turbomachinery. Therefore, impulse turbines are often used in turbopumps to move fluids with minimal chance of causing cavitation.

1.1 Previous Work

Though there has been a great deal of work in the development of turbomachinery, in general this section will focus only on the major advances that have led to the design of the turbine of this study. The steam turbine's origin takes itself back to the second century B.C. as described by the Greek mathematician, Hero of Alexandria. What is today known as

Hero’s engine was a reaction turbine in which steam was fed to a hollow sphere that was free to rotate pivoted about its center. Connected to the sphere were two nozzles, tangential to the sphere facing in opposite directions. Hero described that steam entered the sphere through the pivot and exited through the nozzles with sufficient velocity to spin his engine and create enough power to open temple doors.[7]

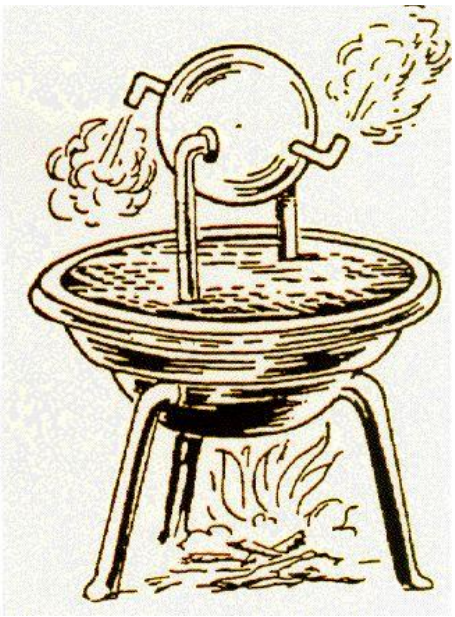

Figure 3: Hero's Engine[9]

In 1629, Braca, an Italian architect wrote describing a turbine consisting of a series of vanes that was spun by a jet of steam. Braca’s idea was later expanded upon in 1642 when Kircher took the concept and increased the number of steam jets from one to two.[1] In 1830, Ericsson invented a turbine that had a series of channels in which steam passed through to propel the turbine. Later in 1843, Pilbrow later proposed the use of two turbines that were staggered such that the fluid injected with a single nozzle impinged on the buckets of both turbines. Pilbrow proposed that the fluid would continue to expand after it had passed through the first turbine and would continue as it passed through the second.[1]

In the 1880's, a Swedish engineer, Dr. Carl Gustaf Patrik de Laval was developing centrifugal separators for the dairy industry when he developed the idea of using steam turbines to power his separators. In 1882 de Laval had completed his first turbine and it was quite similar to Hero's Engine. Steam entered a pipe connected to the turbine's hub and was diverted into two ducts pointed in opposite directions. As the steam exited the ducts, the reaction force caused them to move in the opposite direction of the steam and rotated a shaft at the center of the assembly, from which power was extracted.[1]

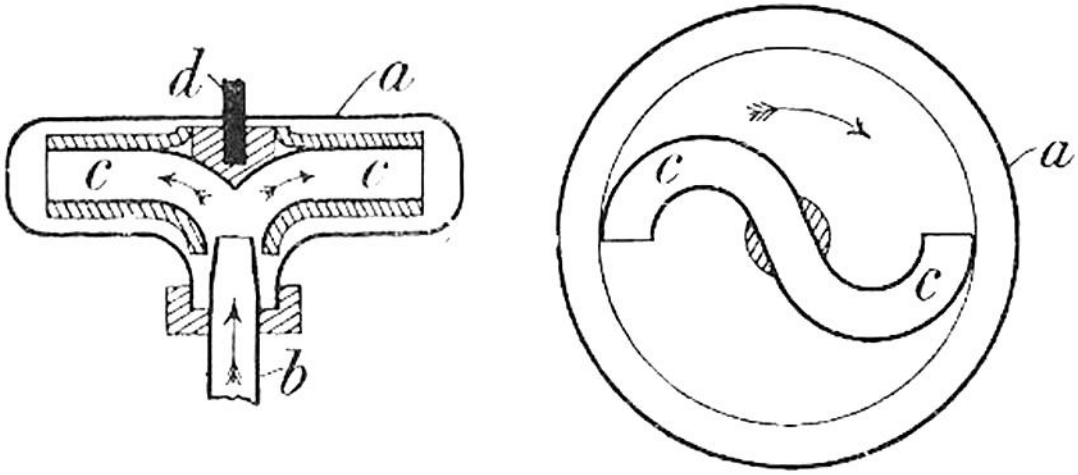

Figure 4: De Laval Reaction Turbine[1]

De Laval later turned his attention to Branca's steam turbine.[7] What de Laval had developed by 1888 was a single stage impulse turbine consisting of concave-convex buckets. Perhaps the most important innovation made by de Laval was to implement a converging-diverging (CD) nozzle. Using a CD nozzle allowed de Laval to build the steam pressure so great that the throat of the CD nozzle was choked, meaning sonic conditions existed.[10] As the steam expanded in the divergent section of the nozzle, the pressure and the temperature of the steam decreased, which allowed the steam to become supersonic and increased the velocity and mass flow rate of the gas.[11] De Laval was efficiently converting most of the

potential energy of the steam into kinetic energy, minimizing the static pressure and maximizing the velocity prior to the steam making contact with the turbine. The kinetic energy of the steam transferred to the turbine, causing it to rotate.[12] It was recorded that de Laval was capable of having his “single-wheel” impulse turbine operate at speeds of 30,000 RPM. [2]

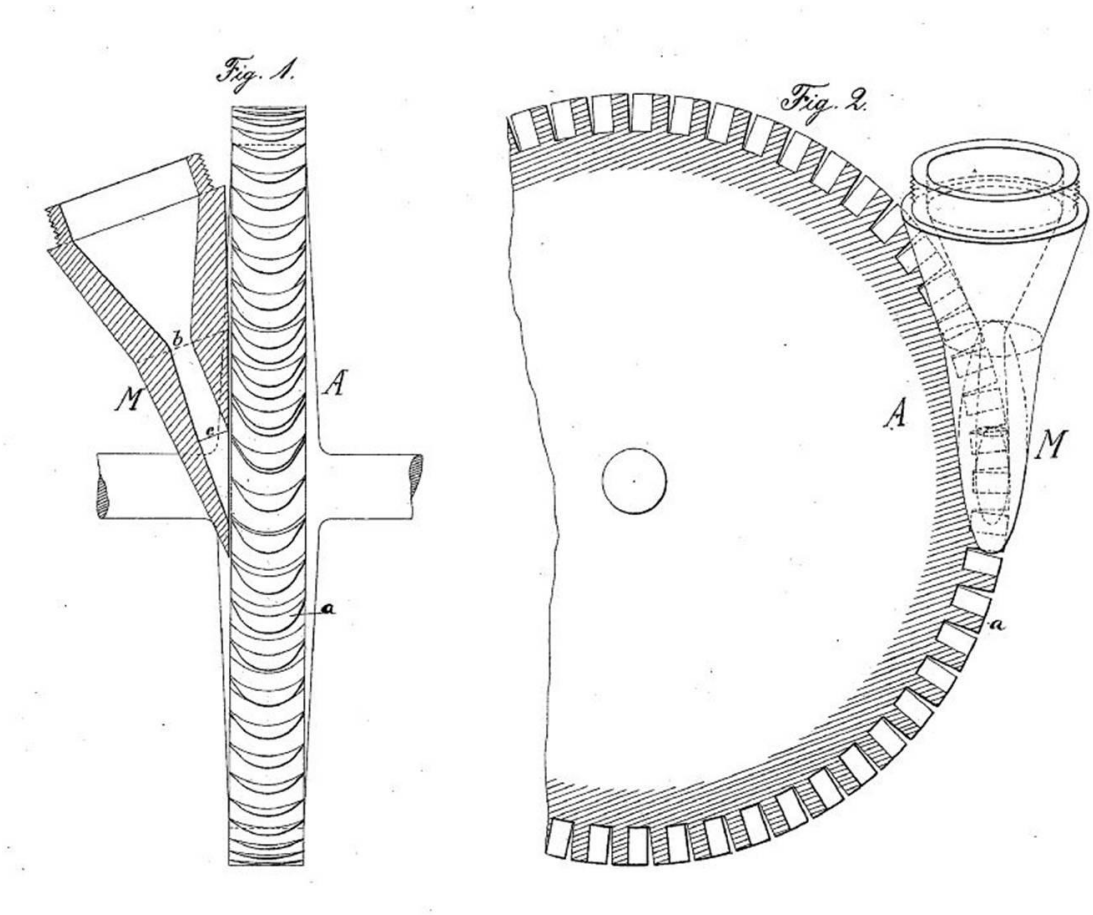

Figure 5: De Laval Impulse Turbine[10]

De Laval went on to apply his turbine for steam powered dynamos. In his dynamos, de Laval had multiple nozzles arranged circumferentially around the turbine. Because of the magnitude of the stresses and thermal loads applied to the turbine, de Laval had the turbines made with the highest grade steels available. Like many of his contemporaries de Laval

realized he could extract more energy from the steam injected into the dynamo by increasing the number of turbine stages.[6]

In 1884, Sir Charles Parsons patented his invention of a reaction steam turbine. Parsons' called for a multistage turbine in which the steam expands in the buckets and the reaction rotates the turbines. Parsons' turbine was similar conceptually to Hero's engine by allowing the expanding steam to be the driver of the turbine.[7]

During the 1880's, a great deal of knowledge of turbomachinery came forth. Finally, workable and economical hardware was developed; largely due to de Laval's contributions to impulse steam turbines and Sir Charles Parsons' patent for a reaction turbine. In the 1890's, Charles Curtis patented a number of turbines of various types and complexities. Curtis had done work to develop impulse, reaction, and multistage turbines; however, he turned his focus to creating a system that possessed buckets representative of both impulse and reaction turbines.[13-16] Curtis later worked alongside the General Electric Company to develop turbines that powered electric generators.[1] Another major participant in this renaissance was Heinrich Zoelly. In 1900, Zoelly first developed a turbine bearing resemblance to Braca's; it was composed of a series of bars, with grooves carved into each bar, propelled by steam.[17] Zoelly later expanded his work, patenting a turbine governor as well as a turbine powered by explosive gas; that being a combustion exhaust powered turbine.[18-19] Additional contributions of multistage impulse turbines were made by Augustine Rateau during the 1890's and early 1900's.[2, 20] Charles Lemale of France was issued a number of patents relating to using an explosive gas to power a turbine and proposed using such an apparatus to propel torpedoes.[21-23]

In 1968, National Aeronautics & Space Administration engineer Louis Goldman of the Lewis Research Center investigated the geometric characteristics of supersonic impulse turbine buckets in which vortex flow was created in the bucket passage. Goldman showed the inlet flow angle as well as the lower-surface Mach number greatly influenced the shape of the bucket. Goldman also found that the ratio of the bucket chord to bucket spacing, or solidity, increased with the Mach number of the lower surface where as increasing the Mach number of the upper surface or the inlet flow angle decreased the solidity. [24]

In the mid 1990's H. Hefazi at California State University performed detailed computational fluid dynamics. Hefazi's goal was to contribute to improving the performance of supersonic impulse turbines by improving shape of the buckets. Hefazi and his colleagues tried to minimize the total pressure losses by altering the geometry of a bucket as well as minimizing shocks in the flow path.[5]

Work surrounding axial flow turbines has evolved into an effective means of propulsion for aircraft. English born Frank Whittle, had filed patents throughout the 1930's for the purpose of jet aircraft propulsion and had a working engine running in 1939.[25] Whittle realized that a turbine was necessary as part of the engine to recover energy from the combusted gases of the engine to drive the compressor as well as other equipment onboard an aircraft.[26] While Whittle developed his engine, Hans von Ohain of Germany was developing a jet engine of his own. Both Whittle and Ohain are both credited as the inventors of the jet engine for their independent, parallel efforts.[27] Moreover, the jet engine relies on the principles of reaction engines.

A growing area of interest has been the development of micro-turbines. Micro-turbines have taken considerable interest as an alternative to fuel cells because they are capable of far

greater power densities. Of considerable interest, J. Piers of Belgium developed a single-stage impulse turbine that was only 0.394” (10 mm) in diameter and was fed hot compressed air. Piers successfully operated his turbine at such fantastic rates as 130,000 RPM, successfully generated 50W of mechanical power and had a peak efficiency of 24%.[28] Similarly in Switzerland, Krähenbühl developed a single-stage impulse micro-turbine what was capable of producing as much power as 124W at 370,000 RPM. Like Piers, Krähenbühl system had a peak efficiency of 24%; however, this efficiency was met while operating at 350,000 RPM.[29] Micro-turbines have also been investigated for powering micro aerial vehicles (MAVs). In 2004, Daniel Holt and Jeffery Kozak of the Rochester Institute of Technology examined using a 0.236” (6 mm) diameter impulse turbine as a potential method to power a MAV that had no dimensions greater than 5.91” (150. mm). Holt and Kozak demonstrated that their turbine was on the same order of magnitude as Lithium Polymer batteries of the day.[25, 30]

1.2 Purpose

One of the greatest drawbacks associated with impulse turbines is the significant costs associated with manufacturing. For most applications, turbines are constructed from very strong materials and must be machined to very small tolerances. What’s more, turbine buckets often have complex curvature which further increases the difficulty machining and increases the cost of manufacture. These high manufacturing costs can quell efforts to use turbines in a wide array of mass-market applications.

The purpose of this thesis is to evaluate an axial flow impulse turbine designed to have significantly reduced manufacturing costs. The focal point in reducing the machining costs is to simplify the geometry of the turbine buckets. The innovation proposed is to trade the

curvature of the bucket for flat surfaces by milling linear slots, at an angle, through the turbine wheel.

Figure 6: Typical Impulse Bucket Channels (Left) and Linear Slot Channels (Right)

A vital requirement was the turbine must be manufactured from conventional, certified materials. Because the aim of this research was to develop and test a turbine for future industrial use, it was necessary to use materials that are commonly available. In order to avoid significant costs and delays in making the turbine available, it was also necessary to use materials already certified by the Federal Aviation Administration and other governing agencies.

In addition to creating the aforementioned turbine, a dynamometer was designed and built to measure the torque produced as well as measure the rotational speed to determine the rotational velocity and the amount of power the turbine was capable of generating. Because the optimum angle of air injected into the turbine changed with variations in the turbine's rotational speed, the supporting equipment of the dynamometer needed to be able to adjust the angle of injection, β, between tests.

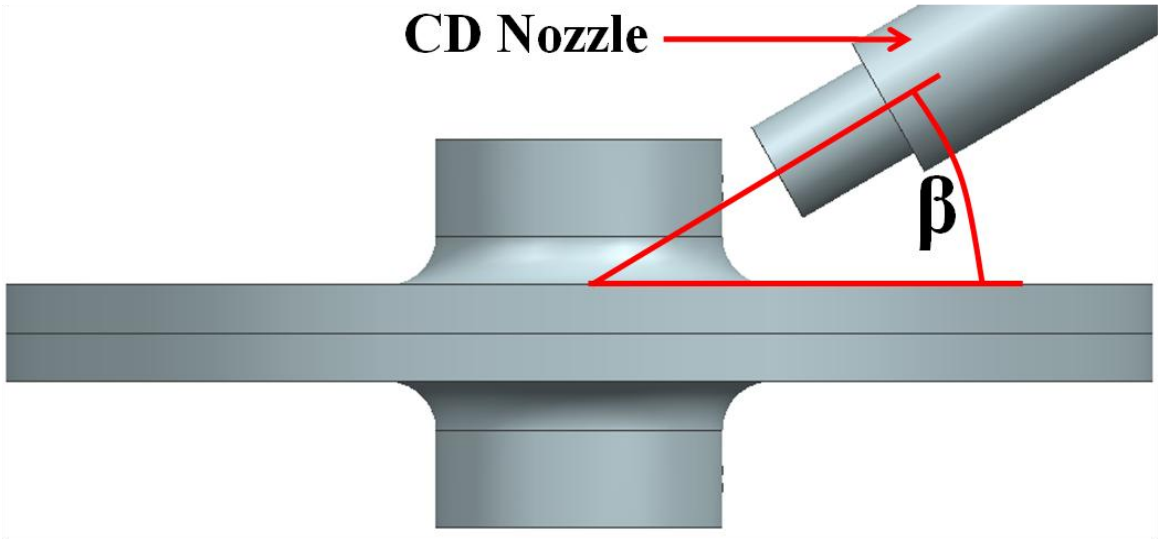

Figure 7: Illustration of the Angle of Injection Between Turbine and CD Nozzle, Scale 2:1

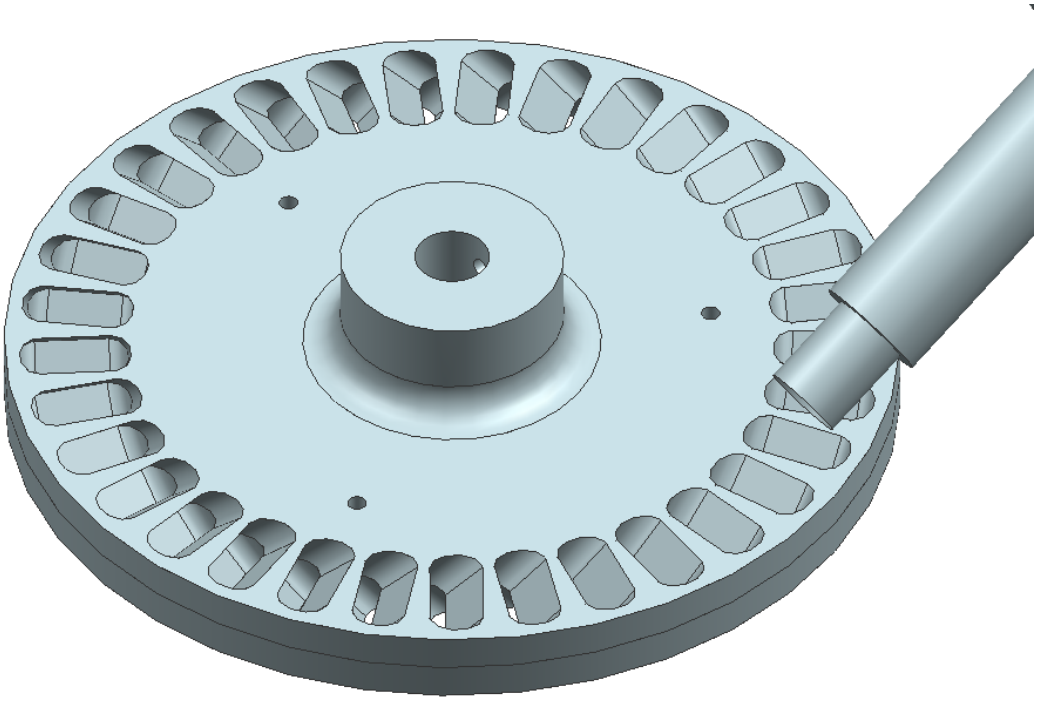

Figure 8: Isometric View of Turbine and CD Nozzle

2.0 Turbine Geometric Layout

The turbine was milled from two steel disks to create the “Left Hand” and “Right Hand” parts. The “Left Hand” and “Right Hand” designations were used to identify the bucket angle path of -45° and +45° respectively.

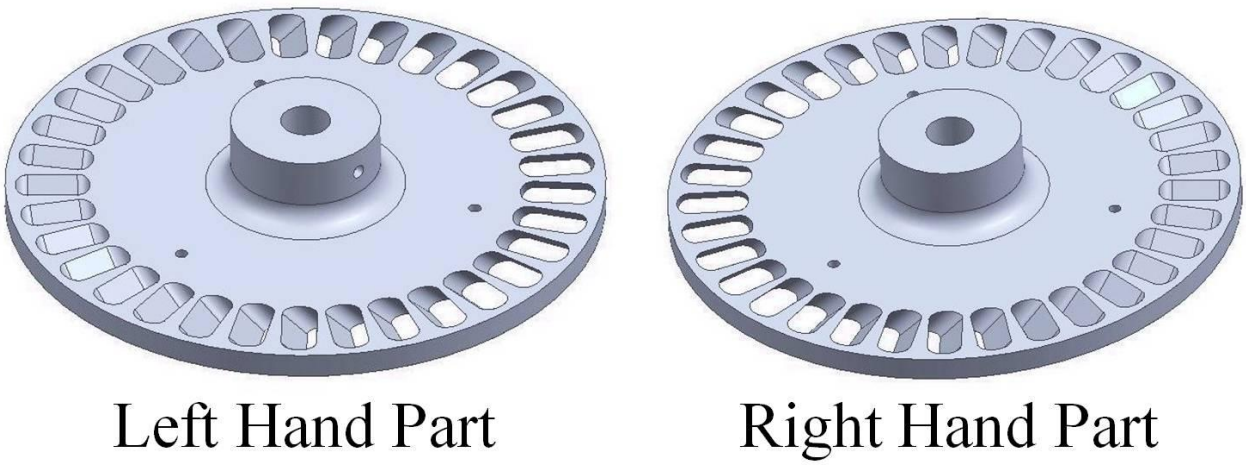

Figure 9: CAD Isometric View of Left Hand & Right Hand Parts

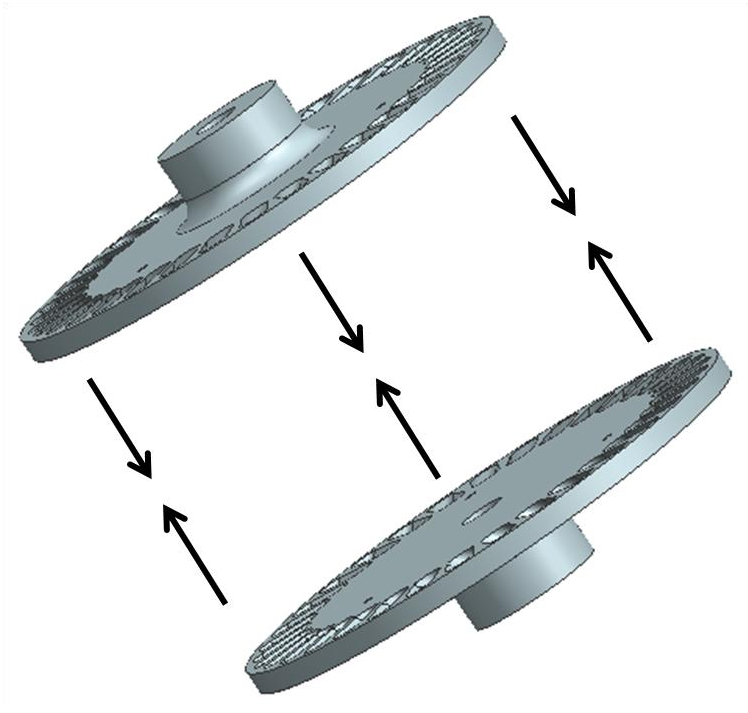

Figure 10: Joining Of The Turbine Disks

The distinction of the two parts was important because the right hand part was mirrored to the left hand part. Both pieces joined at the flat face of each disk, which formed the centerline of the turbine. The turbine was sized for use in small unmanned aerial vehicles (UAV's) which restricted the maximum diameter to 3.00" (76.2 mm). To increase stability of the turbine, each disk was machined to have a hub that was 0.750" (19.1 mm) in diameter and 0.375" (9.53 mm) tall. The center of each disk was bored to accept a 0.354" (9.00 mm) diameter shaft.

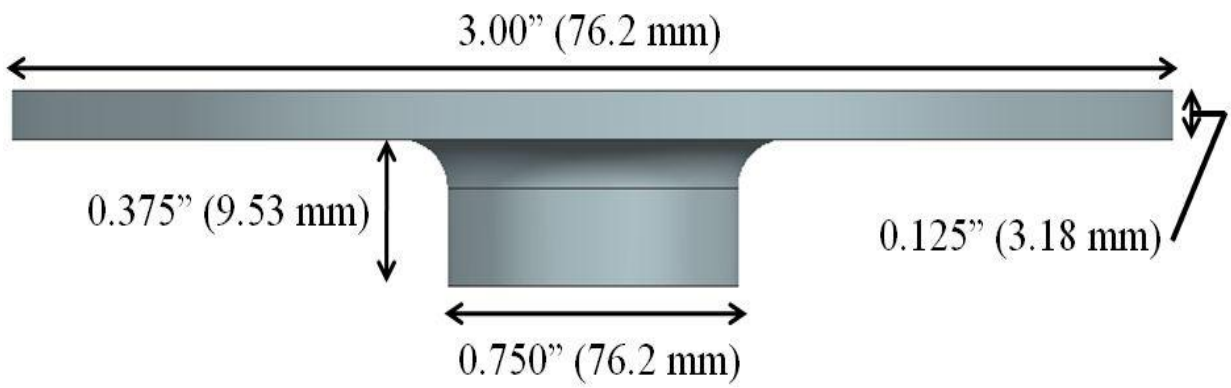

Figure 11: CAD Side View of Left Hand Part, Scale 2:1

To simplify the bucket geometry, slots were bored into both pieces of steel at a 45° angle. When both disks were mated together, the channels turned 90°; the cross-section of the channels resembled that shown in Figure 12.

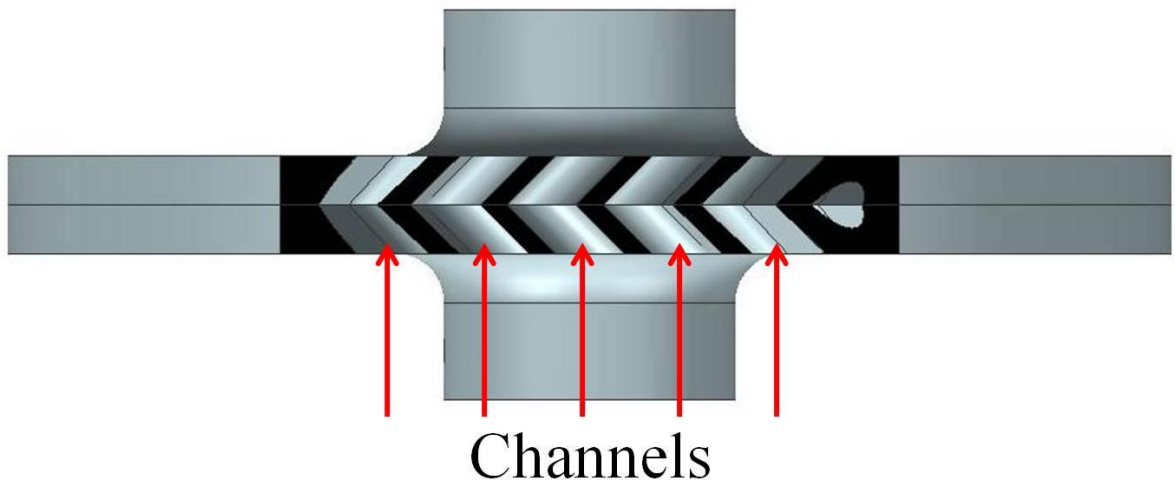

Figure 12: CAD Cutaway View Revealing Linear Slot Channels, Scale 2:1

To retard vibration modes associated with even fractions of the number of slots, the turbine possessed an odd number of buckets; thirty three slots were machined from each disk for this requirement while maximizing the solidity of the turbine. Each slot was milled with a 0.125” (3.18 mm) bore to a width of 0.375” (9.53 mm) along the radius. The end of each slot was 0.050” (1.27 mm) away from the edge of the disk. Bucket tips were not left free; they were connected by a ring of steel that increased the stability of each bucket and helped distribute loads.

The two disks were secured together with three swage pins in 0.062” (1.57 mm) diameter holes in the turbine disk; each hole was 0.875” (22.2 mm) away from the center of the turbine and separated by 120°. After the two disks were mated, each bucket had a uniform chord of 0.250” (6.35 mm). All linear dimensions had a tolerance of ±0.005” (0.127 mm) and all angles had a tolerance of 0.2°.

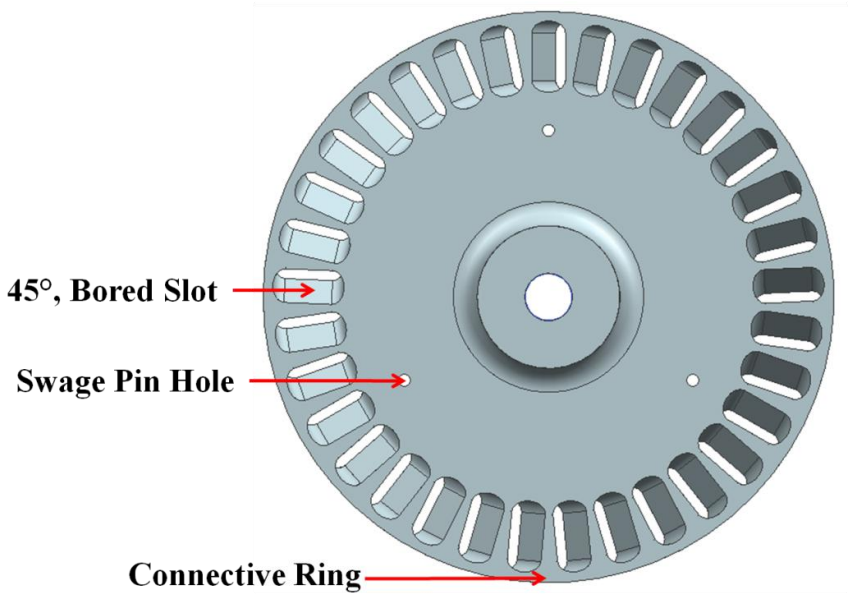

Figure 13: CAD Top View of Turbine, Scale 1:1

3.0 Theoretical Calculations

This section presents all the calculations used throughout the course of this investigation. Beginning with the methodology used in designing the nozzle, this section then details how power, efficiency, and blade Mach number were determined. The section concludes with additional formulas used to determine flexural stiffness of the shaft and the viscosities of the fluids.

3.1 Nozzle

In order to maximize the energy of the compressed air supply, it was necessary to expand the gas to the ambient pressure by use of a converging-diverging (CD) nozzle. The CD nozzle allowed the pressure of the air to build such that a pressure wave moving at the speed of sound occurred in the narrowest part of the nozzle, the throat. When the pressure wave was allowed to reach such speeds, it was impossible for the pressure wave to propagate into the divergent section. When this phenomenon occurred, the nozzle was said to be choked because the mass flow rate could not be increased any further for the nozzle. The characteristics of the air at the throat and exit as well as the geometry, were determined for a conical nozzle that was expanded isentropically. In the following equations, a subscript "1" is used to denote a property at the throat and a subscript "2" is used to indicate properties at the nozzle exit. A superscript "*" is used to indicate properties at the sonic condition.

The first step was to use the ratio of total pressure to ambient pressure and solve for the exit Mach number in the following relation:[34]

$$\frac{P_o}{P} = \left[1 + \left(\frac{\gamma-1}{2}\right) * M^2\right]^{\frac{\gamma}{\gamma-1}} \qquad (1)$$

After the exit Mach number was known, the temperature of the sonic condition at the throat was found.[34]

$$\frac{T_2}{T^*} = \frac{\frac{\gamma+1}{2}}{1+\frac{\gamma-1}{2}*M^2} \tag{2}$$

The speed of sound for the sonic condition was determined using the following relation, using the calculated value of T* for the temperature.[11]

$$a = \sqrt{\gamma * R * T} \tag{3}$$

This value, more specifically, represented the speed of sound at the throat of the nozzle when choked. The specific gas constant used was that of dry-air, 1.4. Due to the fact the nozzle throat was choked, the gas velocity was equal to the speed of sound by the following relation:[11]

$$M = \frac{V}{a} \tag{4}$$

Additionally, using the ambient temperature and the nozzle exit Mach number, the speed of sound and velocity of the air was found using equations 3 and 4, respectively.

At this point, all the gas properties necessary to determine the nozzle dimensions were known. For the purposes of this project, the cross sectional area at the throat was sized to match the exit diameter of a non-divergent air gun nozzle in the laboratory. To determine the required cross sectional area of the nozzle exit, the following relationship was used:[31]

$$A_2 = A_1 / \left[\left(\frac{\gamma+1}{2}\right)^{\frac{1}{\gamma-1}} * \left(\frac{p_2}{p_1}\right)^{\frac{1}{\gamma}} * \frac{V_2}{V_1}\right] \tag{5}$$

Using trigonometry the required length of the nozzle was determined using the nozzle throat and exit diameters and the divergent section half-angle, α:

$$L = \frac{(d_2 - d_1)/2}{\tan \alpha} \quad (6)$$

The two-dimensional geometry of the nozzle divergent section is shown below in Figure 14.

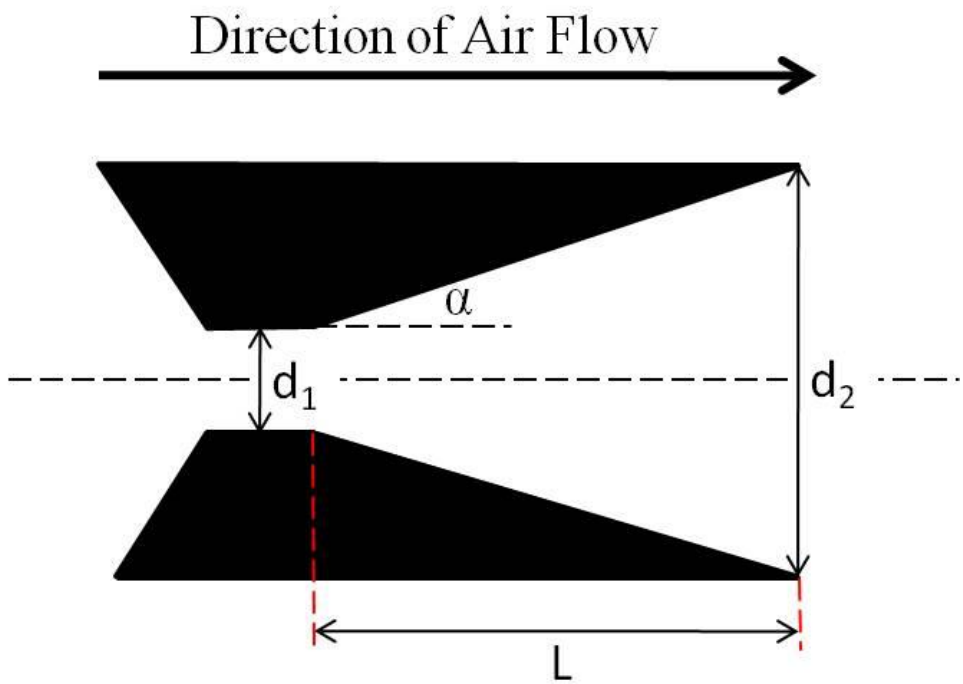

Figure 14: Geometry Of A Conical CD Nozzle Divergent-Section

3.2 Power And Efficiency

Input power from the kinetic energy of the air was determined for the sonic condition at the throat of the nozzle. The density of the air for the exit condition was found using Ideal Gas Law.

$$P_2 = \rho_2 * R * T_2 \quad (7)$$

Using the exit Mach number and the density of air at the nozzle exit, the density of the air for the sonic conditions at the throat was determined.[34]

$$\frac{\rho_2}{\rho^*} = \left[\frac{\frac{\gamma+1}{2}}{1+\frac{\gamma-1}{2}*M^2}\right]^{\frac{1}{\gamma-1}} \quad (8)$$

After the properties of the air at the throat were determined, the mass flow rate for the sonic condition was calculated.[11]

$$\dot{m}^* = \rho^* * a^* * A_1 \tag{9}$$

Enough information was gathered so that the power of the kinetic energy of the air ejected from the nozzle was determined. The following equation was derived from the equation for kinetic energy, substituting mass with the mass flow rate to obtain power:

$$P_{Air} = \frac{1}{2} * \dot{m} * V_1^2 \tag{10}$$

The shaft power extracted by the turbine was related to the torque produced by the turbine and its angular velocity:[34]

$$P_{Shaft} = \tau * \omega \tag{11}$$

Recalling the angular velocity was found with the following equation with the units of radians per second:

$$\omega = \frac{(RPM*2\pi)}{60} \tag{12}$$

The efficiency of the turbine was the ratio of the shaft power output by the turbine to the available power of the air into the turbine:

$$\eta = \frac{P_{Shaft}}{P_{Air}} \tag{13}$$

3.3 Bucket Mach Number

The Mach number of the turbine buckets was determined by first solving for the linear velocity of the turbine buckets.

$$V = \omega \times r \quad (14)$$

For the purpose of this investigation, the radius was measured from the center of the turbine to the midpoint of the turbine bucket span, 1.263" (32.1 mm). The bucket Mach number was found by dividing the velocity by the speed of sound of the ambient conditions, calculated in section 3.1, as per equation 4.

3.4 Flexural Stiffness

The flexural stiffness of the dynamometer shaft was a significant consideration in the design of the apparatus. The moment of inertia of the circular-shaft was found with the following relationship:[35]

$$I = \frac{1}{4} * \pi * r^4 \quad (14)$$

The stress due to flexure of the shaft was determined in the following relationship in which "M" represents the moment.[35]

$$\sigma = \frac{M * c}{I} \quad (15)$$

3.5 Viscosity

The viscosity was unknown for both the corn syrup and the molasses. A falling sphere viscometer was used with a steel sphere and a tall cylinder. Using Stoke's law, the force of drag was equal to the weight of the steel ball. After the velocity of the sphere in the fluid was determined, the viscosity, μ, was solved.[33]

$$F = 3 * \pi * \mu * d * V \quad (16)$$

4.0 Experimental Apparatus And Procedures

The purpose of this chapter is to provide a detailed description of the experimental apparatus as well as the methodology followed during the experiment. The experiment was conducted in the Adaptive Aerostructures Laboratory of the Aerospace Engineering Department at the University of Kansas. The facilities of the Adaptive Aerostructures Lab include several tools and machines that were used to construct the test apparatus. Lab facilities used included an infrared tachometer, Instron 3345 Universal Testing Machine, an 11.2 lb_f (50 N) load cell, and a Windows PC with Instron Bluehill™ v2.5 software used to collect load cell data. Compressed air was available at the lab and was used to supply power to the turbine. Additional manufacturing was conducted at the Aerospace Engineering Department's facilities at the Lawrence Municipal Airport.

4.1 Computer Aided Design Model

Prior to manufacturing the turbine and components of the test stand, it was essential to have a three-dimensional understanding of how all the components were positioned in the test stand. Using NX 6.0, a computer aided design (CAD) program developed by Siemens AG, every major component and structural element discussed within Section 4.0 was modeled and assembled in the CAD into the complete model of the test stand. The CAD model aided in sizing several components and helped ensure that there were no interferences with moving parts.

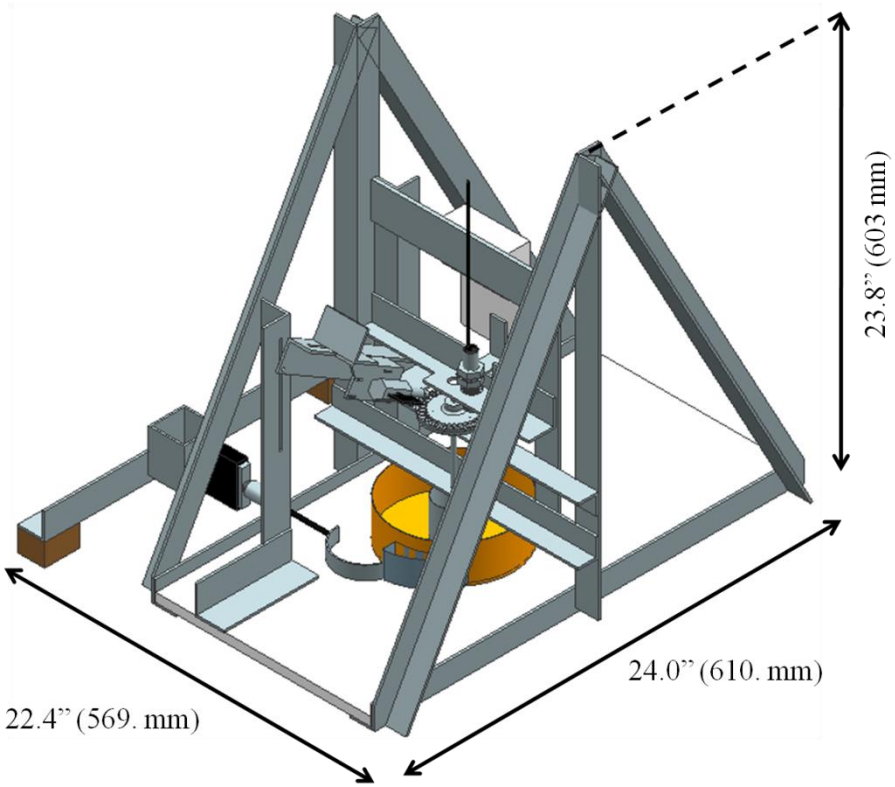

Figure 15: CAD Isometric View of Dynamometer Assembly

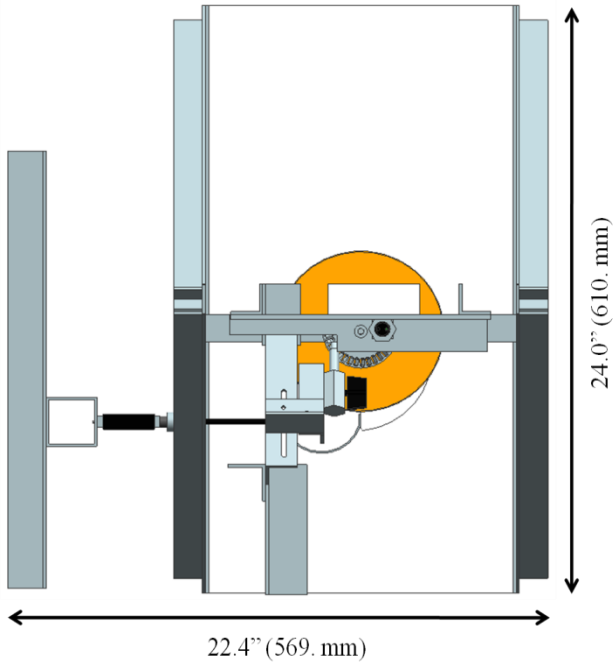

Figure 16: CAD Top View of Dynamometer Assembly, Scale 1:8

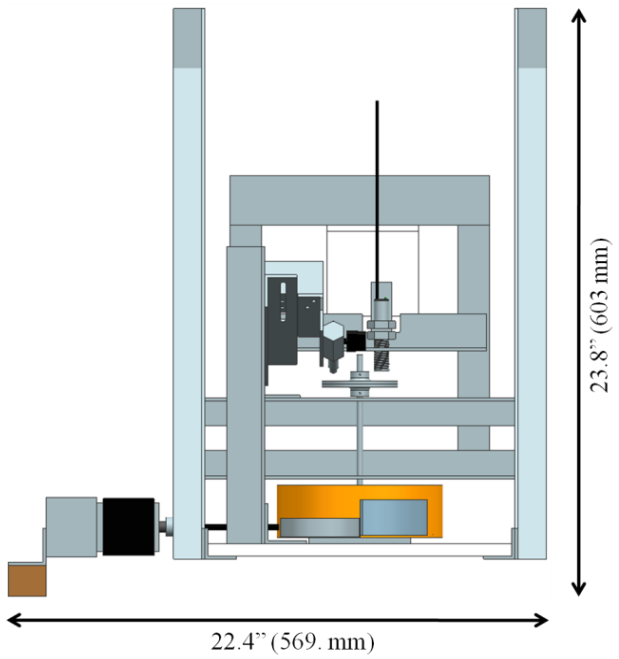

Figure 17: CAD Front View of Dynamometer Assembly, Scale 1:8

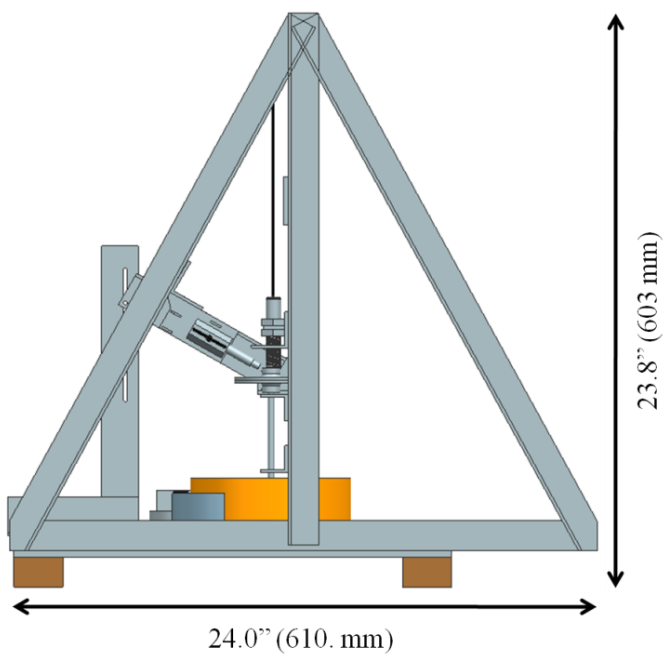

Figure 18: Side View of Dynamometer Assembly, Scale 1:8

4.2 Linear Slot Turbine

The linear slot turbine was composed of two disks made of AISI 1020 steel, mirror images of each other. In addition to the dimensions presented in Section 2.0, each hub had a tapped hole to accommodate a 4-40 set screw to secure the disk to the shaft.

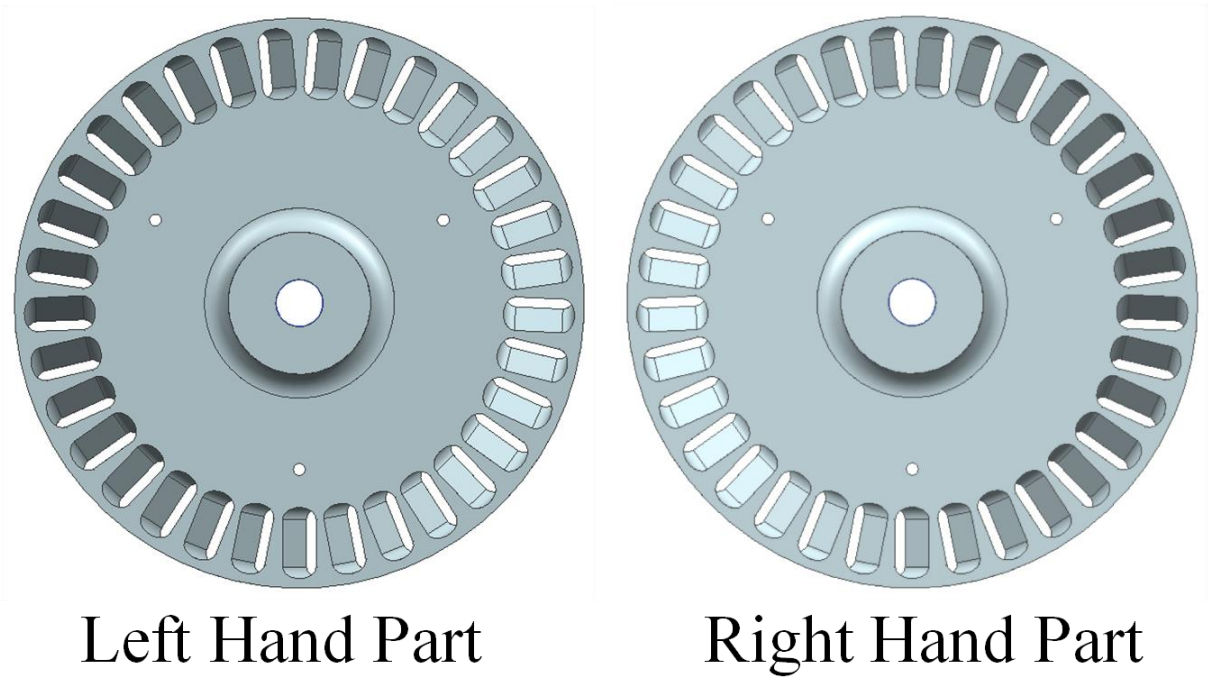

Figure 19: CAD Top View of Left Hand & Right Hand Parts, Scale 1:1

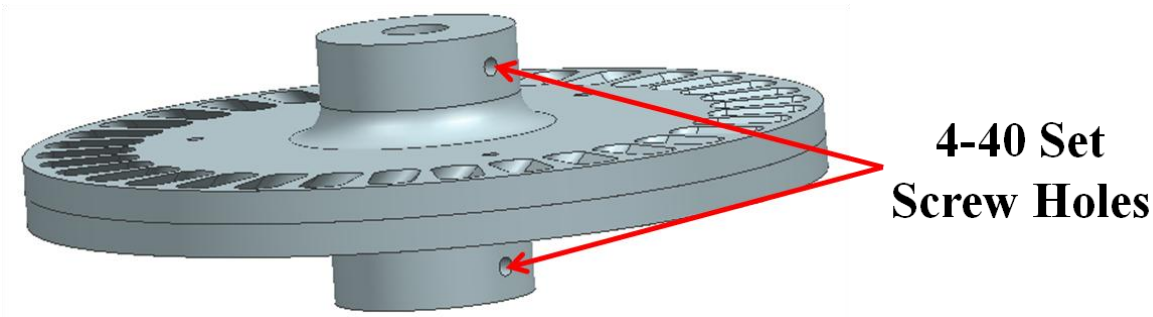

Figure 20: CAD of Both Parts Mated Together

Both parts of the turbine were also designed so that through the turbine disk, there were three alignment holes 0.062” (1.57 mm) in diameter, 0.875” (22.2 mm) from the hub, spaced 120° apart. Once both parts were machined, they were aligned, mated, and secured together with three swage pins through the alignment holes. Once the two disks were mated together, a 90° degree angle formed in each slot where the two disks met. Due to machining errors, there was a slight misalignment at the intersection of each slot. To correct the misalignment, each 90° corner was sanded with 80-grit sandpaper until the edges of the two disks were flush and slightly rounded.

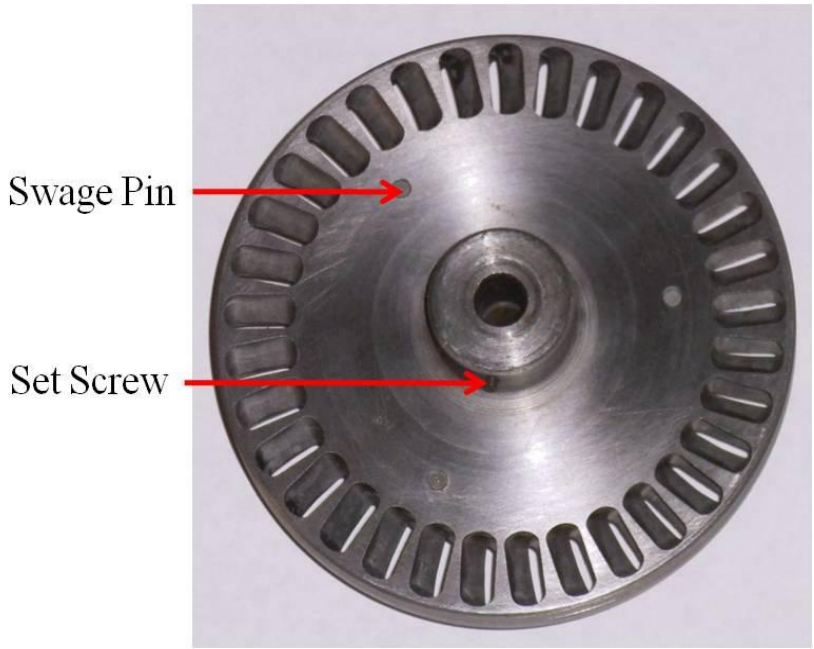

Figure 21: Assembled Linear Slot Turbine, Scale 1:1

4.3 Test Stand Structure

The structure was composed of a piece of 0.500” (12.7 mm) thick plywood measuring 12.0” x 24.0” (305 mm x 610 mm) as well as several pieces of 1.25 in (31.8 mm) extruded aluminum L-channel. The base of the structure was composed of the plywood board with two pieces of the aluminum L-channel, 24.0” (610 mm) long, attached to both sides of the board with a total of four 8-32 fasteners. The primary structural frame was composed of two A-

frames made of the L-channel, extending 22.0” (559 mm) tall, with an additional vertical L-channel that extends from the base to the apex of the A-frame. Some material was removed from each piece of L-channel near the apex to allow the three pieces to be joined. Where the three members of each A-frame met, they were attached together with a single 8-32 fastener. With 8-32 fasteners, the three members of each A-frame connected to one of the horizontal pieces of L-channel that was fixed to the plywood board as shown in Figure 22.

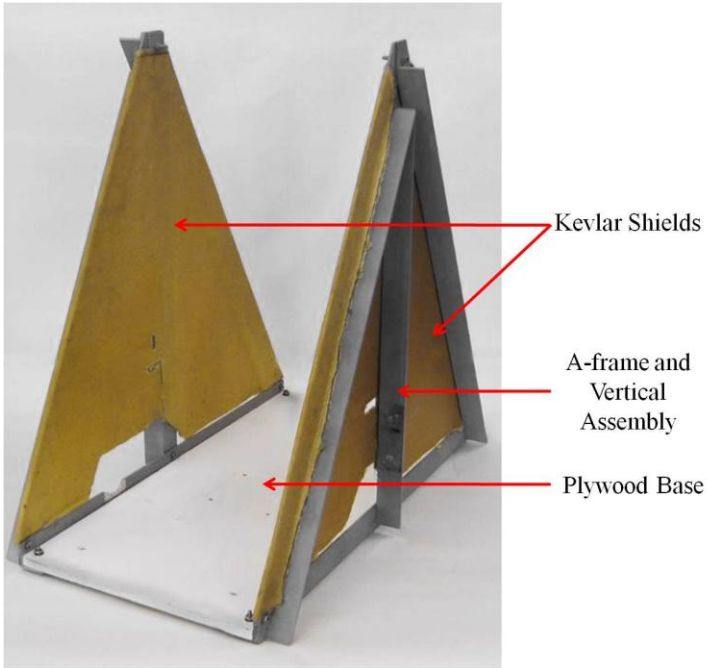

Figure 22: Apparatus Main Structure

A Kevlar shield was added to each A-frame as a precaution to protect lab personnel in case the turbine, or any part of the experiment, broke free. Each shield was composed of a Kevlar 3-ply preimpregnated biweave. Using each A-frame as a mold, each shield was wrapped around the A-frames, placed in a vacuum bag, and cured in an oven.

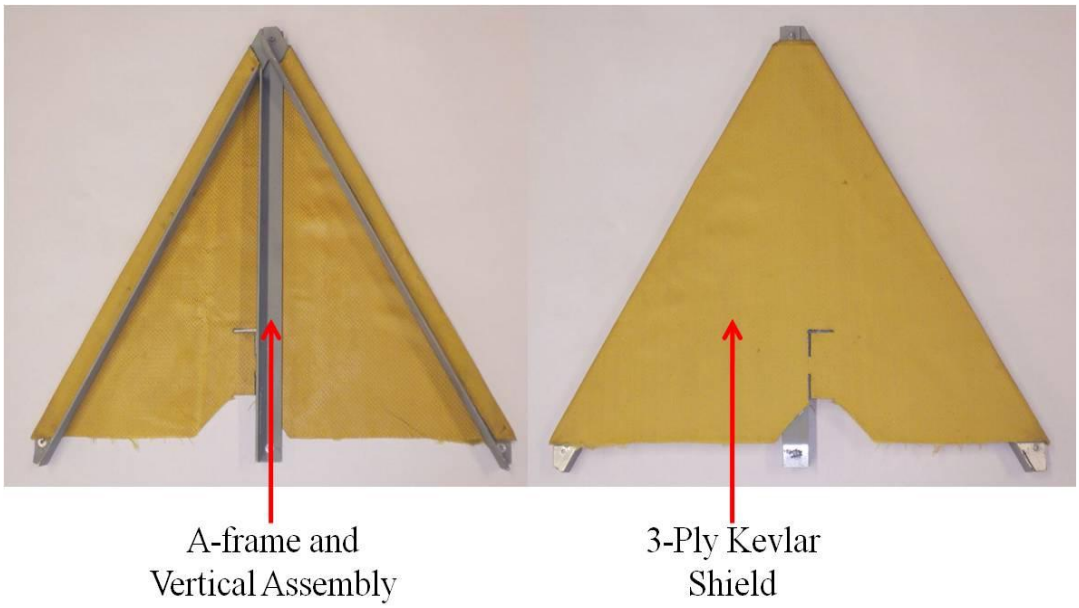

Figure 23: A-frame And Kevlar Assembly, Scale 1:10

Two horizontal pieces of L-channel were used to span between the two vertical members of the A-frames, one mounted directly above the other; measuring from the top of the plywood base, the bottom of the lowest horizontal was 2.44” (62.0 mm) and the top of the second horizontal was 5.81” (148 mm) above. Each end of the horizontal members was attached to the vertical members with 8-32 fasteners. At the center of both horizontal members, a 0.625” (15.9 mm) hole was match drilled to provide clearance of the inner race of the ball bearings discussed in section 4.4. To keep the bearings aligned and in place, 0.250” (6.35 mm) thick aluminum supports were manufactured with a 0.942” (23.9 mm) hole drilled in the center, in which the bearings were press-fit. The bearing supports were attached to each of the horizontal members with two 6-32 fasteners. The ball bearings were further constrained by stainless steel shaft collars, as discussed in the following section.

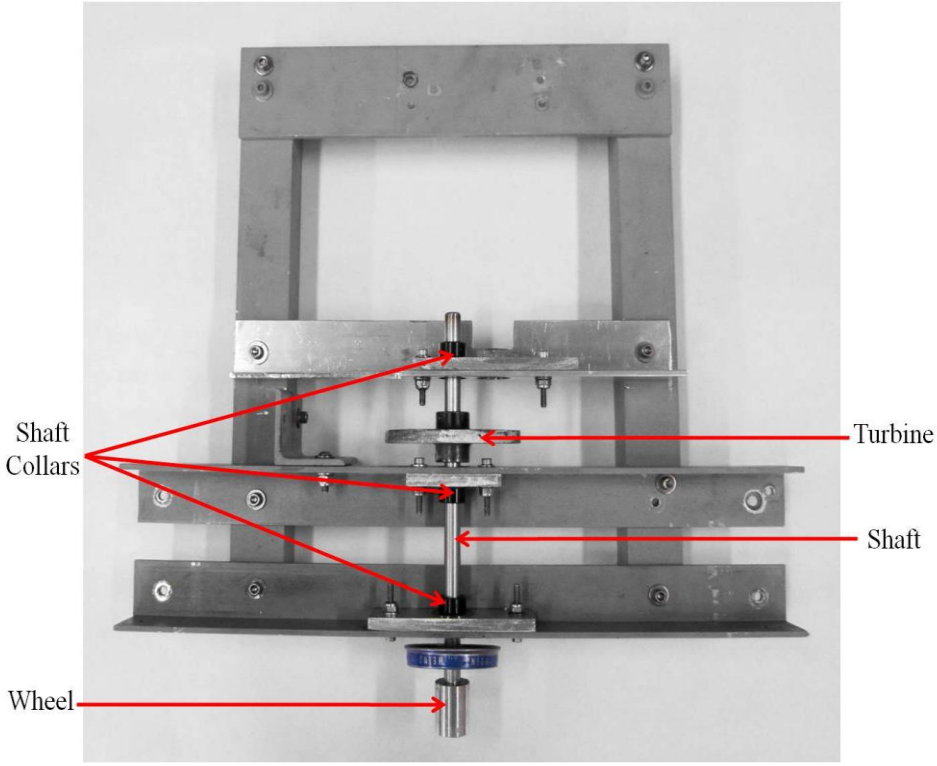

Figure 24: Turbine-Shaft Assembly, Scale 1:4

Attached to the two horizontal L-channel members, that spanned the two A-frames, was a central structure necessary to provide additional support of the shaft as well as the tachometer. Two vertical pieces of L-channel that were 12.2” (310 mm) long and 7.63” (194 mm) apart were attached to the horizontal members, equidistant from the center of the horizontal members, with four 8-32 fasteners. A third horizontal member composed of L-channel was attached to the verticals, with two 8-32 fasteners, such that the bottom of this member was 1.77” (45.0 mm) above the uppermost of the two spanning horizontal members. This third horizontal L-channel, like the other two had a 0.625” (15.9 mm) hole was match drilled to allow freedom of the ball bearings inner race. An aluminum support identical to that used on the other two horizontal members was used to support and hold the third ball bearing in place. This member was positioned such that it supported the shaft above the turbine to prevent the shaft from deflecting due to moments that were caused by the turbine

during tests. A second hole that was 0.75” (19.1mm) in diameter was drilled in the third horizontal member, with an edge distance of 0.063” (1.60 mm) from the bearing hole, to permit access of the infrared tachometer to the turbine. Additional material was machined away to allow complete access of the swing arm discussed in section 4.6, as well as the tachometer support. The details of the central structure are shown in Figure 25.

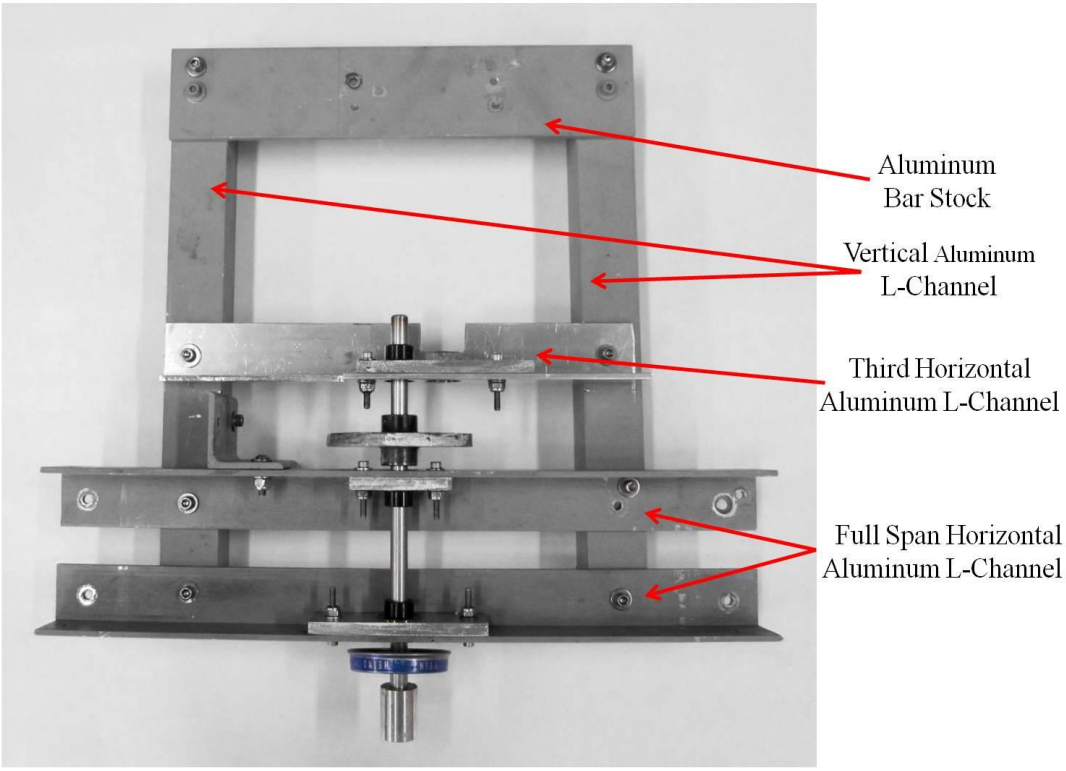

Figure 25: Apparatus Central Structure, Scale 1:4

At the top of the two vertical members, a piece of 0.188” (4.78 mm) by 2” (50.8mm) aluminum bar stock was attached with two 8-32 fasteners at each end of the bar.

A support made of plywood was constructed to hold the tachometer in place above the turbine. The plywood support was attached to the aluminum bar with a pair of 8-32 fasteners and hung down toward the turbine. A steel bracket for the tachometer was attached to the bottom of the plywood support, positioned so that the tachometer fit through the center of the 0.750” (19.1 mm) hole in the third horizontal member as shown in Figure 26.

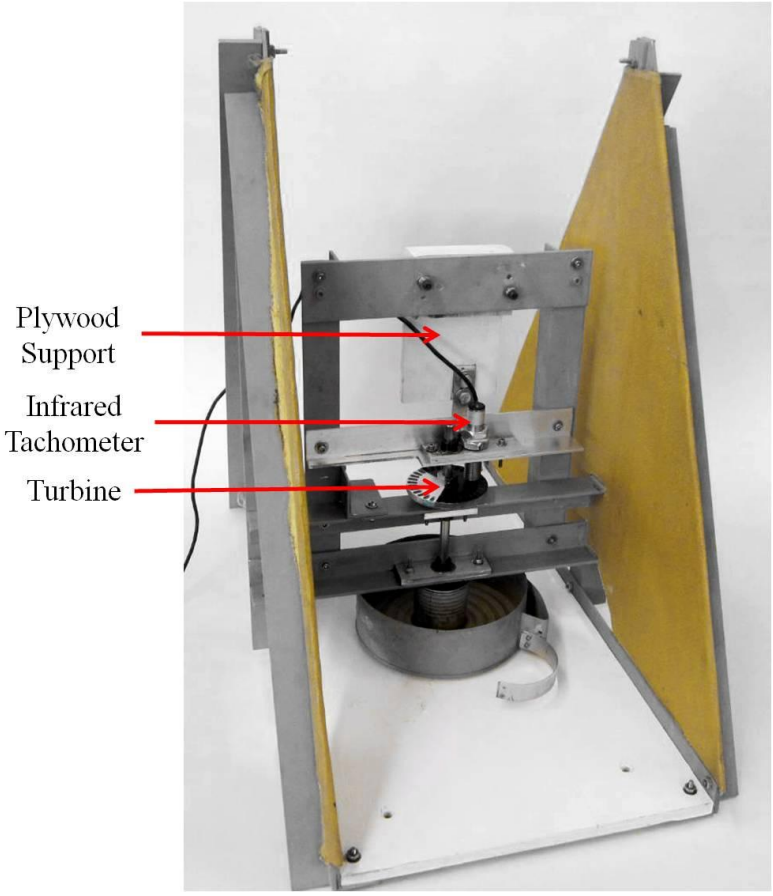

Figure 26: Tachometer and Supporting Structure

4.4 Hydraulic Brake Dynamometer

To measure the torque produced by the turbine, a hydraulic brake dynamometer was used. The turbine was attached to a 0.354” (9.00 mm) diameter vertical steel shaft, 2.00” (50.8 mm) from the end. The turbine was held in place against the shaft with two 4-40 set screws. To prevent the set screws from coming loose due to vibrations, each screw was bonded with Loctite 271 Threadlocker. The shaft was supported by SKF 609-2Z deep groove ball bearings attached to the three horizontal members mentioned in section 4.3. Deep groove bearings were necessary so that the bearings were not torn apart by thrust loads. To prevent the shaft from translating up or down through the bearings, shaft collars were placed on the shaft, lightly making contact with the inner race of the bearing. The shaft collars also ensured

the bearings did not come loose from the aluminum supports. The set screws of the shaft collars were bonded with Loctite 271 to prevent the shaft collars from coming loose during tests. The opposite end of the shaft was press-fit into an aluminum wheel. The wheel had an ID of 0.352” (8.94 mm), 0.002” (0.051 mm) less than the diameter of the shaft. Detailing the rest of the geometry of the wheel, the OD was 0.750” (19.1mm) and 0.982” (24.9 mm) tall. A weight imbalance of the turbine-shaft-wheel system was present which required removing some material from the outer-most part of the turbine. To balance the turbine-shaft system, it was placed on a pair of leveled razorblades. While laying on the razorblades, the turbine-shaft system rotated as the heaviest part of the turbine was pulled toward the ground by gravity. When the system came to rest, a mark was placed on the turbine at its lowest point to identify the heavy portion of the turbine. Material was then removed from the heavy portion of the turbine with a grinding wheel. The turbine-shaft system was then placed back on the razorblades and the balance check was repeated until balanced.

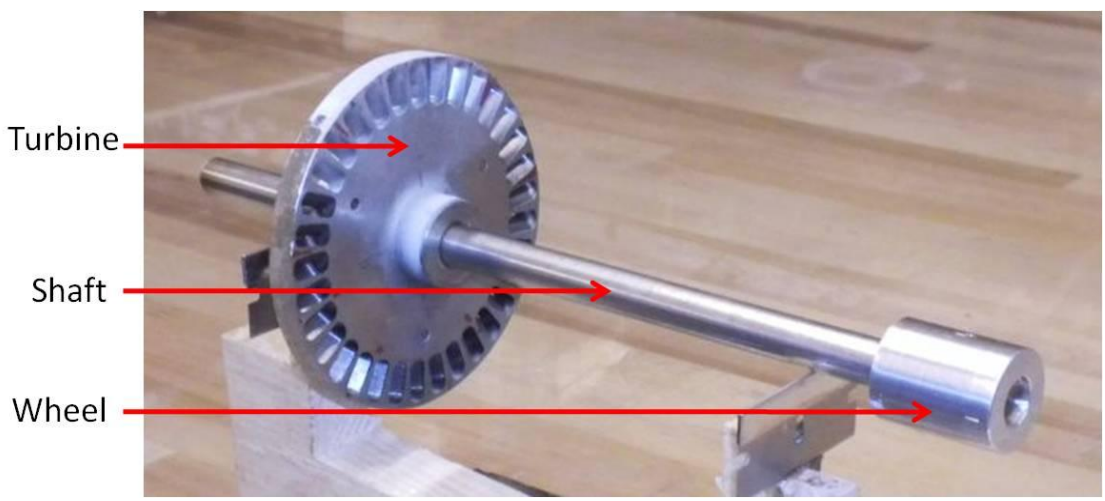

Figure 27: Turbine-Shaft Assembly

An open-top steel container measuring 6.50” (165 mm) ID and 2.00” (50.8mm) tall was mounted atop a square turntable; the other side of the turntable was connected to the plywood base of the test stand’s structure. Inside the container at its center was a steel drum bonded in

place with Loctite Hysol 9412. The drum measured 1.91” (48.5 mm) tall, 2.00” (50.4mm) ID, and 2.02 in. (51.3 mm) OD. The drum housed viscous fluids used in the analysis. To prevent the fluids from escaping the drum, a small metal lid, with a hole in the center to permit access to the shaft, was affixed to the top of the drum and temporarily secured with electrical tape. To prevent fluid from escaping through the central hole of the lid, a 0.375” (9.53 mm) ID, 1.50” (38.1 mm) OD neoprene rubber washer sat atop the lid. It was necessary that the washer ID be slightly larger than the shaft diameter to prevent the washer from being destroyed during tests. The rest of the container was used to store additional mass to damp vibrations caused by fluid dynamics in the dynamometer; these vibrations were found to cause erroneous data by causing the drum system to strike the load cell erratically.

Attached to the exterior of the container wall was a 1.50 in. (38.1 mm) tall extension, made from 0.030 in. (1.00 mm) aluminum sheet, bonded to the wall with Loctite Hysol 9412. The extension was attached to the container such that a vertical face extended from the drum normal to the wall, supported by the rest of the extension. A hemispherical constrained-layer damper (a device constructed of two thin pieces of aluminum sandwiched about a single layer of double-sided tape) was attached to the container extension to help reduce vibrations transmitted from the dynamometer to the load cell. The constrained-layer damper was 0.75” (19.1mm) tall with an average radius of curvature of 1.56” (39.6 mm). Each piece of aluminum of the damper was 0.056” (1.42 mm) thick.

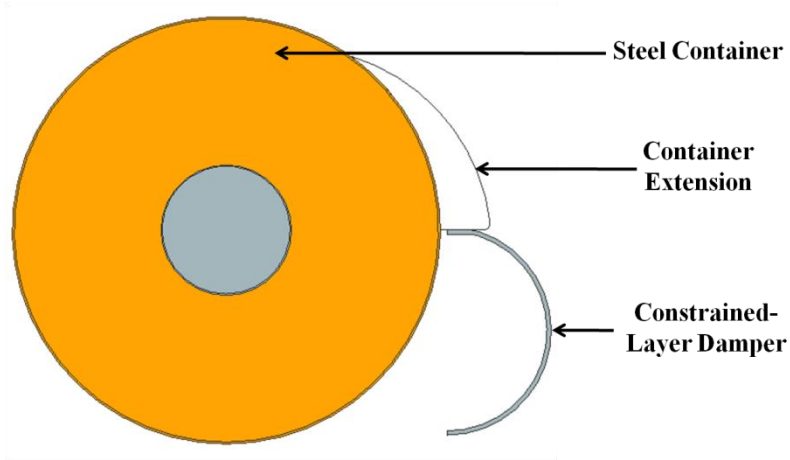

Figure 28: Top View of Container Extension Interface, Scale 1:3

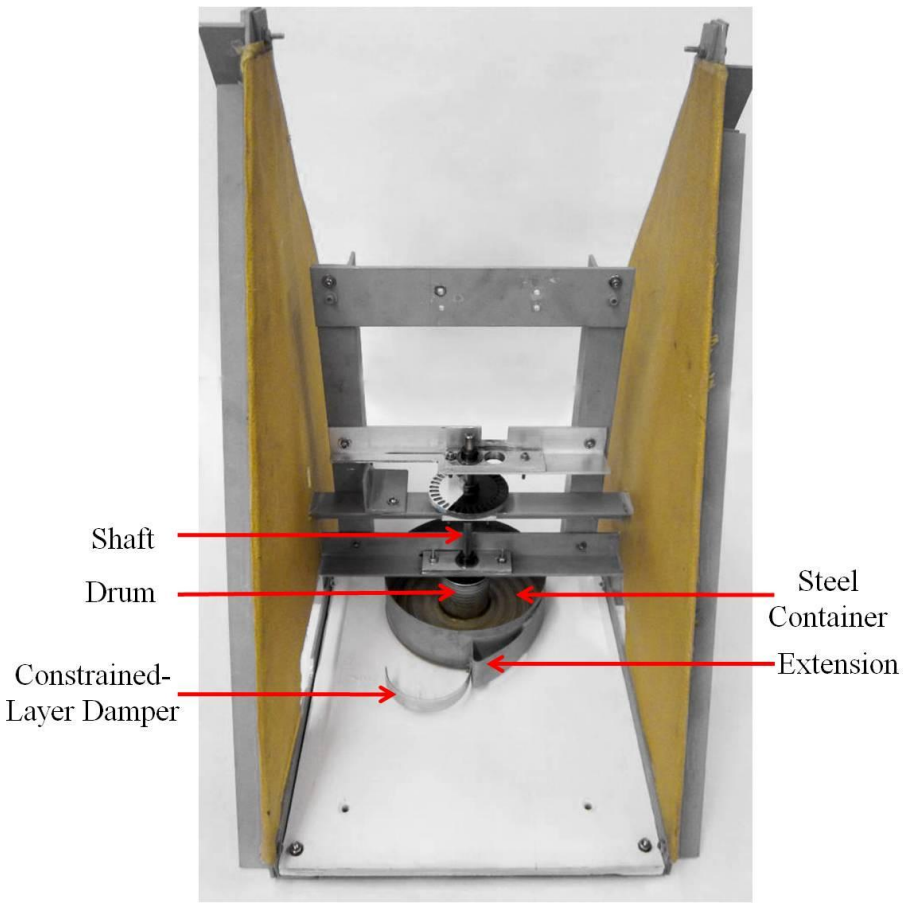

Figure 29: Dynamometer Assembly, Scale 1:5

Suspended by the shaft, the aluminum wheel was placed inside the drum such that the axis of the turbine-shaft-wheel assembly was on the same axis as the drum; with the wheel

only 0.063” (1.60 mm) above the bottom of the drum. During each test, the drum was filled to 1.00” (25.4 mm) with one of the fluids described in section 4.8.

4.5 Injector

To accelerate the velocity of the compressed air into the turbine, a converging-diverging conical nozzle was machined on a lathe. For conical nozzles, the optimum half angle is generally between 12° and 18°; because optimization was beyond the scope of this investigation, the half angle was machined to be the median value of that range, 15°.[31] The nozzle was designed for an inlet total pressure of 82 psia (565 kPa) with a throat radius of 0.063 in (1.60 mm). The resultant exit radius was 0.078 in (1.98 mm), within 0.004” (0.102 mm) tolerance of the calculated exit diameter. The nozzle was attached to a manual, inline ball valve so that air flow was controlled at the dynamometer. Between the air supply line and the ball valve was a pressure gage accurate to 1 psia to measure the steady state inlet pressure.

4.6 Inclination Structure

The ball valve connected to the nozzle was attached to a “swing arm” with a pair of steel hose clamps through slots machined into the swing arm. The swing arm was an assembly constructed of three pieces of aluminum L-channel that were attached to a pivot on the test stand’s structure.

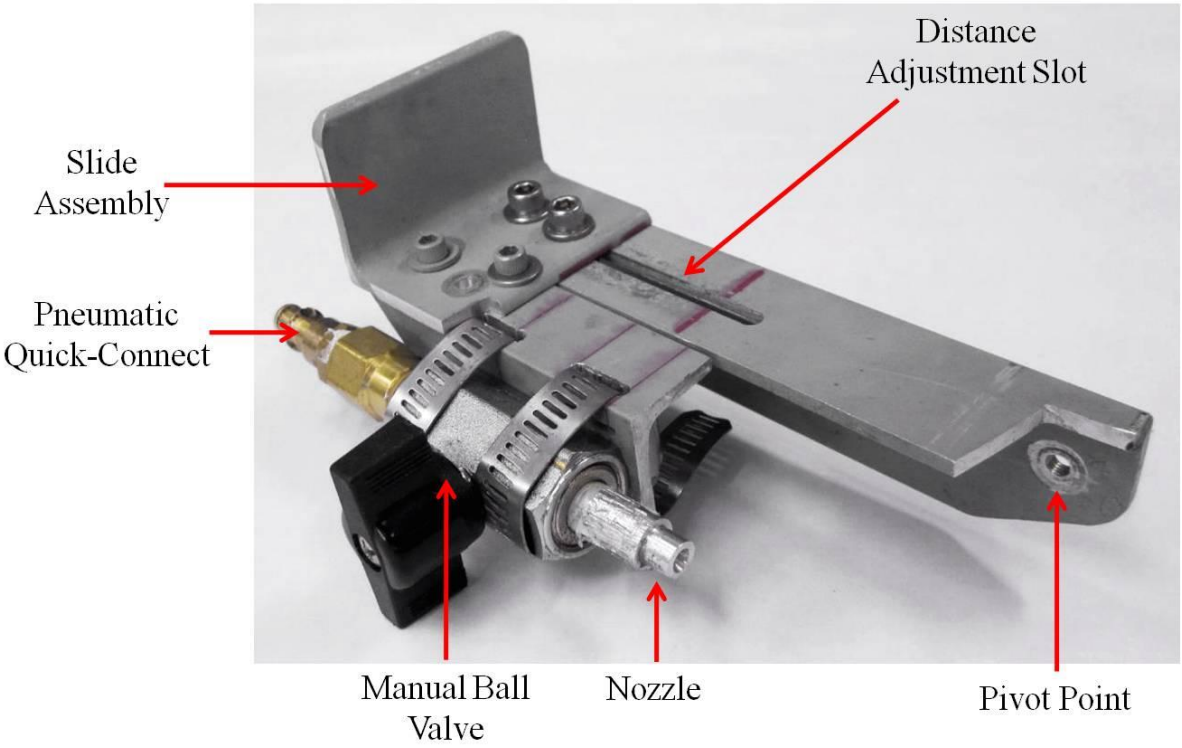

Figure 30: Swing Arm Assembly

The pivot was positioned so that the swing arm could be adjusted to any angle of injection between 15° and 45° relative to the turbine plane; the angle was set about the pivot point as shown in Figure 33. Additionally, the pivot was located so that the nozzle was aimed directly at a turbine bucket, tangent to the turbine, for all swing arm angle settings.

In Figure 31, a CAD model of the swing arm has been divided into two primary components, red and blue, with the attached nozzle and valve shown in grey.

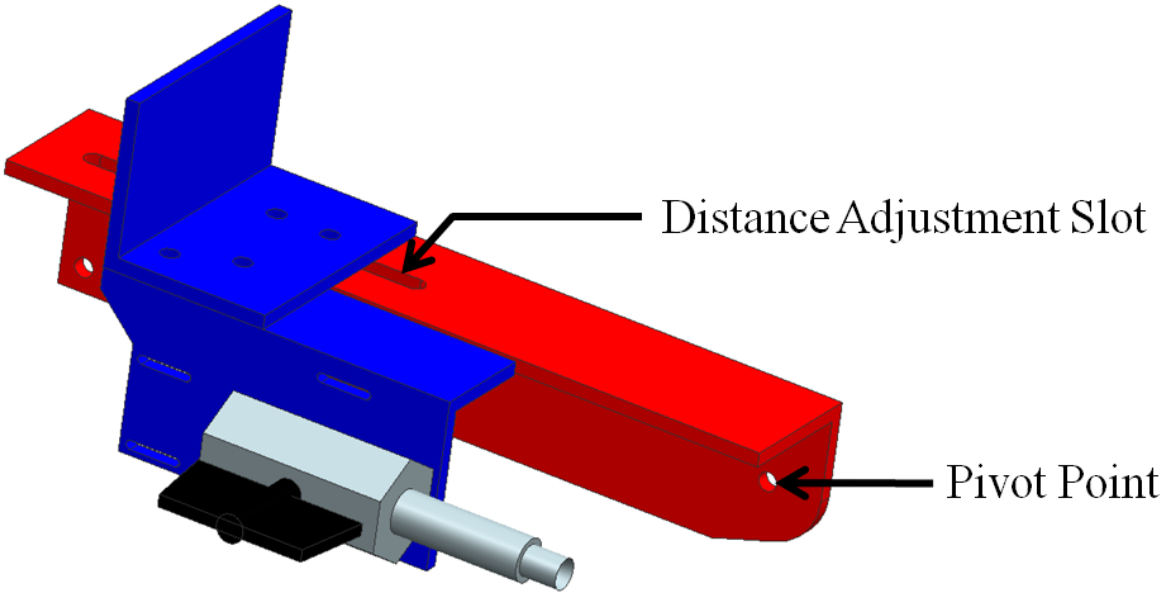

Figure 31: CAD Model of Swing Arm Assembly

The red component was attached to the test stand structure at the pivot point, about which the angle of inclination was set. The red component also attached to a support, described later, with an 8-32 fastener through the hole shown in the left side of component. The blue component was used to set the distance between the nozzle and the turbine. The blue component had two 10-24 fasteners that fit into a slot machined into the red component. The two fasteners guided the blue component along the slot to the desired distance and were then tightened to hold it in place. The blue component was adjusted to minimize the distance between nozzle and the turbine to maximize the power from the kinetic energy of the air ejected from the nozzle. The slot was 0.180” (4.57 mm) wide and 3.96” (101 mm) long.

To support the weight of the swing arm, pressure gage, and airline a support was manufactured from two pieces of aluminum L-channel. The base of the support was 5.38” (137 mm) long and was attached to one end of the second piece of L-channel at a 90° angle. The second piece of L-channel was 13.4” (340 mm) long and had a slot milled into it that was 0.160” (4.06 mm) wide and 5.54” (141 mm) long, located 0.875” (22.2 mm) from the

free end. The slot was large enough to accommodate an 8-32 fastener attached to the end of the swing arm.

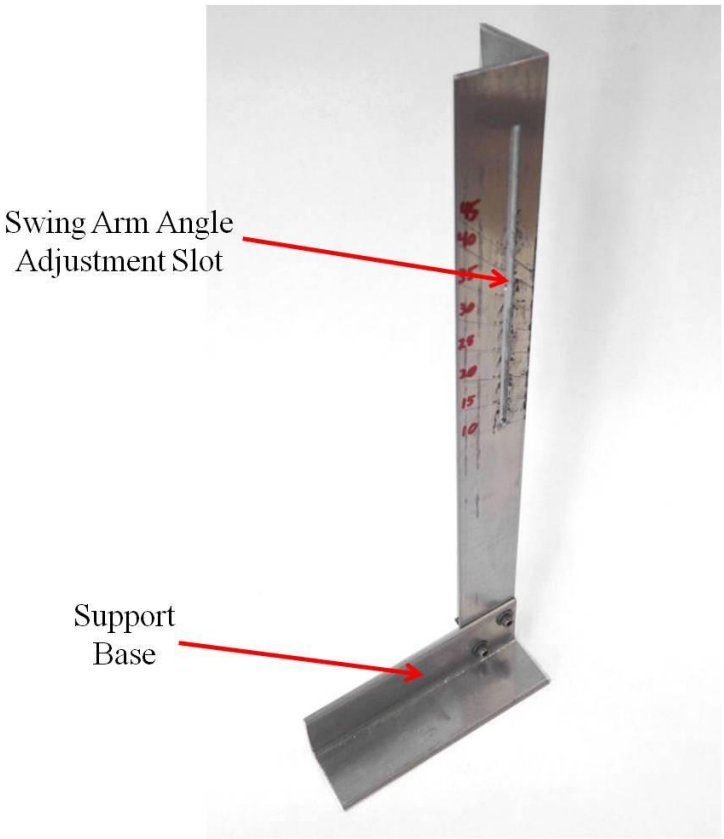

Figure 32: Swing Arm Support

The fastener at the end of the swing arm was placed in the slot; tightening the fastener locked the angle between the swing arm and the support. After the desired angle was set, the base of the support was clamped to the plywood base to hold it in place. To expedite testing, lines were scribed into the support for each angle used during the test.

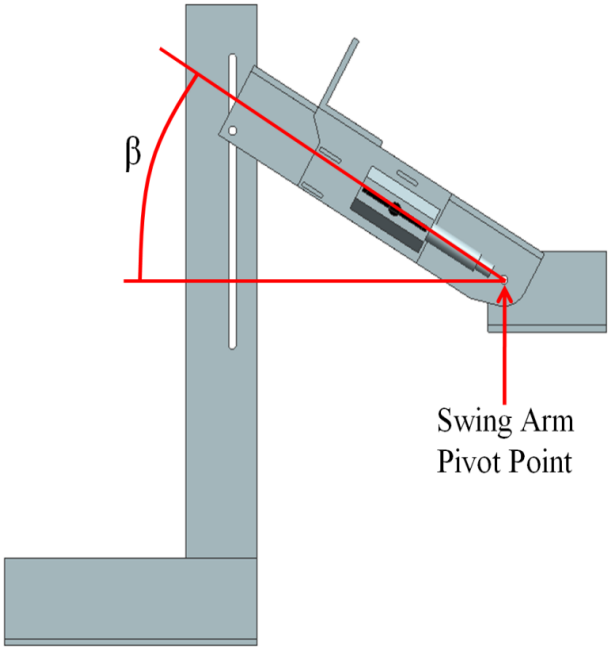

Figure 33: CAD Side View of Adjustable Angle Between Swing Arm & Support, Scale 1:4

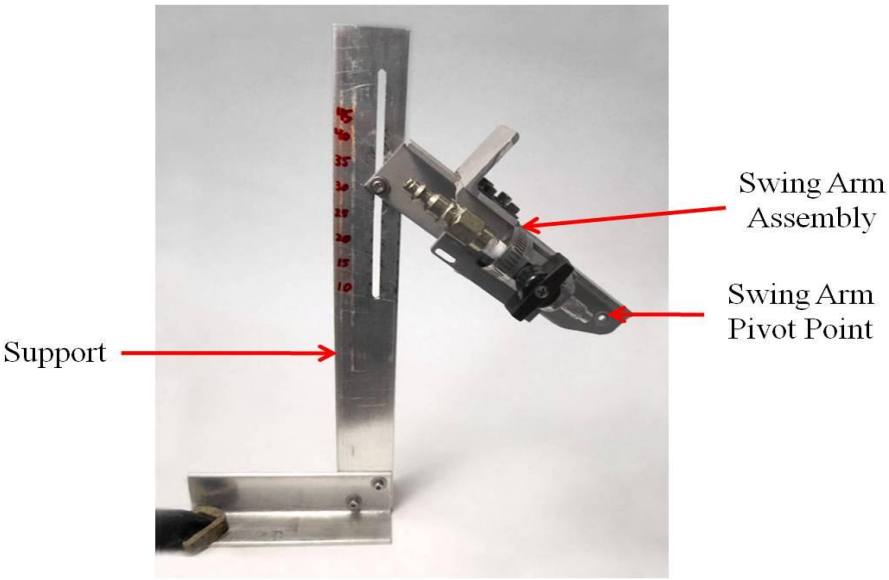

Figure 34: Swing Arm And Support, Scale 1:5

4.7 Instrumentation

To measure the rotational speed, a Monarch Instrument IRS-P infrared tachometer was mounted to a bracket attached to the wooden support mentioned in Section 4.3. The tachometer was positioned 0.188” (4.78 mm) directly above the turbine. To get accurate

measurements of the turbine speed, the top surface of the turbine was painted such that a 1/3 section was white and the remaining 2/3 was black; per the tachometer's instructions.

Figure 35: Turbine Paint Scheme For Infrared Tachometer, Scale 1:1

Rotational speed was shown on a liquid crystal display of a Monarch Instrument Nova-Strobe DB Plus portable stroboscope connected to the tachometer.

To determine the torque produced by the turbine, an Instron 2519-102 11.2 lb_f (50.0 N) S-beam load cell was used to measure the tip-force produced at the container's extension. The load cell was attached to 17.9" (455 mm) long piece of aluminum L-channel, with a bracket manufactured from aluminum 1.75" (44.5 mm) square tube that was positioned 6.31" (160. mm) away from the dynamometer. Wooden blocks were used to raise the load cell to be the same height as the container extension; the L-channel was raised 1.22" (31.0 mm) from the concrete work surface and was secured to the work surface with two 0.250" (6.35 mm) Tapcon concrete screw anchors. The load cell and support structure were not attached to the test stand to prevent any vibrations transmitted from the dynamometer from corrupting the measurements. The load cell was placed so far away from the dynamometer that the

constrained-layer damper could not make contact with the load cell. To close the gap between the load cell and the damper a 4.35” (110. mm) long, 0.250” (6.35 mm) diameter carbon fiber composite rod was attached to the load cell.

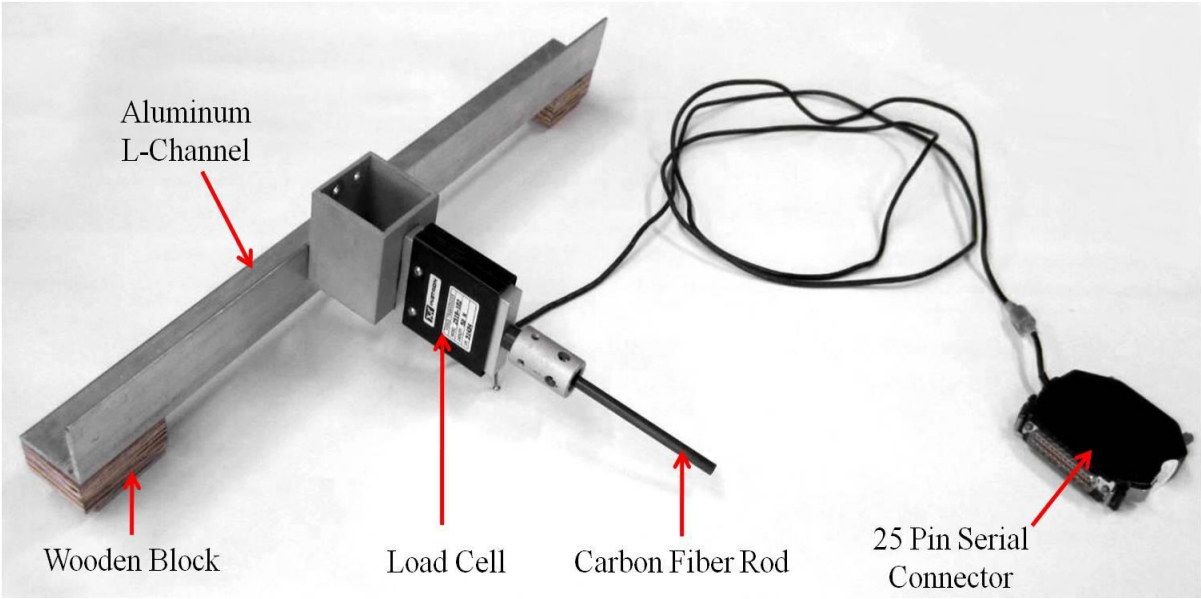

Figure 36: Load Cell Assembly

The total pressure of the compressed air supply was measured just upstream of the CD nozzle with a digital pressure gauge. The pressure gauge used was an Omega DPG6000L, semiconductor strain gauge pressure transducer, and was capable of measuring pressures as great as 500 psi (3,450 kPa), accurate to 1 psi (6.89 kPa).

4.8 Fluid Viscosities

Viscosities were unknown for two of the fluids used: corn syrup and molasses. The viscosities of both of these fluids were determined using a 35.0” (889 mm) tall, 1.63” (41.4 mm) diameter falling sphere viscometer. The viscometer was constructed from a PVC pipe with clear Plexiglas cap at the bottom. The sphere weighed 0.0184 lb_f (0.0818 N) and had a diameter of 0.500” (12.7 mm). The sphere was positioned just above the fluid in the center of the viscometer and dropped into the fluid. The sphere was timed from the moment it entered

the fluid until it reached the Plexiglas at the bottom. The amount of time it took for the sphere to reach the bottom of the viscometer was used to determine the velocity of the sphere in the fluid, which was used to calculate the viscosity.

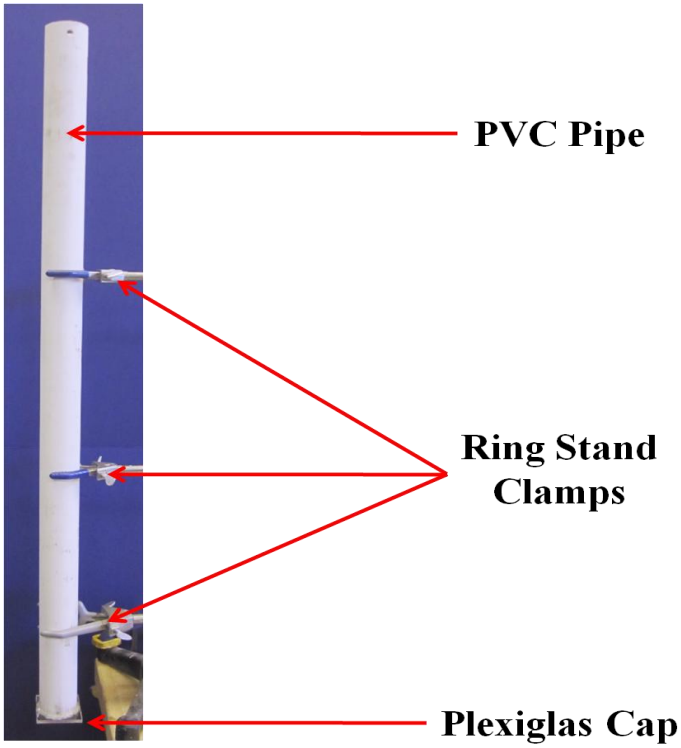

Figure 37: Viscometer, Scale 1:10

Table 1: Fluids & Viscosities[32-33]

Fluid	**μ (Pa*s at 25°C)**
Corn Syrup	5.57
Molasses	7.40
30 Minute Epoxy Resin	1.71

The viscosities reported for corn syrup and molasses in Table 1 are average values from repeated tests. The standard deviation of the results was 1.33e-8 Pa*s for the corn syrup and 2.31e-8 Pa*s for the molasses.

4.9 Operation of the Dynamometer

As air was injected from the nozzle into the buckets of the turbine, the turbine rotated clockwise; which also cause the shaft and aluminum wheel in the fluid of the drum to rotate clockwise. As the wheel spun, the shear forces of the fluid against the drum caused the fluid to spin in the drum in the same direction. As the shear forces between the fluid and the drum wall increased, the drum was forced to rotate which in turn caused the constrained-layer damper to press against the carbon fiber rod and load cell. The constrained-layer damper damped vibrations from the dynamometer transmitted to the load cell to mitigate erroneous force measurements.

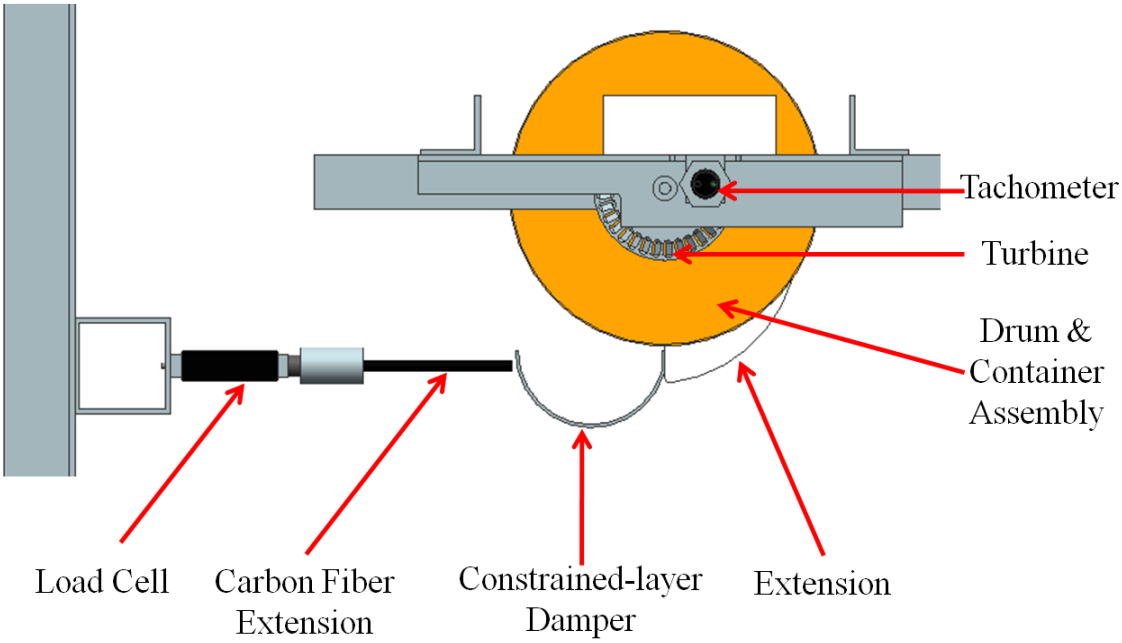

Figure 38: CAD Top View of Dynamometer-Load Cell Interface, Scale 1:4

The transmission of inertia from the wheel to the drum through the fluid was the torque being applied from one surface to the next; because no fluid was lost, mass was conserved and there were no appreciable losses in torque. As the constrained-layer damper & extension

pressed against the load cell, the force measurements were recorded as a time-history using Instron Blue Hill v2.5 software.

During each test, the drum was filled 1.00” (25.4 mm) with one of three viscous, fluids. Each of the fluids used were chosen because of their viscosities; different fluids of high viscosities being necessary to impart various amounts of resistance to the wheel in the drum. By varying the resistance against the wheel, a greater variation of torque and RPM values could be measured.

4.10 Test Procedures

The tachometer calibration was verified per the included instructions by aiming the tachometer at a non-“energy efficient” fluorescent light bulb; the tachometer should read about 7200 RPM which is approximately 120 Hz. After the tachometer was deemed functional, it was installed on the test stand. Both the PC and the Instron 3345 were powered up; once both systems were running, the Bluehill™ software was launched and the appropriate run file was opened. The calibration of the load cell was verified by orienting the load cell vertically and placing calibrated weights, as great as 2.21 lb_f (9.81 N), atop the load cell and verifying the correct measurement with Bluehill™. To prepare the experiment, one of the fluids was poured into the drum to a depth of 1.00” (25.4 mm). The dynamometer A-frames and substructure were then attached to the L-channel connected to the plywood base; taking care to place the shaft in the drum and align it properly. Electrical tape was then applied to the drum and its lid to prevent the fluid from leaking out of the drum during tests. The apparatus was then secured to a large concrete slab with four 0.250” (6.35 mm) Tapcon concrete screw anchors. Next, steel pellets and weights were added to the container to

increase the system mass and reduce vibrations transmitted from the drum to the dynamometer.

The swing arm was set at the initial angle of 15° and secured to the support with an 8-32 fastener. The base of the support was then secured to the plywood base with a "Quick-Grip" type bar-clamp. The distance between the nozzle and the turbine could then be adjusted along the slot in the swing arm, and then secured by tightening the two fasteners in the slot. The turbine was then given one revolution to ensure it would not strike the nozzle.

Next, a digital pressure gauge, connected to the compressed air line, was attached to the ball valve using a 0.250" (6.35 mm) pneumatic quick connect. To ensure the tachometer was properly viewing the turbine, the tachometer was turned on and the turbine was spun by hand at a low RPM. Finally, the load measured by the load cell was balanced with the Bluehill™ software and the drum was turned so that the constrained-layer damper made light contact with the carbon fiber rod attached to the load cell.

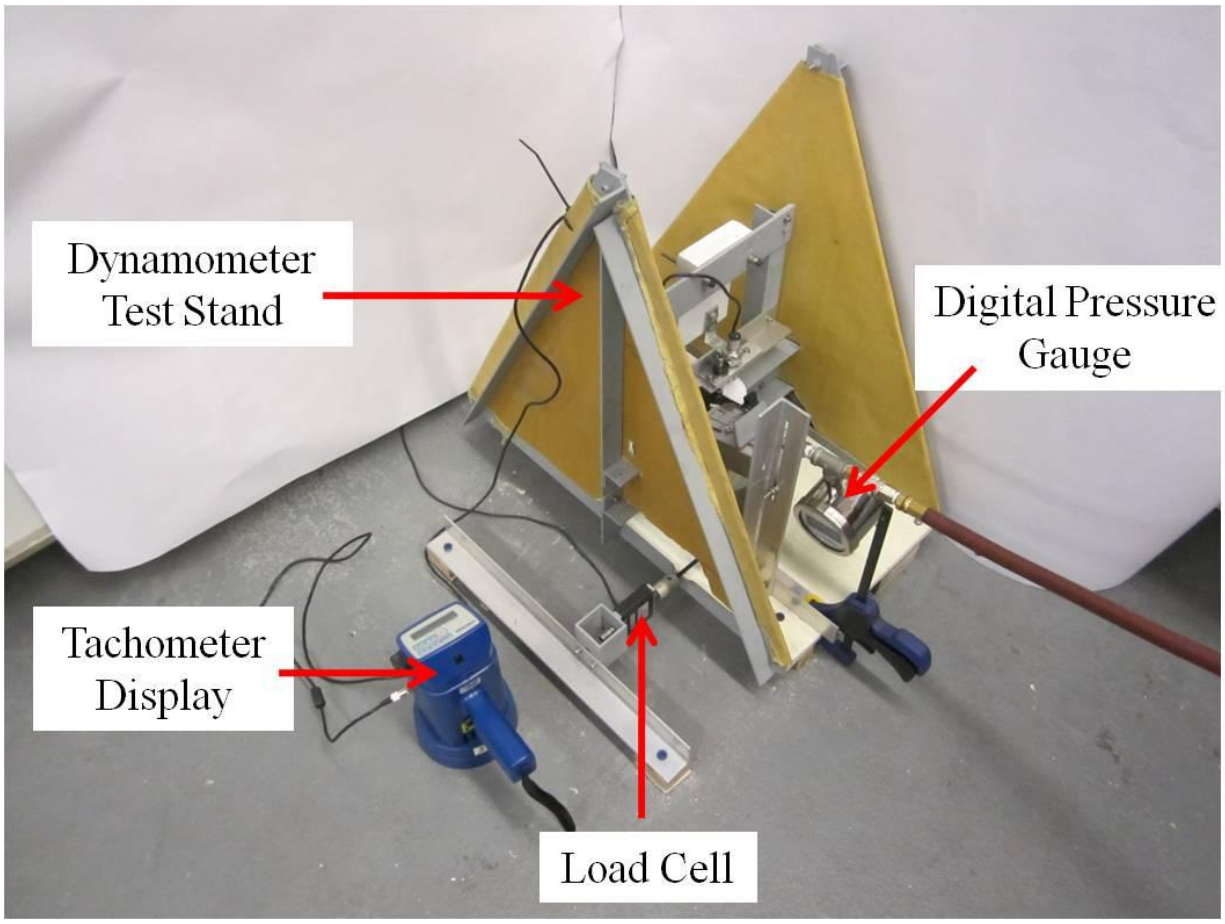

Figure 39: Test Stand Fully Assembled & Prepped for Experiment

At this point, the experiment was ready for testing. Each test began by initiating the data logging of the load cell using the Bluehill™ Software. Immediately afterwards, the ball valve was opened to full which allowed the compressed air to flow through the nozzle and rotate the turbine. When the turbine and the dynamometer reached steady state (defined as when the RPM variance became less than 100) the total pressure of the air supplied to the nozzle as well as the RPM was recorded. The ball valve was then closed, de-energizing the turbine and dynamometer followed by ceasing the data logging with Bluehill™. This test was then repeated twice for the same angle.

The fasteners in the slot of the swing arm were loosened and the nozzle was retracted away from the turbine. The fastener connecting the swing arm to the support was loosened, β

was increased by 5°, and then the fastener was tightened to lock the arm in place against the support. Then the distance between the nozzle and the turbine was brought to a safe minimum. The test was then repeated three times at this new angle. The angle was subsequently increased by 5° and tested three times at each angle until a maximum angle of 45° was achieved. This maximum angle value was so determined because it is equal to the angle of each bucket of the turbine, relative to the plane of rotation.

After completing the angular sweep with one fluid, the test stand was removed from the concrete and the A-frames were detached from the base. The upper structure of the test stand was separated from the base to clean the wheel and the drum of fluid using mild detergent and water. The procedure was then repeated with the other fluids.

5.0 Test Results

During testing, the laboratory was maintained at 75°F (23.9°C) and the daily average atmospheric pressure was 15 psia (103 kPa). The total pressure varied from 73 to 80 psia (503-552 kPa). The pressure range created nozzle exit Mach numbers that ranged from 1.69 to 1.75. The power of the air flow was estimated to be 0.781-0.867 hp (582-647 W). For the vast majority of the tests, the pressure was maintained between 78 and 79 psia (538-545 kPa). Knowing the nozzle flow conditions, the optimum bucket Mach number of the turbine, being half the nozzle exit Mach number, ranged from 0.845 to 0.875 which required the turbine to rotate between 86,900 & 90,000 RPM.

The data gathered was only part of the operational envelope of the turbine. Data was collected at the rotational speeds between 29,500 and 33,100 RPM. The reader should be reminded that rotational speed was not controlled but was a product of the pressure of the air injected from the nozzle, the angle of injection between the nozzle & turbine, and the resistance of the dynamometer. The upper limit of the rotational speed was limited by pressure of the compressed air supply. Force measurements were taken at a rate of 100 samples per second. A Matlab script was used to filter the force measurements using a moving average for 20 samples and multiplied the load by the radius from the shaft center to the load cell, 3.55”, to get torque values. Linear trends were then found where the torque was steady state.

Results for all three fluids showed every measurement with β equal to 15° was a significant outlier from the rest of the data. When the inclination structure was set to a 15° β, the amount of air that entered the turbine from the nozzle was significantly less than at greater angles. Additionally, the nozzle could not be positioned as close to the turbine as at greater inclinations

without risking contact with the turbine during operation. For these reasons, the 15° β cases have been omitted from the results.

5.1 Results of Dynamometer Loaded With Corn Syrup

The 20° cases operated with an average rotational speed 31,700 RPM. The average torque produced was 0.0588 in*lb_f (0.00664 N*m) and the average power produced was 0.0296 hp (22.1 W). While operating at those speeds, the average bucket Mach number was 0.308. As the angle of injection was increased to 25° there was an increase in the average rotational speed to 32,900 RPM, resulting in an average bucket Mach number of 0.320; the greatest rotational speeds were attained at this angle. While at 25°, the average torque decreased to 0.0538 in*lb_f (0.00609 N*m) and the average power slightly decreased to 0.0280 hp (20.9 W). When the angle of injection was increased to 30°, the average rotational speed decreased to 32,700 RPM, with an average bucket Mach number of 0.318. The average torque increased to 0.0561 in*lb_f (0.00634 N*m) and the average power produced had increased to 0.0292 hp (21.8 W).

Increasing the angle of injection to 35°, rotational speed further decreased, averaging 32,700 RPM. The average bucket Mach number decreased from the value of the 30° case to 0.318. The torque and power increased from the 30° case to an average of 0.0607 ft*lb_f (0.00686 N*m) and 0.0315 hp (23.5 W) respectively. When the angle of injection was increased to 40°, the rotational speed continued to decrease, averaging 32,100 RPM; also resulting in an average bucket Mach number of 0.312. The average torque increased to 0.0690 in*lb_f (0.00780 N*m). At this angle, the average power peaked at 0.0351 hp (26.2 W). Finally, at 45° angle of injection, there was a decrease in rotational speed, bucket Mach number, torque, and power produced. The average rotational speed decreased to 31,400

RPM; the lowest speed among the six angles of injection. The average bucket Mach number associated with that speed was 0.306. Torque for the three test at this angle averaged 0.0536 in*lb_f (0.00606 N*m). The average power produced was the lowest among the six angle cases, 0.0267 hp (19.9 W). The full range of results for each parameter from the eighteen tests with the dynamometer loaded with corn syrup is summarized in Table 2.

Table 2: Turbine Measurements With Corn Syrup For Viscous Fluid

β	RPM	Bucket Mach No.	τ (in*lb_f)	P (hp)	η
20°	31,500-31900	0.306-0.310	0.0556-0.0610	0.0283-0.0307	3.36-3.59
25°	32,700-33,100	0.318-0.322	0.0511-0.0578	0.0268-0.0301	3.09-3.47
30°	32,600-33,000	0.317-0.321	0.0553-0.0581	0.0286-0.0300	3.37-3.56
35°	32,500-32,800	0.316-0.319	0.0590-0.0624	0.0307-0.0325	3.59-3.74
40°	31,800-32,200	0.309-0.313	0.0638-0.0790	0.0325-0.0404	3.81-4.72
45°	31,300-31,600	0.304-0.307	0.0514-0.0555	0.0255-.0277	2.99-3.24

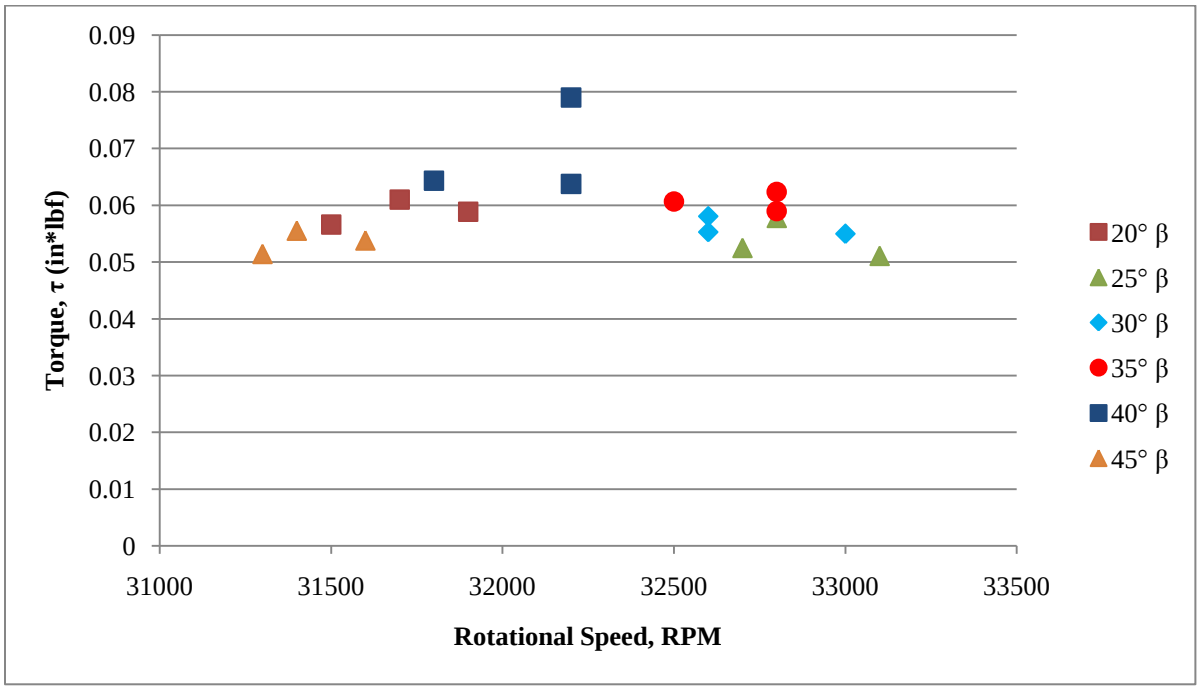

Figure 40: Dynamometer Loaded With Corn Syrup, Torque Vs. Rotational Speed

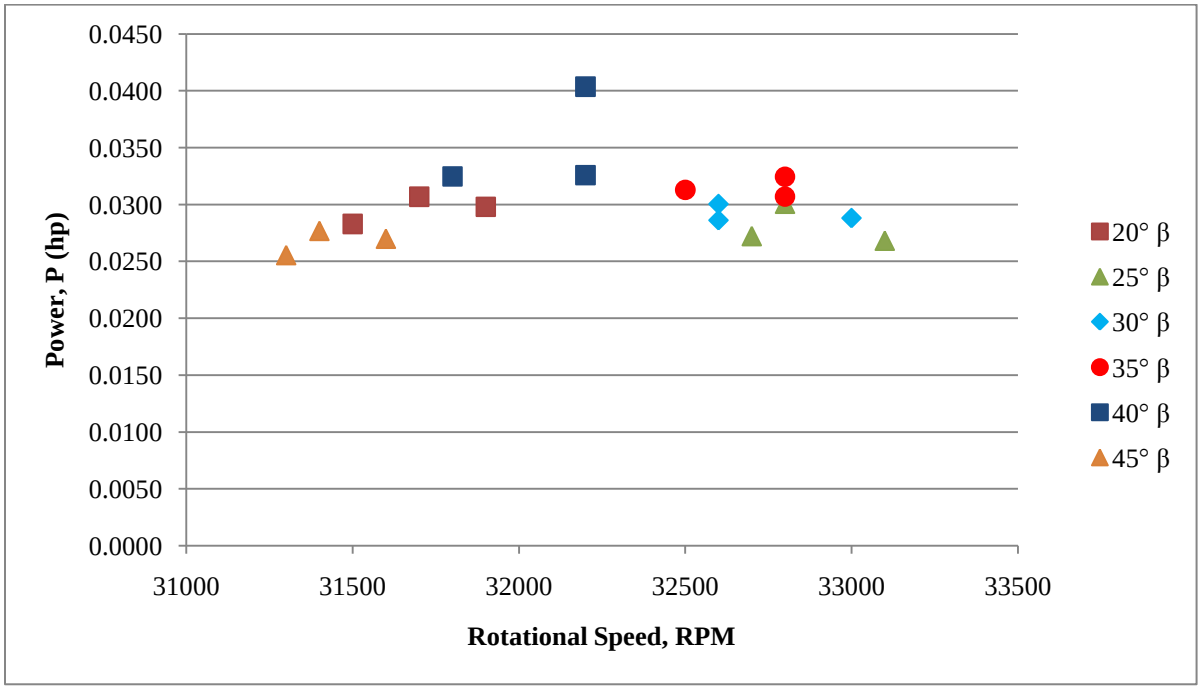

Figure 41: Dynamometer Loaded With Corn Syrup, Power Vs. Rotational Speed

Throughout the angular sweep, the power from the compressed air ranged from 0.843 to 0.867 hp (629-647 W). The efficiencies of the turbine that resulted ranged 2.99% to 4.72%. The efficiencies are plotted against the rotational speed in Figure 42. Because power was the product of torque & rotational velocity and the range of velocity was relatively small, the data scatter for power vs. rotational speed in Figure 41 looks very similar to the scatter for torque vs. rotational speed in Figure 40. Also, the variation in power from the kinetic energy of the air was small, not more than 0.024 hp (17.9 W); this small variation of input power is why the scatter of Figure 42 looks very similar to that in Figure 41.

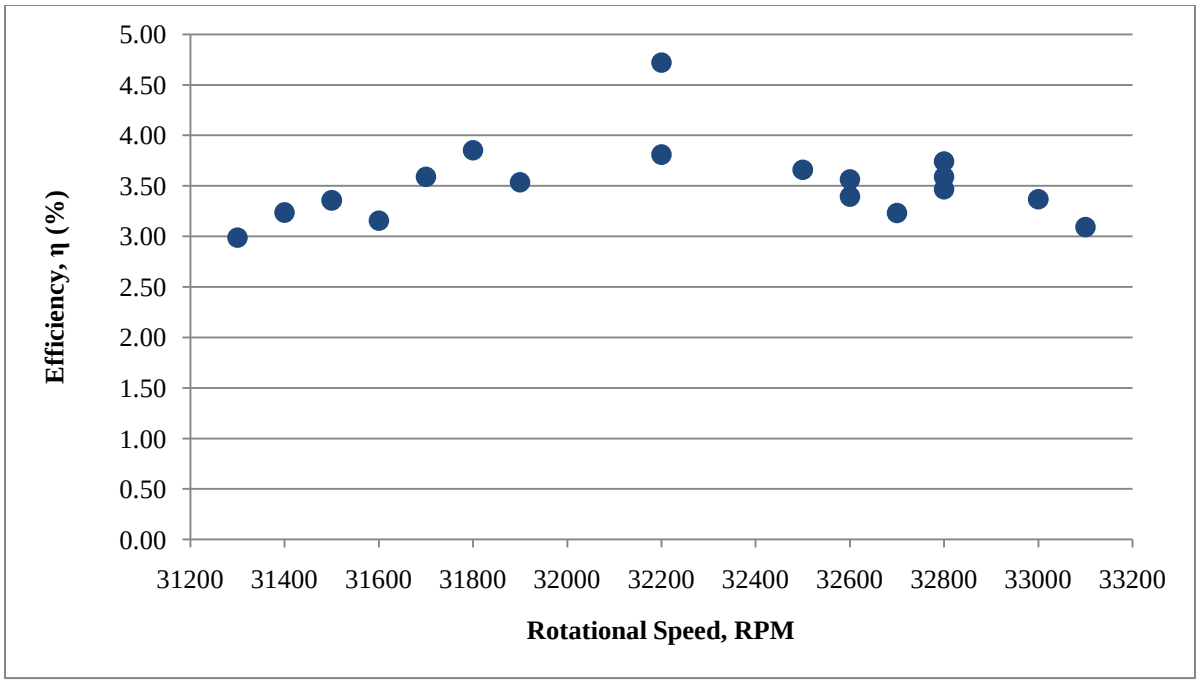

Figure 42: Dynamometer Loaded With Corn Syrup, Efficiency Vs. Rotational Speed

The data was based on the average torque measured while the dynamometer operated at steady state. The error bands based on the torque measurements, as it applies to efficiency, is shown in Figure 43. The lower bound of the error was 0.88 and the upper bound was 3.44.

The magnitude of the upper bound of the error band was attributed to dynamics between the dynamometer and the load cell. Occasionally, the dynamometer and shear layer damper assembly would recoil a small, finite distance away from the load cell. When torque overcame the recoil, the dynamometer would recontact the load cell with enough momentum sufficient to cause a spike in the torque measurements, as shown in Appendix A. This error band was representative of the data for each of the fluids used in the dynamometer during this investigation.

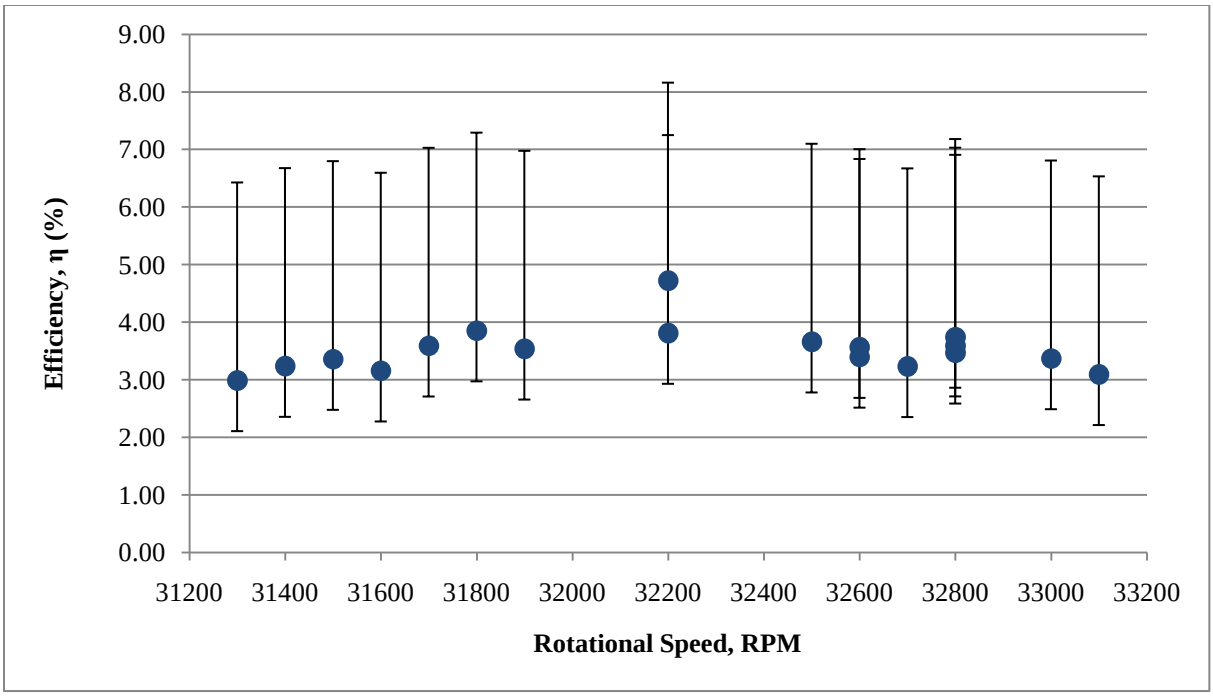

Figure 43: Efficiency Error Band for Dynamometer Loaded With Corn Syrup

When comparing the angle of injection to the averaged rotational speeds achieved at each angle, the speeds increase until the injection angle reaches 25°. At the 25° setting, the averaged rotational speed achieves a maximum value of 32,900 RPM. As the angle of injection was increased, the rotational speeds gradually decreased. The rate of decrease of rotational speeds increased as the injection angle exceeded 35°. This trend is shown below in Figure 44.

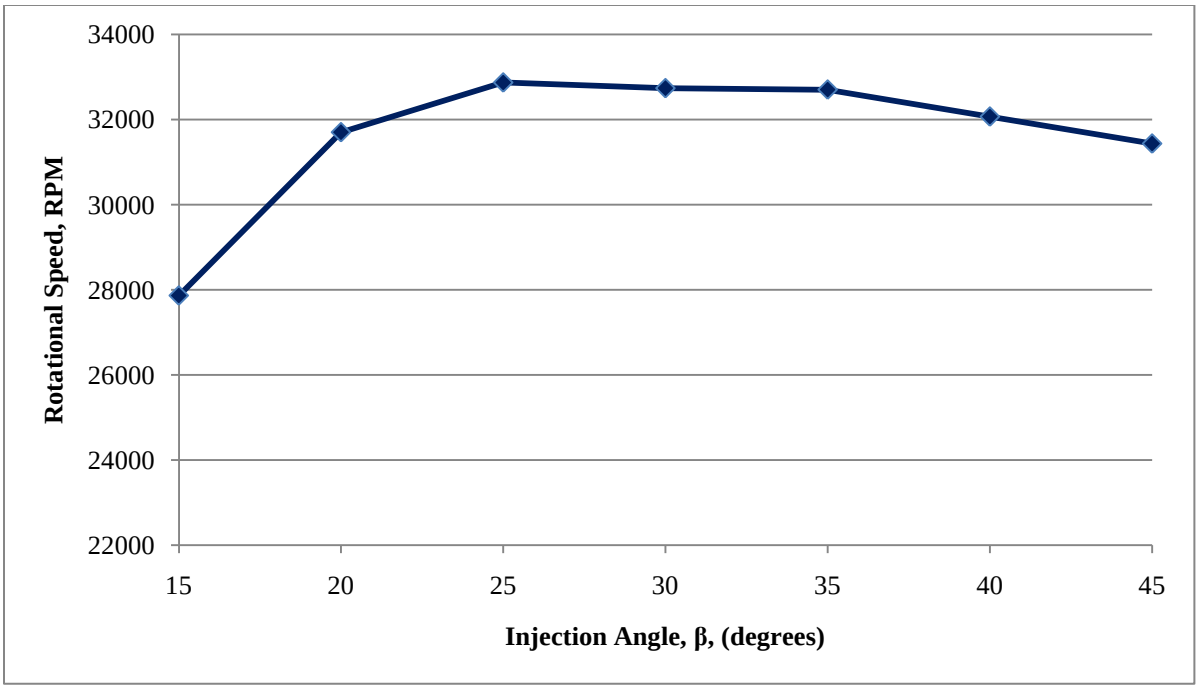

Figure 44: Dynamometer Loaded With Corn Syrup, Rotational Speed Vs. Angle of Injection

5.2 Results of Dynamometer Loaded With Molasses

At 20°, the turbine was able to attain an average rotational speed of 31,000 RPM and the average bucket Mach number was 0.302. The average amount of torque and power produced at 20° was 0.0569 in*lb_f (0.00643 N*m) and 0.0280 hp (22.2 W) respectively. There was a substantial increase in the rotational speed as the angle of injection was increased to 25°. Speeds reached their max, averaging 32,700 RPM with an average bucket Mach numbers of 0.318. The average torque increased to 0.0575 in*lb_f (0.00650 N*m). The power produced increased from the previous angle of injection, averaging 0.0298 hp (22.2 W). When the angle of injection was increased to 30°, the average rotational speed decreased to 32,400 RPM and the bucket Mach numbers decreased to an average of 0.315. The average torque decreased to 0.0558 in*lb_f (0.00630 N*m). The power produced also slightly decreased to an average of 0.0287 hp (21.4 W).

As the angle was increased to 35°, the average rotational speed decreased further to 32,000 RPM; the bucket Mach number also decreased to an average of 0.311. The average torque slightly increased to 0.0560 in*lb_f (0.00633 N*m). The average power created slightly decreased from the 30° cases, averaging 0.0284 hp (21.2 W). Increasing the angle to 40° showed the rotational speed continued to decrease to an average of 31,800 RPM and the average bucket Mach number decreased to 0.309. There was a significant increase in torque compared to the previous angle, averaging 0.0770 in*lb_f (0.00870 N*m). The average power produced increased significantly to a peak value of 0.0388 hp (28.9 W). When the angle was at 45°, there was a decrease in all values. The average rotational speed was at the minimum value for the six angles of attack, 29,700 RPM. The resulting average bucket Mach number was 0.289. The average torque was 0.0754 in*lb_f (0.00852 N*m) and the average power produced was 0.0355 hp (26.5 W). The full range of results for each parameter from the eighteen tests with the corn syrup is summarized in Table 3.

Table 3: Turbine Measurements With Molasses Syrup For Viscous Fluid

β	**RPM**	**Bucket Mach No.**	**τ (in*lb_f)**	**P (hp)**	**η**
20°	30,800-31,300	0.300-0.304	0.0516-0.0671	0.0252-0.0330	2.95-3.91
25°	32,600-32,800	0.317-0.319	0.0541-0.0630	0.0271-0.0327	3.32-3.88
30°	32,300-32,500	0.314-0.316	0.0528-0.0593	0.0271-0.0306	3.22-3.58
35°	32,000	0.311	0.0528-0.0605	0.0268-0.0307	3.13-3.65
40°	31,700-32,000	0.308-0.311	0.0726-0.0798	0.0368-0.0402	4.31-4.77
45°	29,700	0.289	0.0730-0.0770	0.0344-0.0363	4.40-4.65

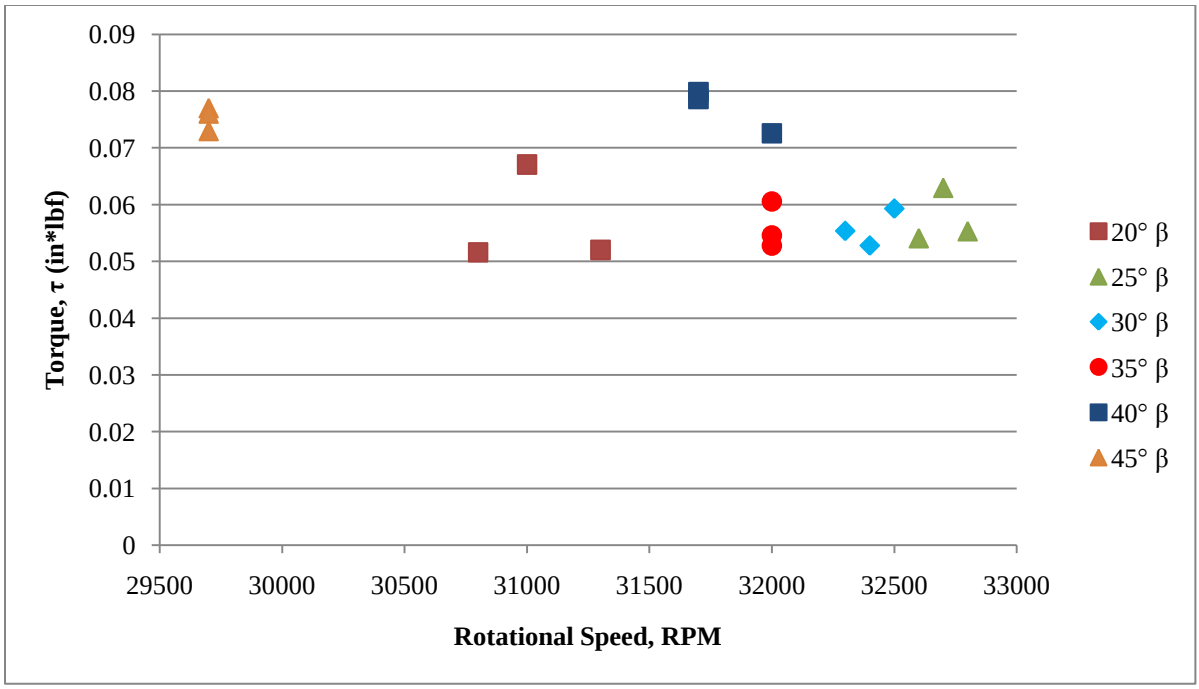

Figure 45: Dynamometer Loaded With Molasses, Torque Vs. Rotational Speed

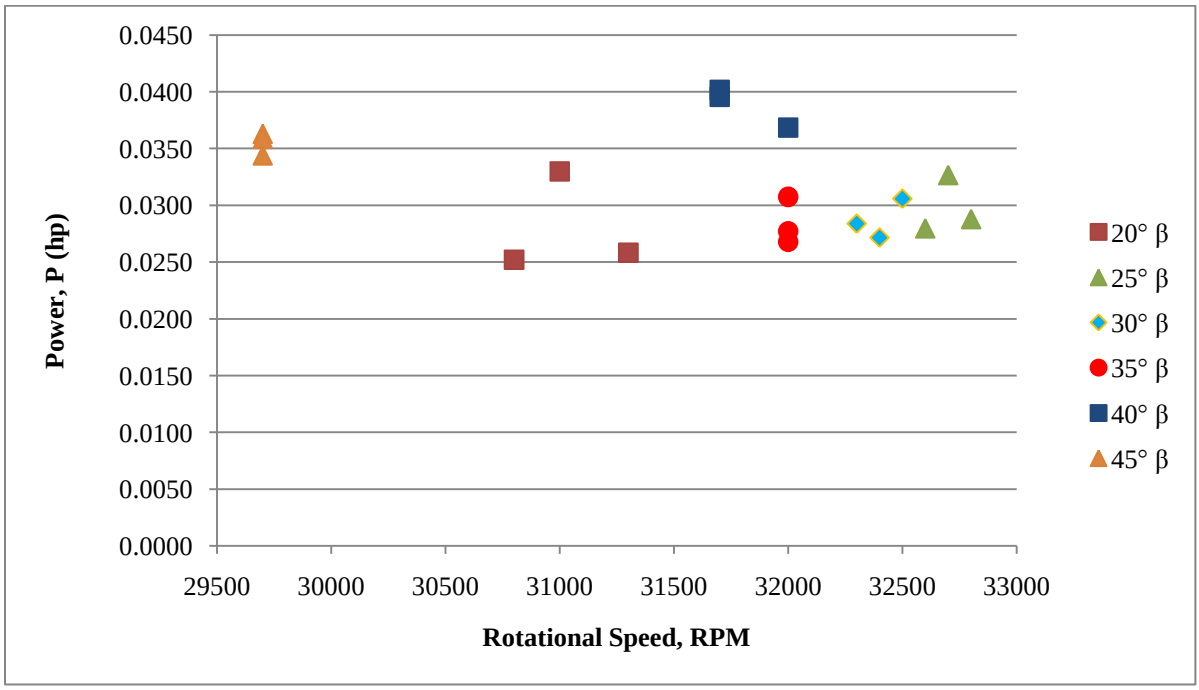

Figure 46: Dynamometer Loaded With Molasses, Power Vs. Rotational Speed

Throughout the angular sweep, the power from the kinetic energy of the compressed air ranged from 0.781 to 0.855 hp (582-638 W). The efficiencies of the turbine that resulted ranged 2.95% to 4.77%. The efficiencies are plotted against the rotational speed in Figure 47. Because power was the product of torque & rotational velocity and the range of velocity was relatively small, the data scatter for power vs. rotational speed in Figure 46 looks very similar to the scatter for torque vs. rotational speed in Figure 45. Also, the variation in power from the kinetic energy of the air was small, not more than 0.074 hp (55.2 W); this small variation of input power is why the scatter of Figure 47 looks very similar to that in Figure 46. All tests taken at angles of injection ranging from 20° to 40° had between 0.843 hp (629 W) and 0.855 hp (638 W) of input power from the air; however, tests at 45° angle of injection had 0.781 hp (582 W) of input power from the air. Reduction in air power during the 45° tests was due to a drop in the available air pressure.

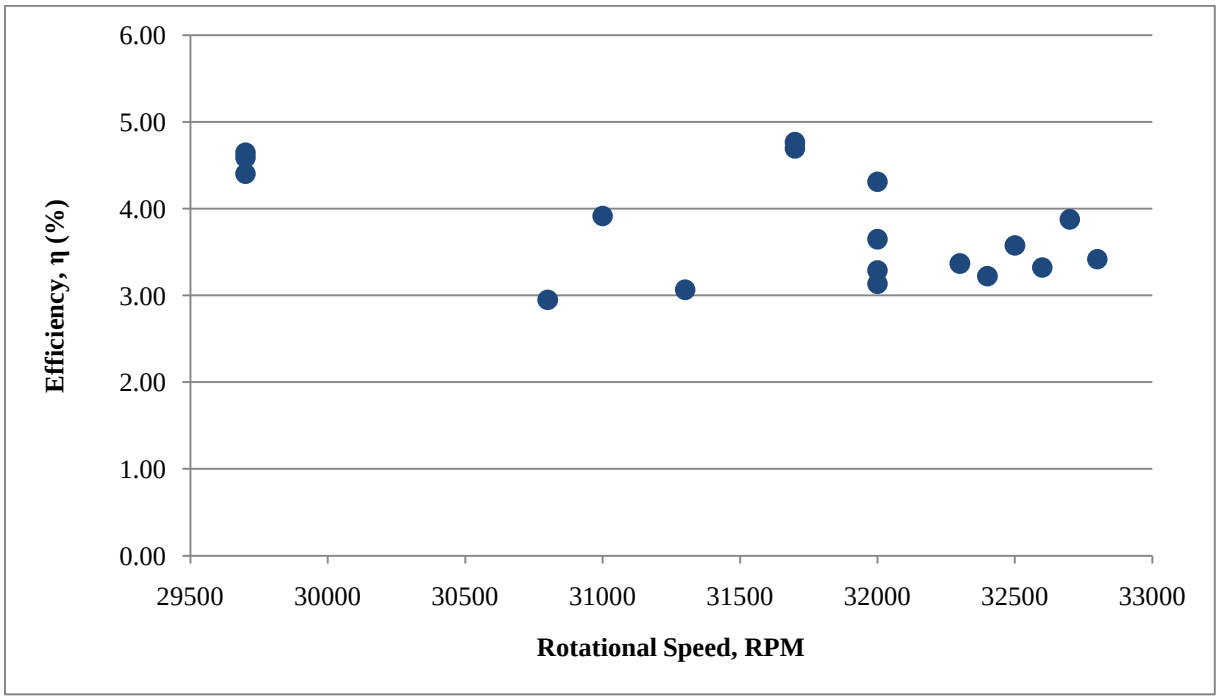

Figure 47: Dynamometer Loaded With Molasses, Efficiency Vs. Rotational Speed

Figure 48: Dynamometer Loaded With Molasses, Rotational Speed Vs. Angle of Injection

When comparing the angle of injection to the averaged rotational speeds achieved at each angle, the speeds increase until the injection angle reaches 25°. When set to 25°, the averaged rotational speed maximized to 32,700 RPM. When the angle of injection was set to greater inclinations, the rotational speeds gradually decreased throughout the remainder of the tests. This trend is shown above in Figure 48.

5.3 Results of Dynamometer With Resin Results

With the angle of injection set to 20°, the turbine operated at an average rotational speed of 31,800 RPM and the average bucket Mach numbers achieved was 0.310. The average torque was 0.0462 in*lb_f (0.00522 N*m) and the average power produced was 0.0234 hp (17.4 W). When the angle was set to 25°, the turbine achieved the maximum speed among the six angle settings; the average rotational speed increased to 32,300 RPM and the average bucket Mach numbers increased to 0.314. The average torque increased to 0.0481 in*lb_f (0.00543 N*m). The average power achieved increased to 0.0246 hp (18.3 W). As the

angle of injection was increased to 30°, the average rotational speed decreased to 31,500 RPM with an average bucket Mach number of 0.306. The average torque and power produced at this angle were 0.0573 in*lb_f (0.00647 N*m) and 0.0286 hp (21.3 W) respectively.

With the angle of injection set to 35°, the average rotational speed further decreased to 31,300 RPM and the average bucket Mach numbers decreased to 0.305. The average torque decreased to 0.0547 in*lb_f (0.00618 N*m). The average power produced slightly decreased to 0.0272 hp (20.3 W). When the angle of injection was set to 40° the rotational speeds continued to decrease, averaging 31,100 RPM. The bucket Mach number for the average speed was 0.303. The average torque further decreased to 0.0518 in*lb_f (0.00585 N*m). The average power achieved at this angle was 0.0256 hp (19.1 W). Finally, at 45° angle of injection, the rotational speed decreased to the minimum achieved among the six angles of injection. The average rotational speed was 29,700 RPM and the average bucket Mach number was 0.289. The average torque increased to 0.0551 in*lb_f (0.00623 N*m). The average power produced increased from the average of the 40° cases to 0.0260 hp (19.4 W). The results above are summarized in the following table.

Table 4: Turbine Measurements With Resin For Viscous Fluid

β	RPM	Bucket Mach No.	τ (in*lb_f)	P (hp)	η
20°	31,700-31,900	0.354-0.356	0.0462-0.0471	0.0230-0.0238	2.68-2.83
25°	32,100-32,500	0.358-0.363	0.0451-0.0510	0.0233-0.0260	2.76-3.04
30°	31,400-31,600	0.351-0.352	0.0536-0.0604	0.0269-0.0301	3.14-3.47
35°	31,200-31,500	0.348-0.352	0.0504-0.0574	0.0250-0.0285	2.96-3.39
40°	31,000-31,300	0.346-0.349	0.0499-0.0534	0.0248-0.0263	2.94-3.12
45°	29,500-29,900	0.329-0.334	0.539-0.0560	0.0254-0.0263	3.02-3.13

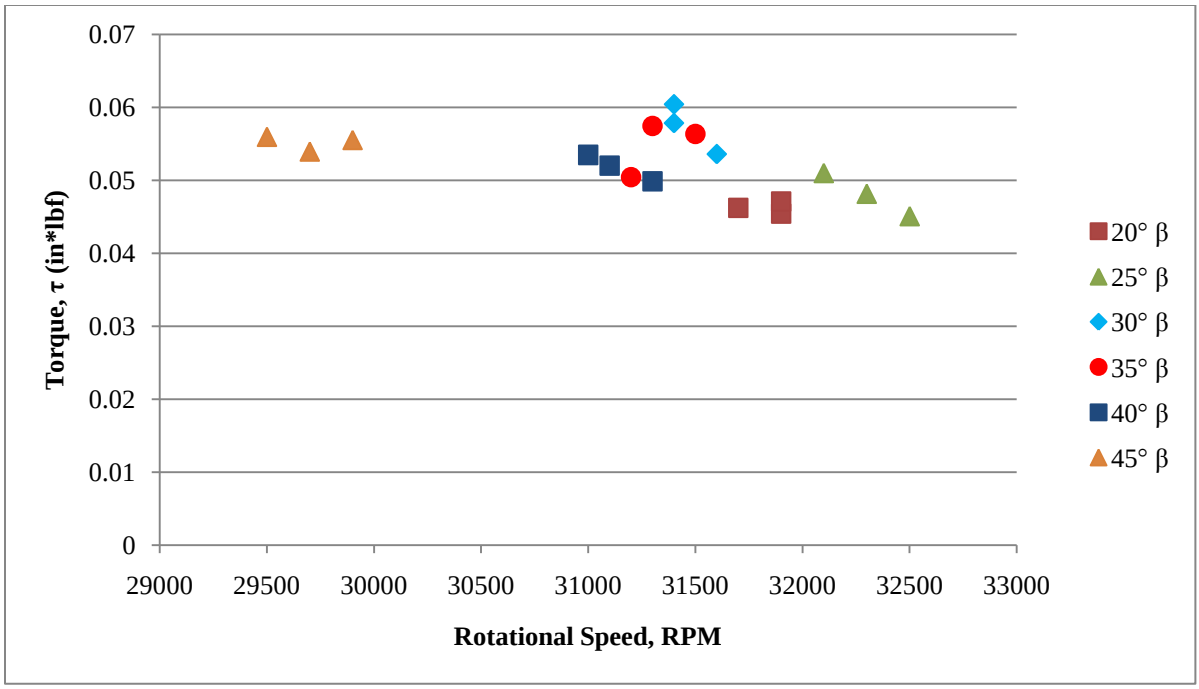

Figure 49: Dynamometer Loaded With Resin, Torque Vs. Rotational Speed

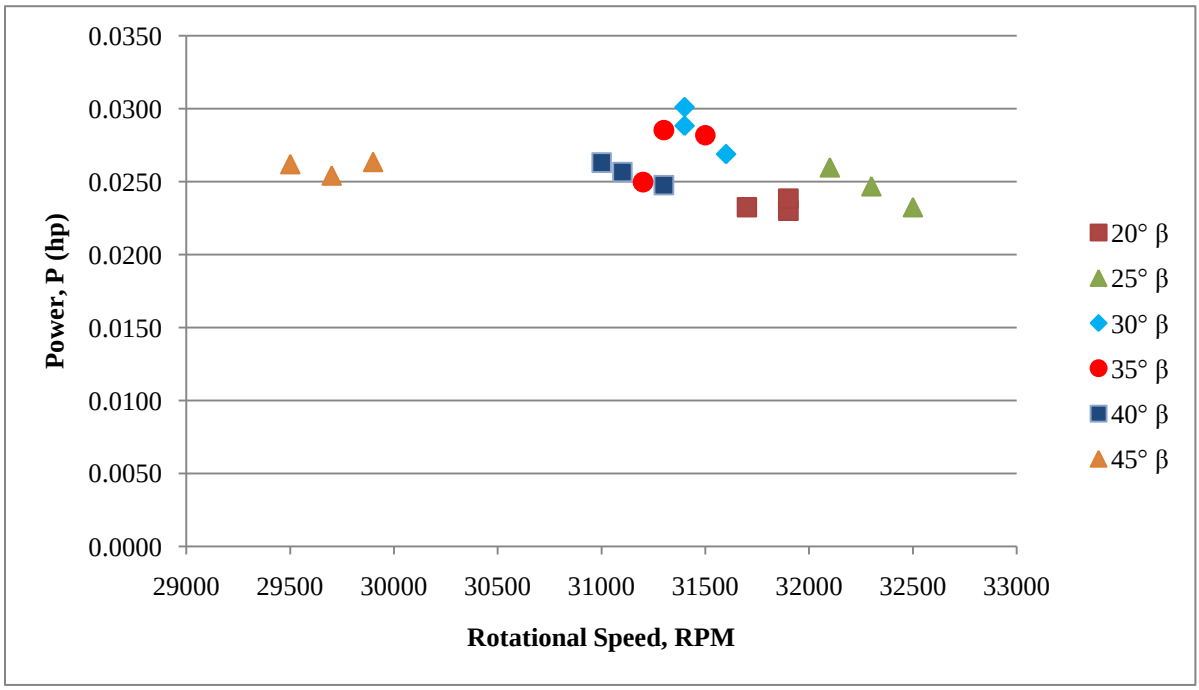

Figure 50: Dynamometer Loaded With Resin, Power Vs. Rotational Speed

Throughout the angular sweep, the power from the compressed air ranged from 0.843 to 0.867 hp (629 to 647 W). The efficiencies of the turbine that resulted ranged 2.73% to 3.47%. The efficiencies are plotted against the angle of injection in Figure 51. Because power was the product of torque & rotational velocity and the range of velocity was relatively small, the data scatter for power vs. rotational speed in Figure 50 looks very similar to the scatter for torque vs. rotational speed in Figure 49. Also, the variation in power from the kinetic energy of the air was small, not more than 0.024 hp (17.9 W); this small variation of input power is why the scatter of Figure 51 looks very similar to that in Figure 50.

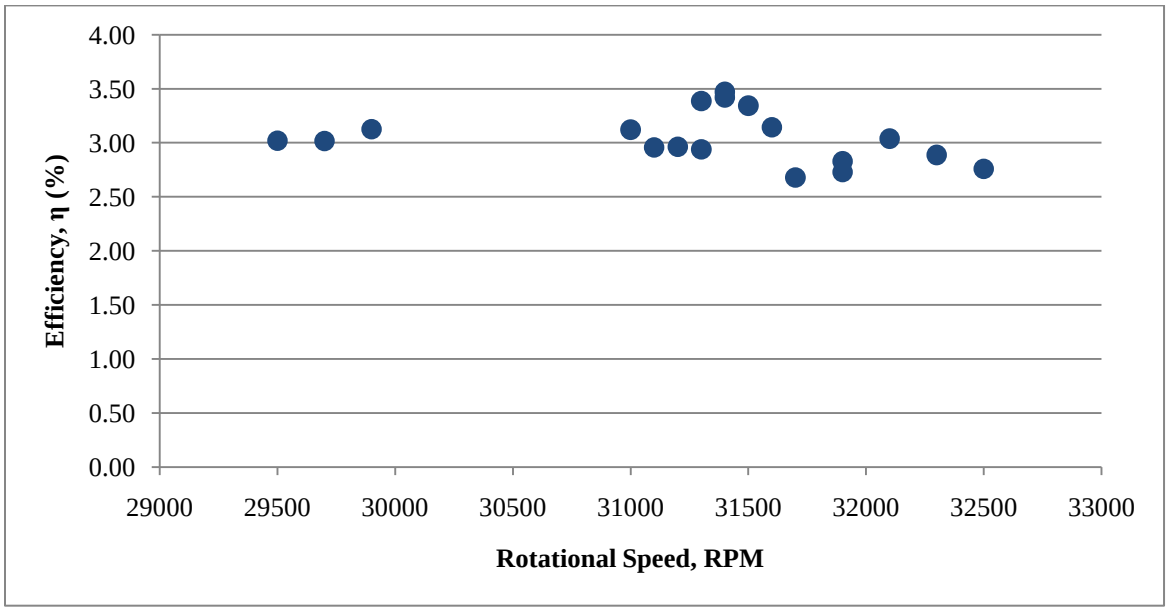

Figure 51: Dynamometer Loaded With Resin, Efficiency Vs. Rotational Speed

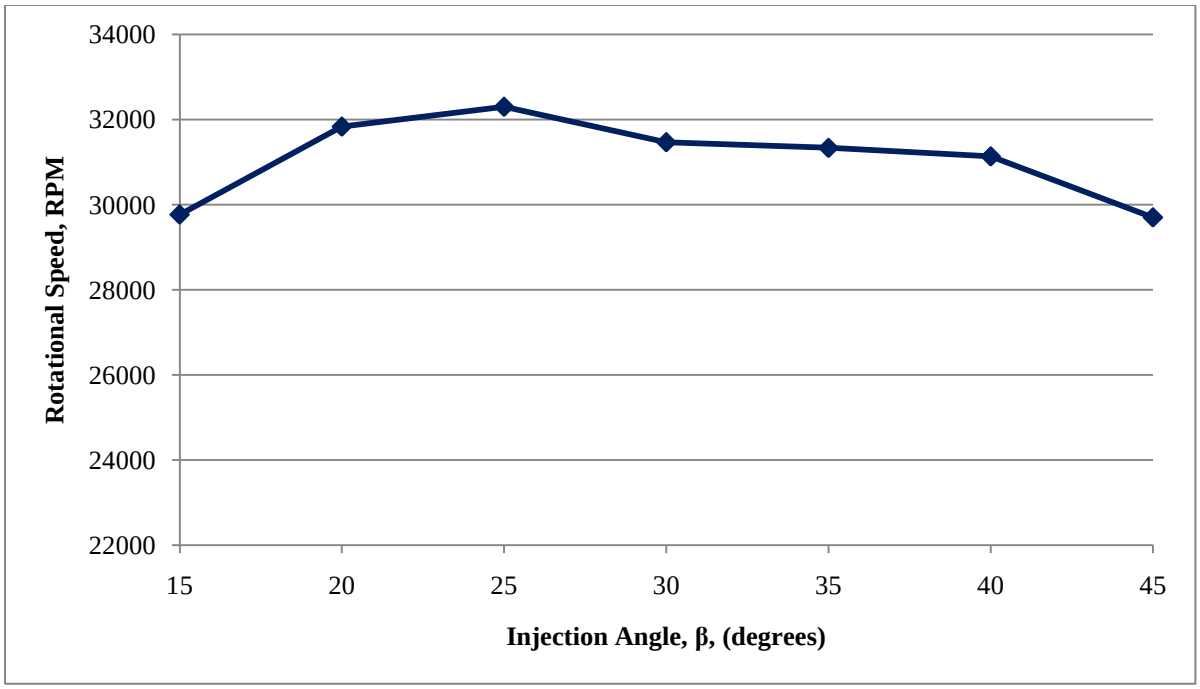

Figure 52: Dynamometer Loaded With Resin, Rotational Speed Vs. Angle of Injection

When comparing the angle of injection to the averaged rotational speeds achieved at each angle, the speeds increase until the injection angle reaches 25°. The averaged rotational speed maximized at this angle to 32,300 RPM. When the angle of injection was set to greater inclinations, the rotational speeds gradually decreased throughout the remainder of the tests with the greatest decreases in speed occurring between 25°-30°. This trend is shown above in Figure 52.

The trends of rotational speed versus the angle of injection for all three fluids are shown in Figure 53 for comparison. Tests with each fluid showed a similar trend; rotational speed increased with the injection angle, maximized at 25º. As the injection angle was further increased, the rotational velocity gradually decreased. For all angles ranging from 20º to 45º, there was little variance in rotational speed, less than 2000 RPM, between the three fluids; this is likely because the fluid viscosities were all of the same order of magnitude.

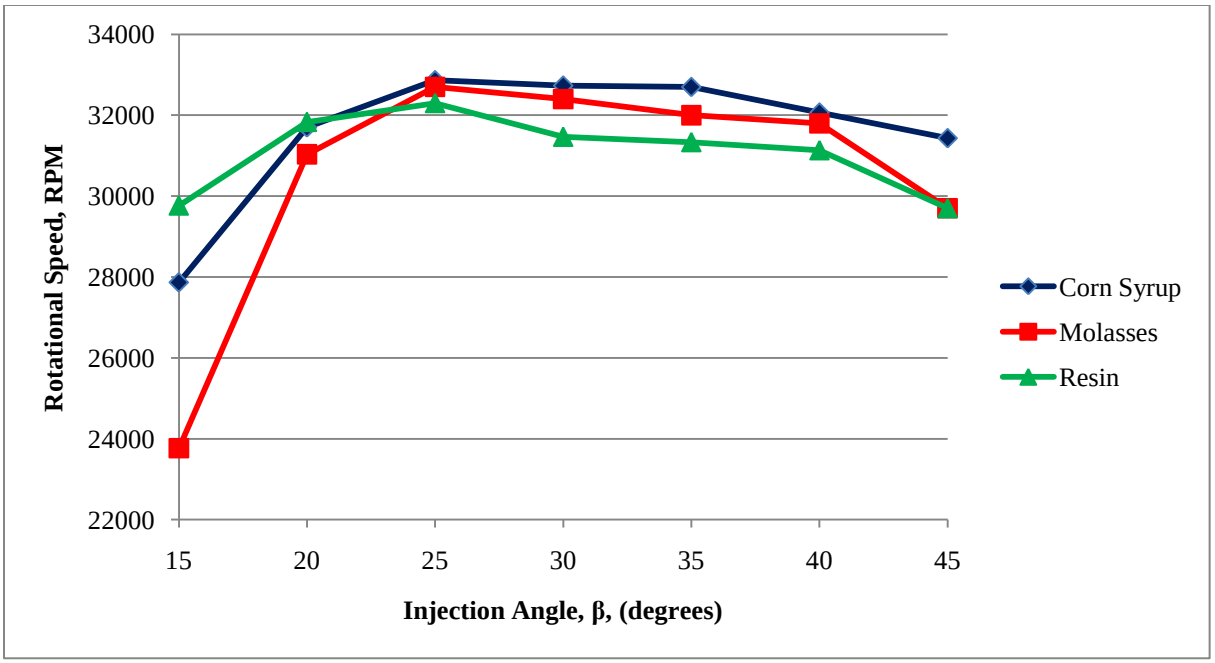

Figure 53: Rotational Speed Vs. Injection Angle

5.4 Air Injection Out of Tangential Plane

There was some concern about the variation in the amount of power determined for a given angle in a given fluid. It was believed that this may be due to small deviations in the direction the air was injected into the turbine. Though the angle of injection was well controlled with the support, there was a finite amount the nozzle could move out of the turbine's tangential plane which permitted the nozzle to be angled inboard and outboard from the bucket center. This angle of deviation from tangential plane has been notated as Δ (the sign convention has been defined as all inboard angles are negative and all outboard angles are positive) and is illustrated in Figure 54.

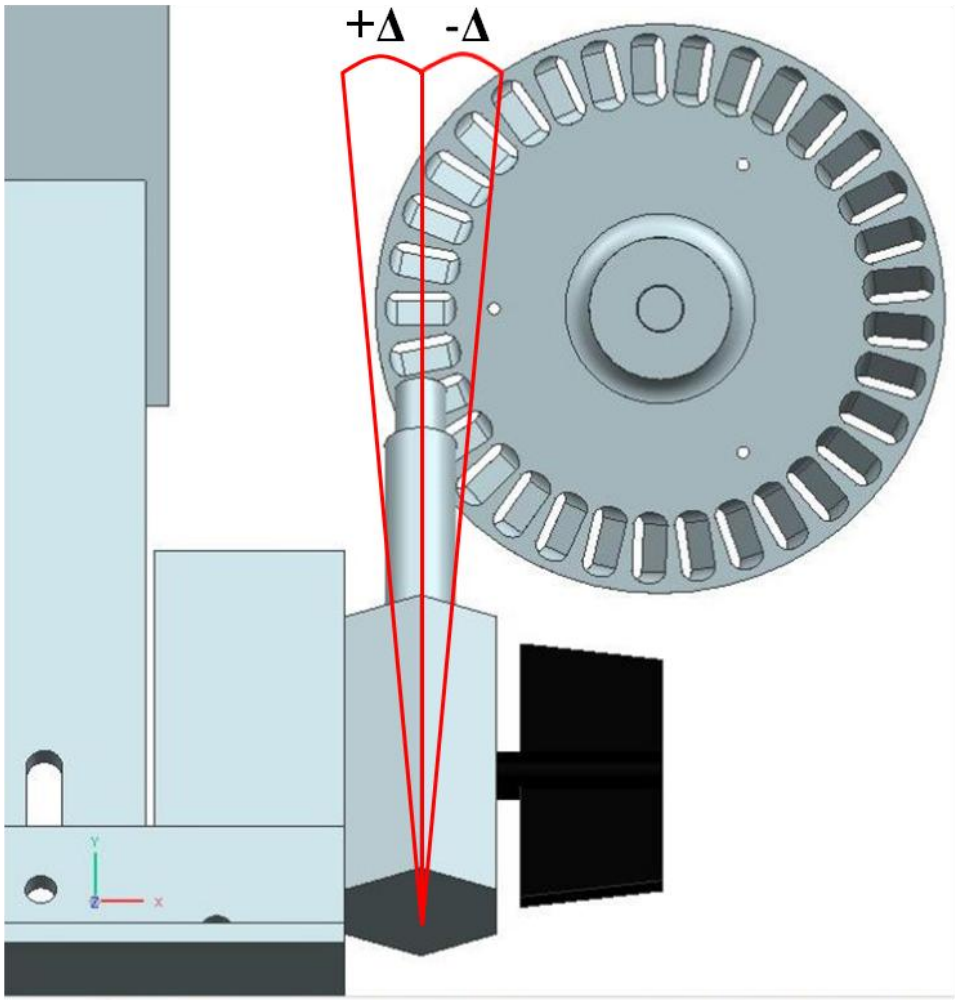

Figure 54: Tangential Deviation Angle, Scale 1:1

This was almost entirely due to the distance adjustment slot of the nozzle swing arm being slightly wider than the 10-24 fasteners used to secure it. Prior to testing, the fasteners in distance adjustment slot were well tightened; however, there was the possibility that it was not aligned perfectly with the bucket center when it was set. Additionally, with the ball valve that controlled nozzle flow mounted directly to the nozzle swing arm, it is possible that operating the ball valve may have imparted enough force on the swing arm to aim the nozzle out of the tangential plane.

To investigate the effects of the injection angle deviating from the tangential plane, the drum of the test stand was filled with molasses to a depth of 1.00” (25.4 mm) with β set to 35°. The swing arm was set for the nominal distance used for all previous tests at that angle. One of the two fasteners of the distance adjustment guide was loosened and the nozzle was pointed as far inboard as possible, 1° from the tangential plane of the turbine. The loose fastener was tightened and the turbine was then run three times at that position. Afterwards the fastener in the distance adjustment guide was loosened and the nozzle was adjusted to the tangent of the turbine. The test was repeated three times at the tangent angle. Finally the nozzle was set so it faced as far outboard from the turbine as possible, 1° from the tangent of the turbine, and run three more times. Though the angular changes were small, it was enough to permit the nozzle centerline 0.131” (3.33 mm) of travel along the bucket span.

During this test, the total pressure at the throat of the nozzle varied from 73-74 psi (503-510 kPa). The lowest power values obtained were when the nozzle was angled 1° inboard. While facing inboard, the turbine obtained an average rotating speed 29,700 RPM and average bucket Mach number of 0.289. The average torque was 0.0477 in*lb_f (0.00539 N*m) and the average power produced was 0.0225 hp (16.8 W). When the nozzle was aimed tangent to the wheel, the turbine showed an increase in power and rotation speed, operating at an average speed of 30,400 RPM and average bucket Mach number of 0.296. The average torque increased to 0.0608 in*lb_f (0.00687 N*m) and the average power produced was 0.0293 hp (21.8 W). The average rotational speed continued to increase when the nozzle was turned 1° outboard, 30,800 RPM with an average bucket Mach number of 0.299. The average torque decreased to 0.0601 in*lb_f (0.00679 N*m); however, the power calculated was the same as for the tangential case. Following a second order polynomial trendline for the nine

tests comparing power to angle out of the tangential plane, the maximum amount of power achievable may be when the nozzle is angled 0.5° outboard. The results of this analysis are shown in Figures 55 & 56 and the full range of the results is detailed in Table 5.

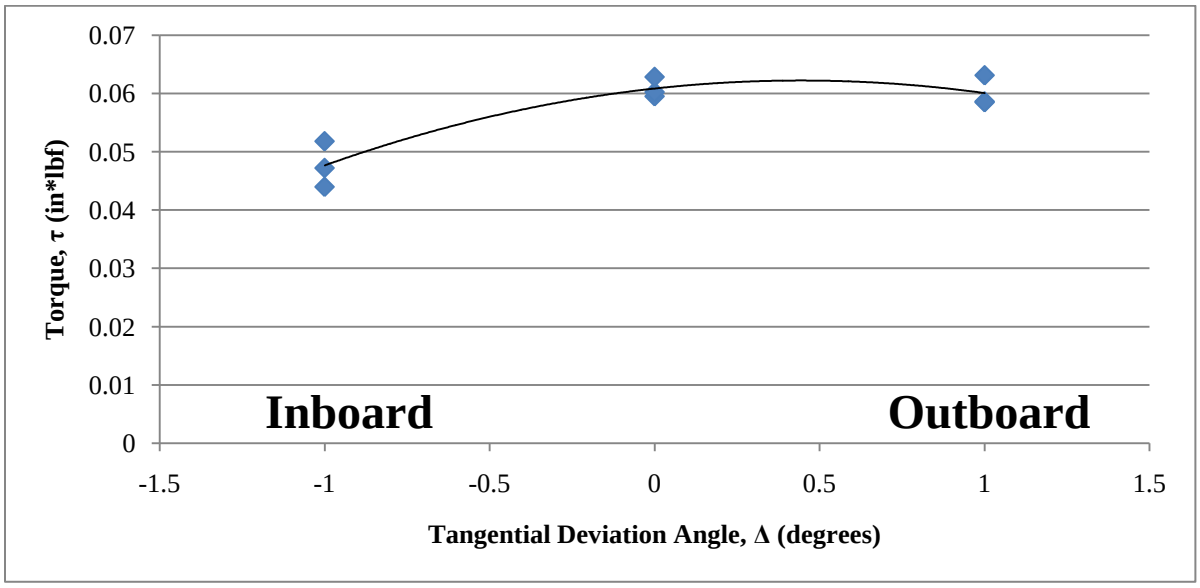

Figure 55: Torque Vs. Tangential Deviation Angle

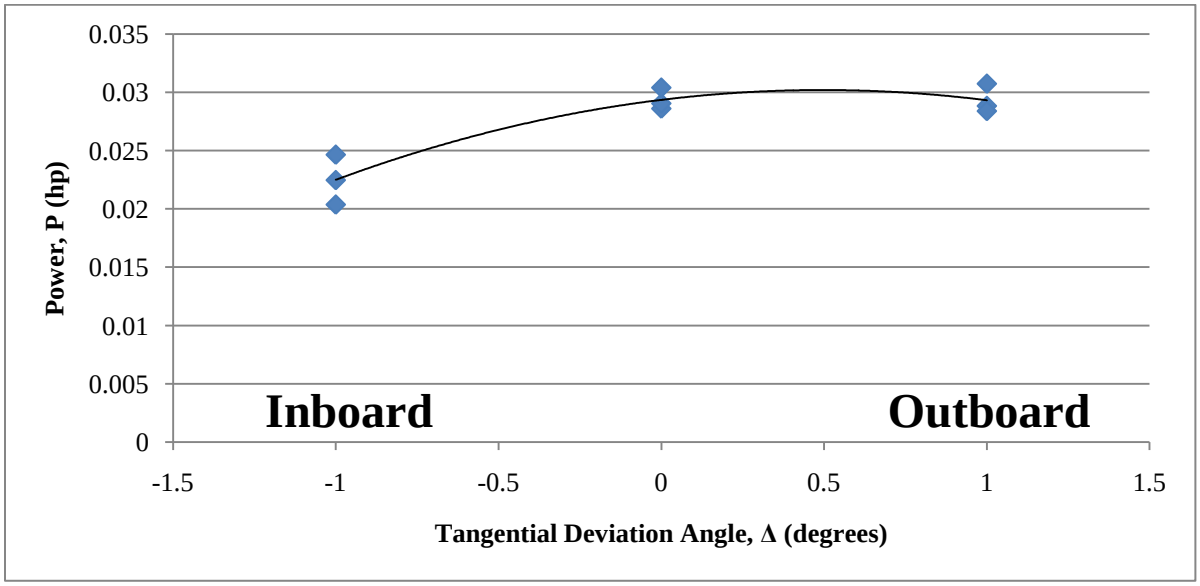

Figure 56: Power Vs. Tangential Deviation Angle

Table 5: Turbine Measurements Comparing Angles Relative To The Tangential Plane

Δ	RPM	Bucket Mach No.	τ (in*lb_f)	P (hp)	η
-1°	29,200-30,000	0.284-0.292	0.0440-0.0518	0.0204-0.0247	2.61-3.11
0°	30,300-30,500	0.295-0.297	0.0595-0.0628	0.0286-0.0304	3.60-3.89
1°	30,600-31,000	0.298-0.301	0.0585-0.0631	0.0284-0.307	3.58-3.93

6.0 Conclusions & Recommendations

6.1 Conclusions

The experiments showed that an impulse turbine with linear shaped slots between the buckets was capable of producing power and high rotational speeds. It can be concluded that the turbine, being supplied compressed air at 73-80 psia (503-552 kPa) with a single CD nozzle was capable of operating at rotational speeds of 29,500-33,100 RPM. The average torques measured for that operating range were 0.0451-0.0798 in*lb_f (0.00510-0.00902 N*m) and produced 0.0230-0.0404 hp (17.2-30.1 W) of power. The average bucket Mach numbers for these speeds ranged 0.287-0.322, less than half the optimum bucket Mach numbers, 0.845-0.875, for the air pressures used.

Injecting air at the turbine at angles shallower than 20° from the plane of rotation yielded significantly lower power and rotational speeds than the values measured at greater angles of injection. This phenomenon occurred because the angle was too shallow to permit sufficient air capture by the buckets. Rotational speeds achieved, for each fluid used in the dynamometer, rapidly increased with increases of the angle of injection until maximizing at 25°. Increasing the injection angle beyond 25° resulted in a gradual decrease in rotational speed, which continued through the maximum angle of 45°.

The average torques calculated for the tests with the dynamometer loaded with corn syrup ranged from 0.0511 in*lb_f (0.00577 N*m) to 0.0790 in*lb_f (0.00893 N*m). Tests with the dynamometer loaded with molasses yielded average torques between 0.0516-0.0798 in*lb_f (0.00583-0.00902 N*m). The average torques for the tests with the dynamometer loaded with resin were lower than both of the other fluids, ranging from 0.0451 in*lb_f (0.00510 N*m) to 0.0604 in*lb_f (0.00682 N*m). The lower measured torque, when the

dynamometer was loaded with resin, was because the resin's dynamic viscosity was much lower than the other two fluids used.

The average shaft power for the tests with the dynamometer loaded with corn syrup ranged from 0.0255-0.0404 hp (19.0-30.1 W). When loaded with molasses, the average power produced ranged from 0.0252 hp (18.8 W) to 0.0402 hp (30.0 W). The average power produced for the tests with the dynamometer loaded with resin ranged from 0.0230-0.0301 hp (17.2-22.4 W). The decrease in power when the dynamometer was loaded with resin was because the resin's dynamic viscosity was much lower than the other two fluids used.

For the tests with the dynamometer loaded with corn syrup, the efficiency of the turbine ranged between 2.99% and 4.72%. The efficiencies from the tests with the dynamometer loaded with molasses also ranged from 2.95% to 4.77%. The tests with the dynamometer loaded with resin yielded a lower band of efficiencies than the previous fluids, ranging from 2.68% to 3.47%. The decrease in efficiency when the dynamometer was loaded with resin was also because the resin's dynamic viscosity was much lower than the other two fluids used.

As the shaft assembly spun, fluid dynamics occurred in the viscous fluid of the drum, which adversely affected the results. The dynamics in the drum impeded the system from quickly reaching steady state conditions; as well as, caused vibrations strong enough to shake the steel container, which produced noise in the data measured by the load cell. The severity of the vibrations was reduced by adding mass to the steel container; however, ultimately the vibrations could not be completely nulled.

Vibrations were highly detrimental to the performance of the turbine. The turbine was attached to the shaft and balanced every time an alteration was made but the system became

unbalanced due to flexure of the turboshaft. Increasing the shaft diameter from 0.236” (6.00 mm) to 0.354” (9.00 mm) increased the shaft’s moment of inertia by a factor of 5.06 and reduced the flexural stress by a factor of 3.38. The reduced flexure of the shaft significantly reduced the vibrations caused by the turbine-shaft assembly. Reduction of the vibrations conserved enough energy sufficient to increase the rotational speed of the turbine by almost 10,000 RPM.

At lower angles of injection, the turbine was largely driven by the reaction from the air changing direction as it passed through the turbine. At higher inclinations, the impulse from the air became the more significant driver of the turbine as the air impinged on the concave surface of the buckets more directly.

Control of the angle of injection, with regards to the tangential plane of the turbine, proved to be somewhat problematic. Comparing the average torque and power produced with 0° Δ to the torque and power with the nozzle directed inboard, -1°Δ yielded a 21.7% reduction in torque and a 23.3% reduction in power when angled inboard. The same comparison was made to aiming the nozzle outboard, 1° Δ. Though there was a 1.29% reduction in torque when the nozzle was aimed outboard, the rotational velocity increased sufficiently that there was no difference in the amount of power produced. Though the potential existed to have a 23.3% difference in power by aiming the nozzle inboard, it is highly unlikely the nozzle was ever aimed this far inboard or outboard unintentionally.

6.2 Recommendations

More power could likely be obtained if the nozzle exit was closer to the turbine. The nozzle was positioned a cautionary distance away from the turbine to prevent mutual damage if an anomaly occurred. The nozzle could indeed be placed closer to the turbine with the

existing design. Ideally, the nozzle exit cross section should be an ellipse to form an inclined nozzle with a shallower half angle in the divergent section. Inclined nozzles have been used with turbines since the late 1800's and are shown on de Laval's patent.[10] However, a different inclined nozzle would be required for each angle of injection.

Vibrations in the dynamometer due to an imbalance of the turbine-shaft system were a problem which was never completely overcome. The imbalance most likely could be reduced by placing the shaft in the chuck of a lathe with the turbine attached to the shaft. The turbine could then be trued to the shaft by removing material from the connective ring with a bit while the lathe's spindle rotated. This method could potentially balance the system better than the method described in section 4.4 and would leave a cleaner surface. This method was not implemented because at the time conceived, there was concern that some of the connective ring had become dangerously thin and this process could potentially compromise the turbine's structural strength.

Though beyond the scope of this research, there is some interest as to how much of a loss in power is attributed to shock formation. The air exiting the nozzle was supersonic and as the flow passed through the buckets, it passed over sharp corners. A shadowgraph or schileren test to analyze the shock structure could be conducted with a model of the slot between two buckets, made from clear polycarbonate. To determine the amount of static pressure lost due to the shocks, it is recommended to construct a model of the slot with pressure ports at the slot inlet and exit. For both models, it is recommended to test at each angle of injection.

To further analyze the power curve it would be necessary to decrease and increase the total pressure applied to the turbine. Decreasing the pressure with the existing experimental

apparatus could be achieved with the addition of a pressure regulator. It is recommended that pressure changes be made incrementally and nozzles be machined for each pressure step to prevent overexpansion. Increasing the pressure without decreasing the mass flow rate may require a different compressed air supply capable of creating much higher pressures. Additional nozzles may be required for the increased total pressures to prevent underexpansion.

Using the line compressed air supply available to the Adaptive Aerostructures Laboratory proved to be somewhat unreliable. Because the compressed air supply was also used by other laboratories and machine shops in Learned Hall, it was often difficult to utilize the maximum pressure the system was capable. A more reliable supply of compressed air could be obtained by using an independent air compressor and reservoir, dedicated only to powering the turbine. Better results could also be obtained with better control of the nozzle inlet pressure with a pressure regulator.

The turntable was not as much a low friction device as initially thought. The turntable also allowed some lateral motion which is believed to have contributed to the noise in the torque measurements. Replacing the turntable with a higher precision bearing system may yield better results.

Better control of the nozzle flow path in the tangential plane of the turbine should produce better results. This could be achieved by integrating a laser beam onto the swing arm. A laser could effectively verify the alignment of the swing arm by aiming it at a target attached to the dynamometer structure. A laser would provide a simple means of checking the alignment of the swing without increasing the mechanical complexity of the apparatus.

Because the dynamometer used was manufactured in house, there is some question as to how accurate the torque measurements were. To verify the results this experiment should be repeated using an Eddy current or other professionally developed dynamometer. Eddy current dynamometers operate by attaching an electric motor to the shaft and varying the load by altering the current. Though such a system requires a gearing system between the shaft and the electric motor, this arrangement avoids fluid dynamics issues that were found to be present in the hydraulic brake dynamometer.

Better real-time data could be gathered by integrating all the instrumentation into a single data acquisition system. By using virtual instrument software, such as National Instruments Labview, the complexity of the data collection system could be reduced as well as increase the fidelity of the data.

7.0 References

[1] Neilson, R. M., *The Steam Turbine*, 3rd ed., Longmans, Green, And Co., New York, 1904.

[2] Giampaolo, T., *The Gas Turbine Handbook: Principles and Practices*, 2nd ed., Fairmont Press, Lilburn, GA, 2003.

[3] Singfield, P., "Low Pressure High Superheat Axial Flow Impulse Steam Turbine Wheel," Xaibe, Belize, 2005.

[4] Anon., "Critical Rotating Components," *TECT Power*, Cleveland, Oh. 2010.

[5] Hefazi, H., Kaups, K., Schmitz, A., and Pearson, L., "A Computational Study of Supersonic Impulse Cascade Performance," *AIAA 34th Aerospace Sciences Meeting and Exhibit*, Reno, 1996.

[6] French, L. G., *Steam Turbines*, The Technical Press, Brattleboro, VT, 1907.

[7] Moyer, J. A., *The Steam Turbine*, Chapman & Hall, London, 1908.

[8] Thakker, A., Sheahan, C., Frawley, and P., Khaleeq, H.B., "Innovative Manufacture of Impulse Turbine Blades for Wave Energy Power Conversion," *Proceedings of The Institution of Mechanical Engineers, Part B: Journal of Engineering Manufacture*, vol. 216, No. 7, 2002, pp. 1053-1059.

[9] Anon., "Rockets In Ancienct Times (100 B.C. To 17th Century)," *Marshall Space Flight Center History Office*, Huntsville, AL, 2010.

[10] de Laval, C. G., Stockholm, U.S. Patent for "Steam-turbine," No. 522,066, Issued 26 Jun. 1894.

[11] Anderson, J. D., *Fundamentals of Aerodynamics*, 3rd ed., McGraw-Hill, Boston, 2001.

[12] Lee, K. T., "An Analytical and Experimental Investigation of Potential Mechanical Work Extraction from Supersonic Jet Flow on High Speed Mini Turbines," M.S. Thesis, Aerospace Engineering Dept., University of Kansas, Lawrence, KS, 2009.

[13] Curtis, C. G., New York, U.S. Patent for "Elastic-Fluid Turbine," No. 566,967, Issued 1 Sept. 1896.

[14] Curtis, C. G., New York, U.S. Patent for "Elastic-Fluid Turbine," No. 591,822, Issued 19 Oct. 1897.

[15] Curtis, C. G., New York, U.S. Patent for "Apparatus For Generating Mechanical Power," No. 635,919, Issued 31 Oct. 1899.

[16] de Laval, C. G., *Centrifugal Pumping Machinery*, McGraw-Hill, London, 1912.

[17] Zoelly, H., Zurich, U.S. Patent for "Turbine Wheel," No. 648,158, Issued 24 Apr. 1900.

[18] Zoelly, H., Zurich, U.S. Patent for "Explosion Gas-Turbine," No. 1,089,892, Issued 10 Mar. 1914.

[19] Zoelly, H., Zurich, U.S. Patent for "Steam or Gas Turbine," No. 705,890, Issued 29 Jul. 1902.

[20] Rateau, A., Paris, U.S. Patent for "Multicellular Turbine," No. 748,216, Issued 29 Dec. 1903.

[21] Lemale, C., Paris, U.S. Patent for "Self-Propelling Torpedo," No. 1,078,687, Issued 30 Dec. 1913.

[22] Lemale, C., Paris, U.S. Patent for "Turbine," No. 919,895, Issued 27 Apr. 1909.

[23] Lemale, C., Alfort, France, U.S. Patent for "Continuous Internal-Combustion Turbo-Motor," No. 789,554, 9 May, 1905.

[24] Goldman, L. J., "Analytical Investigation of Supersonic Turbomachinery Blading II - Analysis of Impulse Turbine-Blade Sections," NASA-TN-D-4422,1968.

[25] Millbrooke, A., *Aviation History*, Jeppesen Sanderson, Englewood, CO, 1999.

[26] Whittle, F., Trumpington, England, U.S. Patent for "Propulsion of Aircraft And Gas Turbines," No. 2,168726, Issued 8 Aug. 1939.

[27] Flack, R. D., *Fundamentals of Jet Propulsion*, Cambridge University Press, New York, 2005.

[28] Peirs, J., Verplaetsen, F., and Reynaerts, D., "A Micro Gas Turbine Unit for Electric Power Generation: Design and Testing of Turbine and Compressor," *9th International Conference on New Actuators*, Bremen, Germany, 2004.

[29] Krähenbühl, D., Zwyssig, C., Hörler, H., and Kolar, J.W., "Design Considerations and Experimental Results of a 60 W Compressed-Air-To-Electric-Power System," *2008 IEEE/ASME International Conference on Mechatronics and Embedded Systems and Applications*, Beijing, 2008, pp. 375-380

[30] Holt, D. B., and Kozak, J.D., "Design, Fabrication, and Testing of a Miniature Impulse Turbine Driven by Compressed Gas," *40th AIAA/ASME/SAE/ASEE Joint Propulsion Conference and Exhibit*, Fort Lauderdale, FL, 2004.

[31] Sutton, G. P., Biblarz, O., *Rocket Propulsion Elements*, 7th ed., John Wiley & Sons Inc., New York, 2001.

[32] Anon., "Discussion of Viscous Properties of Commercial Resin," Champagin, Illinois, Tower Hobbies, 12 Jul, 2010.

[33] Brown, P.P., Lawler, D.F., “Sphere Drag And Settling Velocity Revisited,” *Journal of Environmental Engineering*, vol. 129, Issue 3, 2003.

[34] S. Farokhi, *Aircraft Propulsion*, John Wiley & Sons Inc., Hoboken, NJ, 2009.

[35] Hibbeler, R.C., *Mechanics of Materials*, 5th ed., Pearson Education, Inc., Upper Saddle River, NJ, 2003.

[36] Anon., National Weather Service Report for Lawrence, KS, 3 July, 2010.

[37] Anon., "All Stainless Steel Digital Pressure Gauge DPG6000L Series," Omega Engineering Inc., Stamford, CT.

[38] Anon., "User's Guide DPG6000 Pressure Gauges," Omega Engineering Inc., Stamford, CT.

[39] Anon., "Pocket Laser Tach 200 (PLT200)," Monarch Instrument, Amherst, NH, 2006.

[40] Anon., "IRS - Infrared Optical Sensor," Monarch Instrument, Amherst, NH, 2004.

[41] Anon., "Nova-Strobe DA Plus and Nova-Strobe DB Plus," Monarch Instrument, Amherst, NH, 2002.

[42] Anon., "2519-100 Series Load Cell," Instron, Canton, MA, 2003.

[43] Anon., "A New Impulse Steam Turbine," *The Engineer*, London, 1909.

[44] Hodgkinson, F., Wilkinsburg, PA, U.S. Patent for "Impulse-Wheel For Fluid-Pressure Turbines," No. 763,397, Issued 28 Jun.1904.

[45] Nussbaumer, W.A., Milwaukee, U.S. Patent for "Elastic-Fluid Turbine," No. 849,420, Issued 4 Apr. 1907.

[46] Peirs, J., Reynaerts, D., and Verplaetsen, F., "Development of An Axial Microturbine For A Portable Gas Turbine Generator," *Journal of Micromechanics and Microengineering*, vol. 13, No. 4, 2003, pp. S190-S195.

[47] Wirt, H. L., Schenectady, NY, U.S. Patent for "Elastic-Fluid Turbine," No. 1,490,755, Issued 15, Apr. 1924.

[48] Krähenbühl, D., Zwyssig, C., Hörler, H., and Kolar, J.W., "Theoretical And Experimental Results Of A Mesoscale Electric Power Generation System From Pressurized Gas Flow," *Journal of Micromechanics And Micro Engineering*, vol. 19, No. 9, 2004.

[49] Steinmetz, C., "The Steam Turbine," *Cassier's Magazine*, vol 32, 1907.

[50] Anon., "The Evolution Of The Tangential Impulse Turbine," *Engineering*, vol. 116, 1923, pp 163-164.

[51] Jeong, E., Lee, H.G., Park, P.G., and Kim, J., "Tip Clearance Effect On The Performance Of A Shrouded Supersonic Impusle Turbine," *Journal of Propulsion And* Power, Vol. 24, No. 6, 2008, pp. 1295-1300.

[52] Giesecke, F.E., Mictchell, A., Spencer, H.C., Hill, I.L., Dygdon, J.T., Novak, J.E., Lockhart, S., *Tehnical Drawing*, 13th ed., Pearson Education, Inc., Upper Saddle River, NJ, 2009.

Appendix A: Processed Torque Data

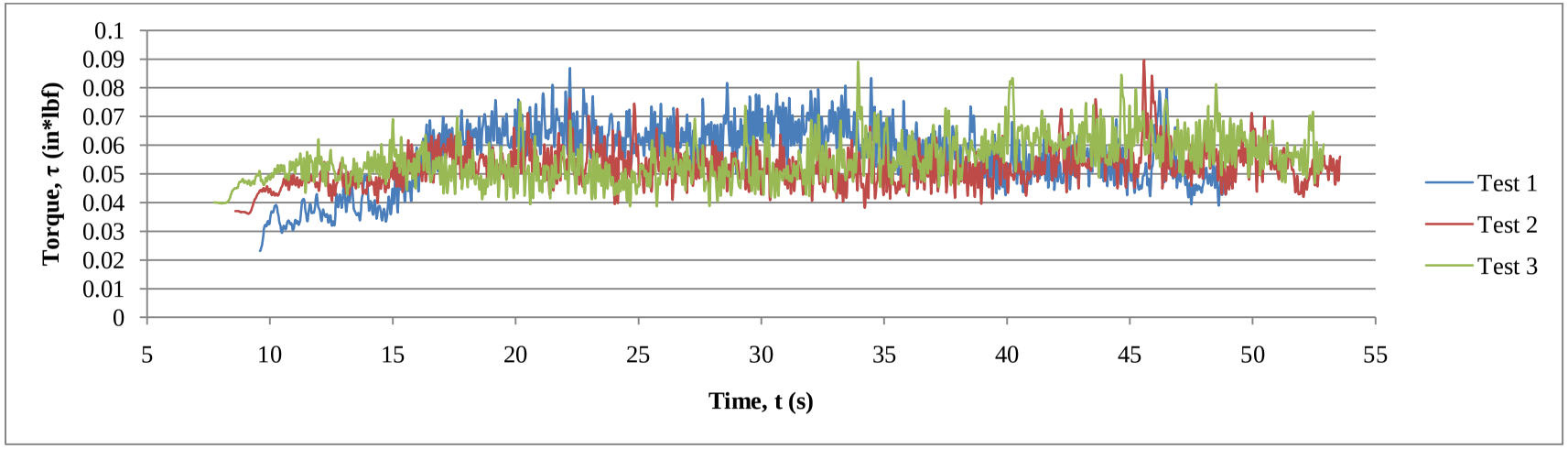

Figure 57: Processed Torque Data, Dynamometer Loaded With Corn Syrup, 15° β

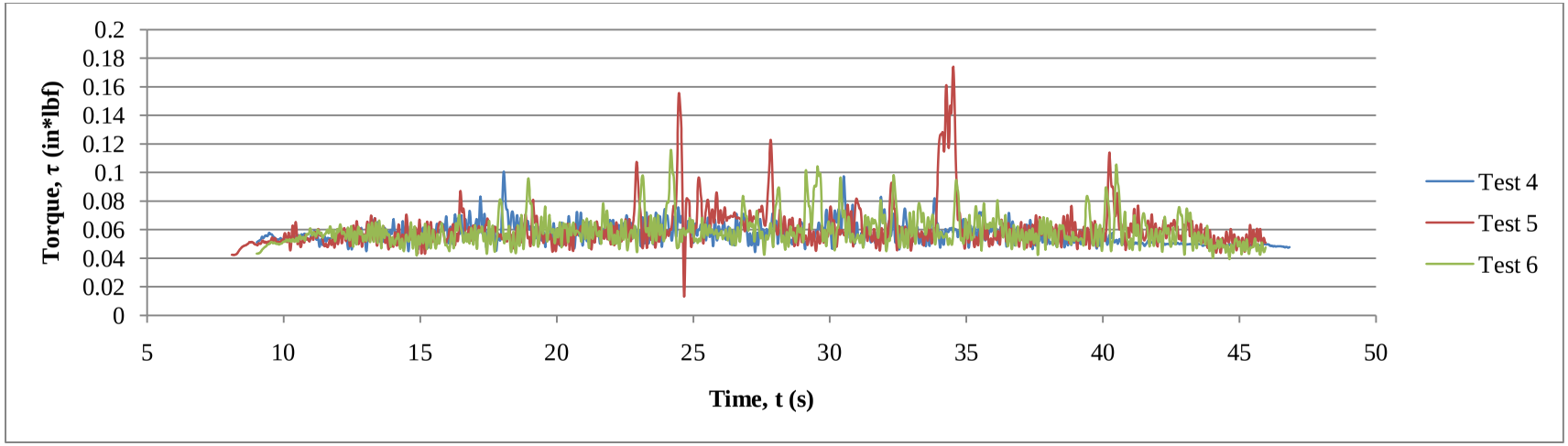

Figure 58: Processed Torque Data, Dynamometer Loaded With Corn Syrup, 20° β

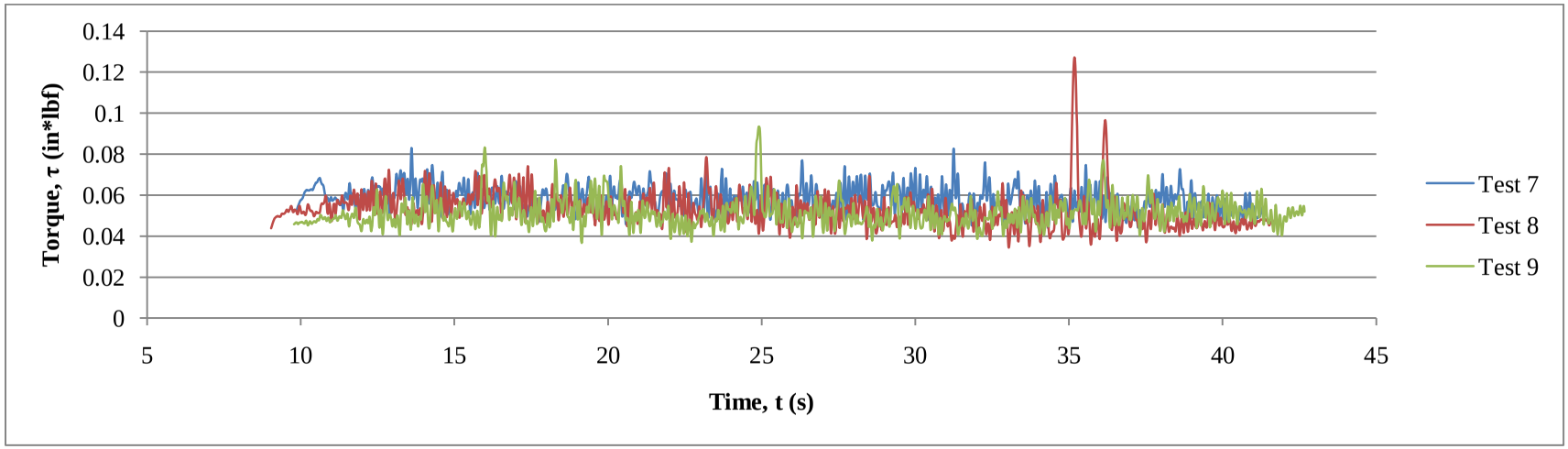

Figure 59: Processed Torque Data, Dynamometer Loaded With Corn Syrup, 25° β

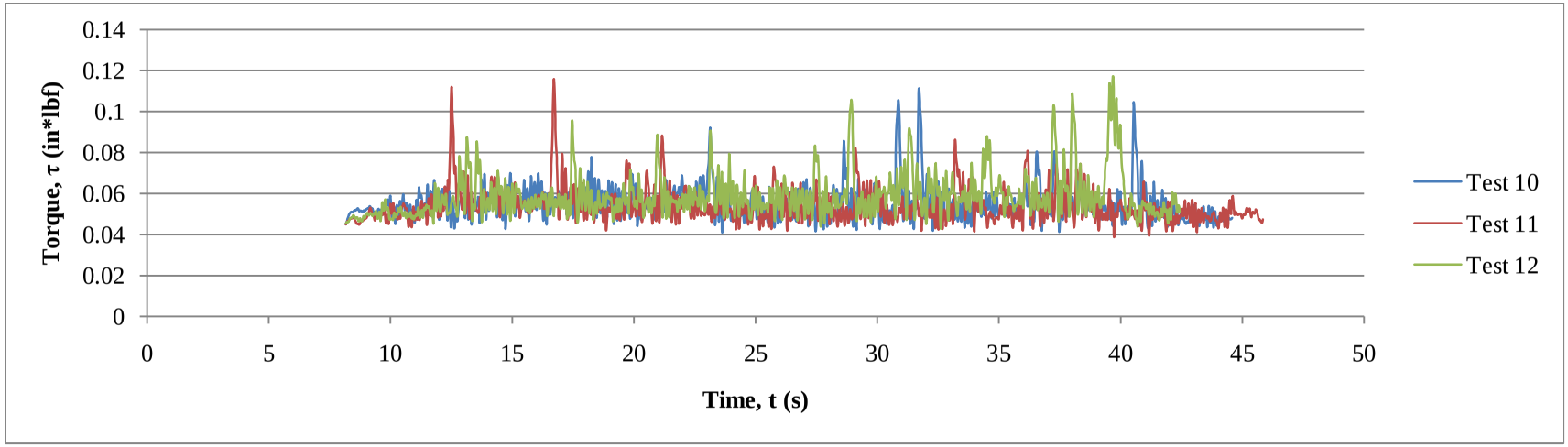

Figure 60: Processed Torque Data, Dynamometer Loaded With Corn Syrup, 30° β

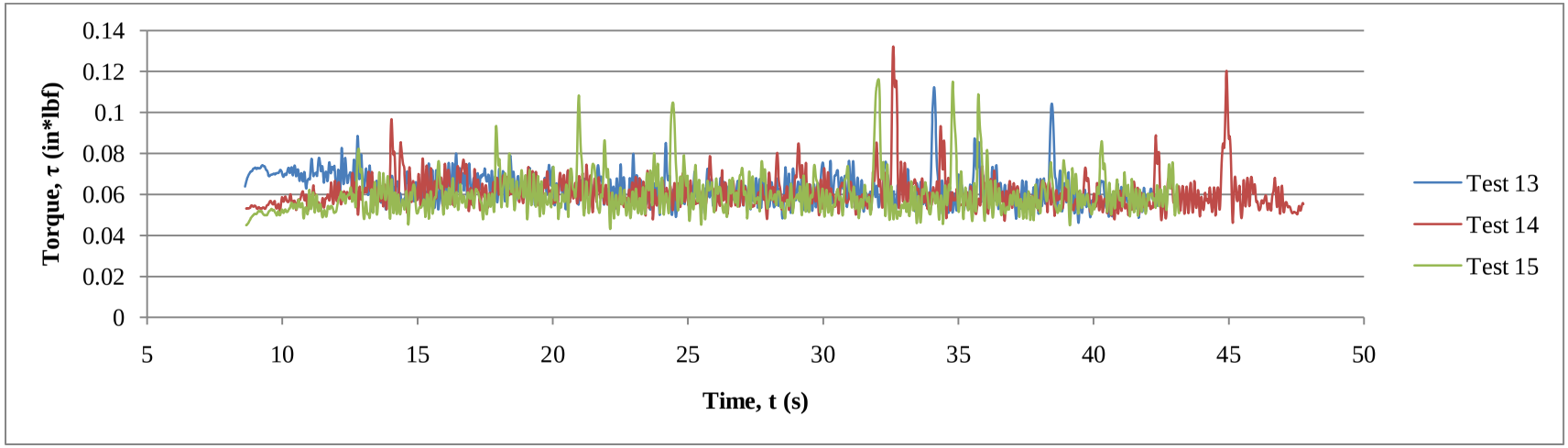

Figure 61: Processed Torque Data, Dynamometer Loaded With Corn Syrup, 35° β

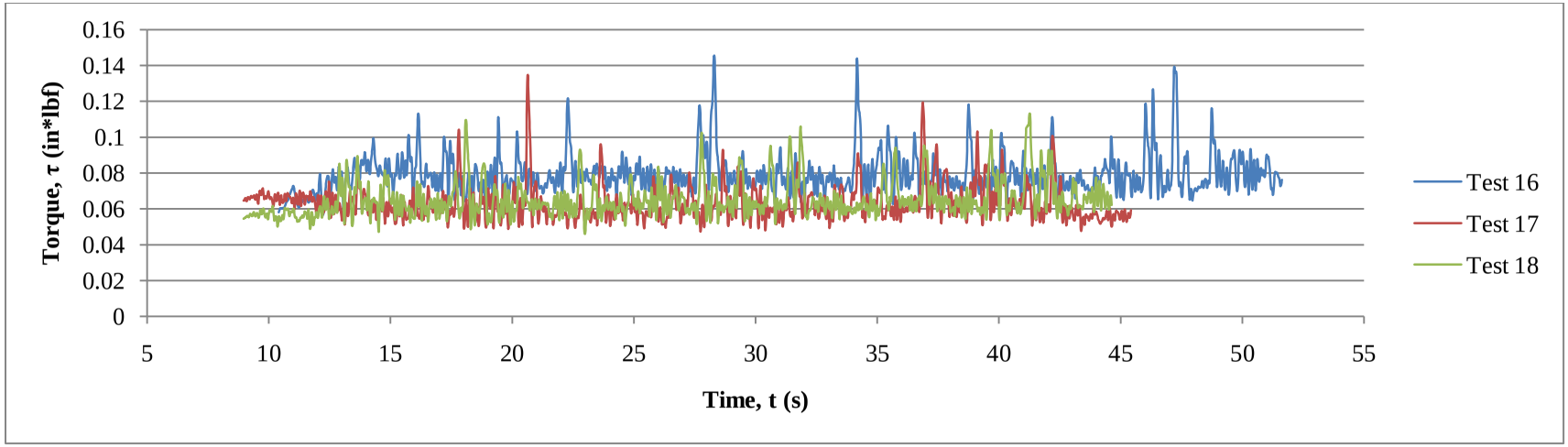

Figure 62: Processed Torque Data, Dynamometer Loaded With Corn Syrup, 40° β

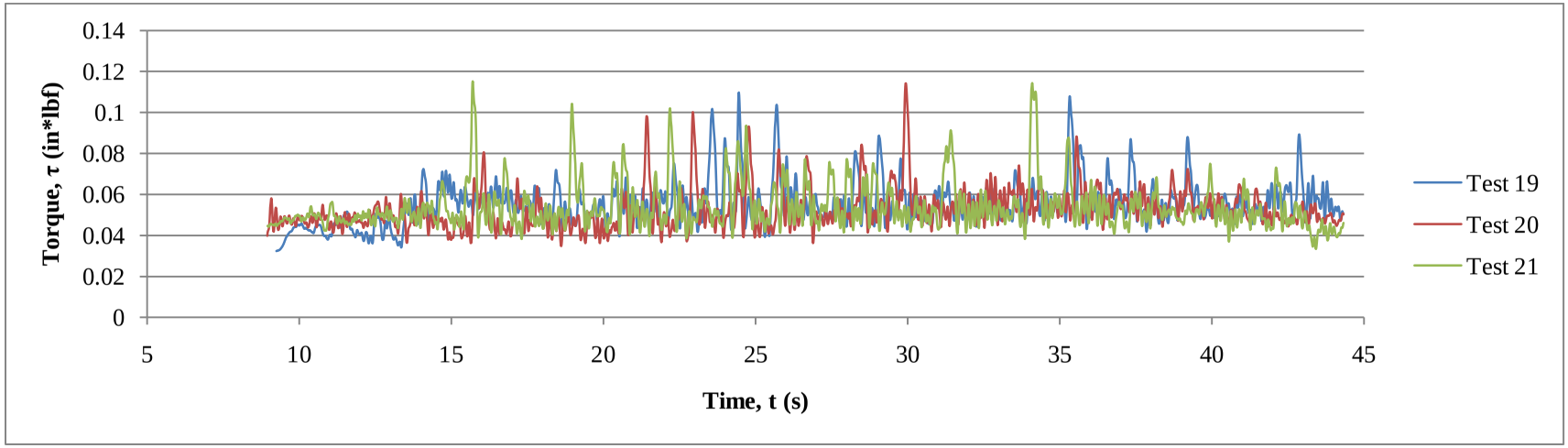

Figure 63: Processed Torque Data, Dynamometer Loaded With Corn Syrup, 45° β

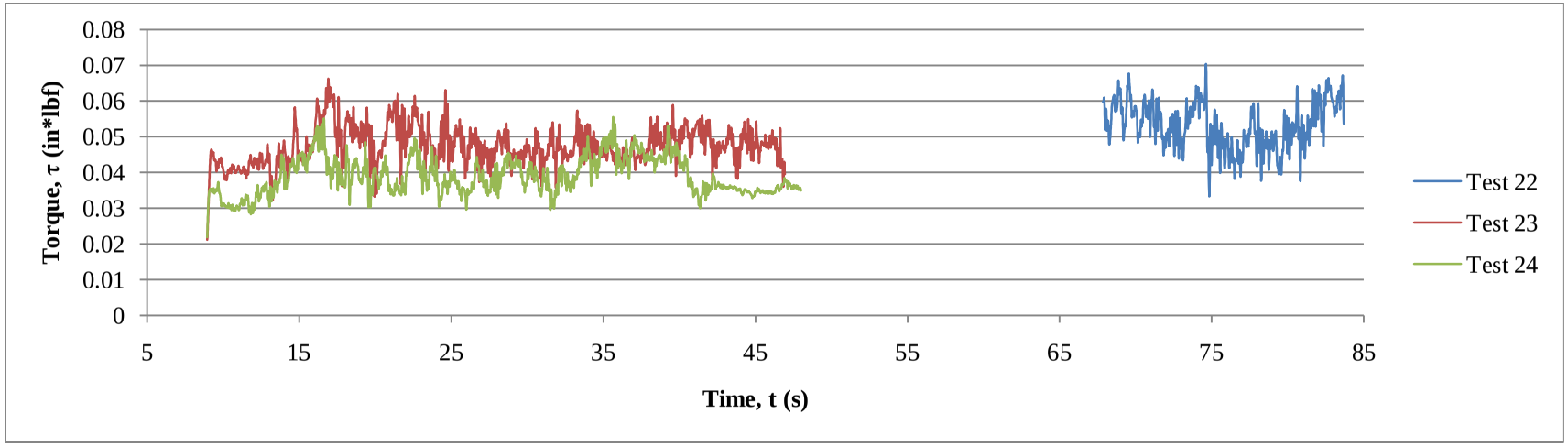

Figure 64: Processed Torque Data, Dynamometer Loaded With Molasses, 15° β

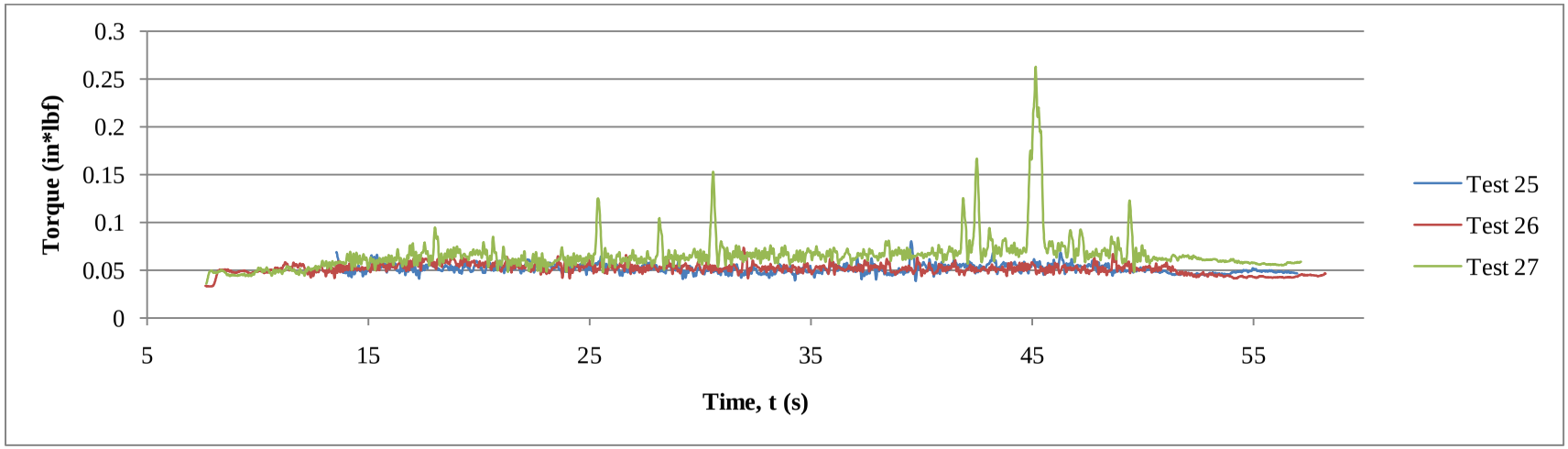

Figure 65: Processed Torque Data, Dynamometer Loaded With Molasses, 20° β

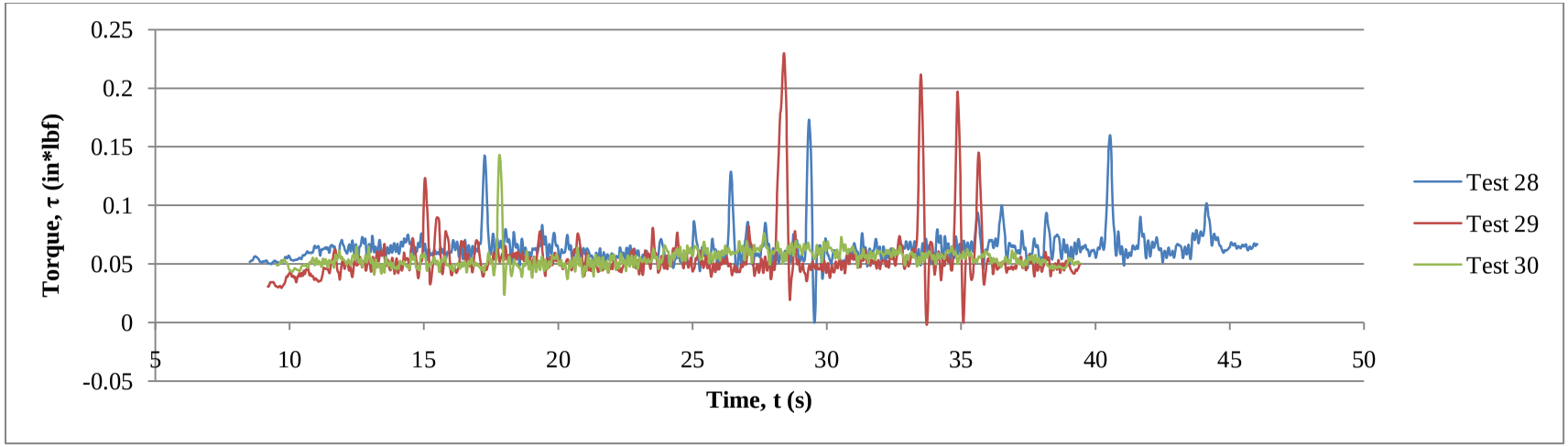

Figure 66: Processed Torque Data, Dynamometer Loaded With Molasses, 25° β

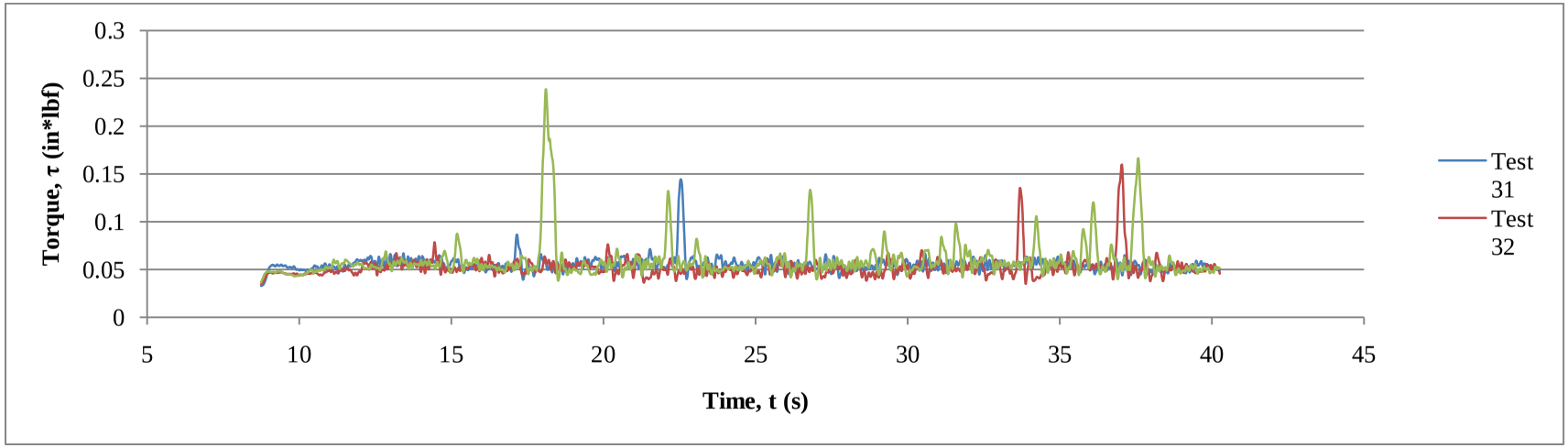

Figure 67: Processed Torque Data, Dynamometer Loaded With Molasses, 30° β

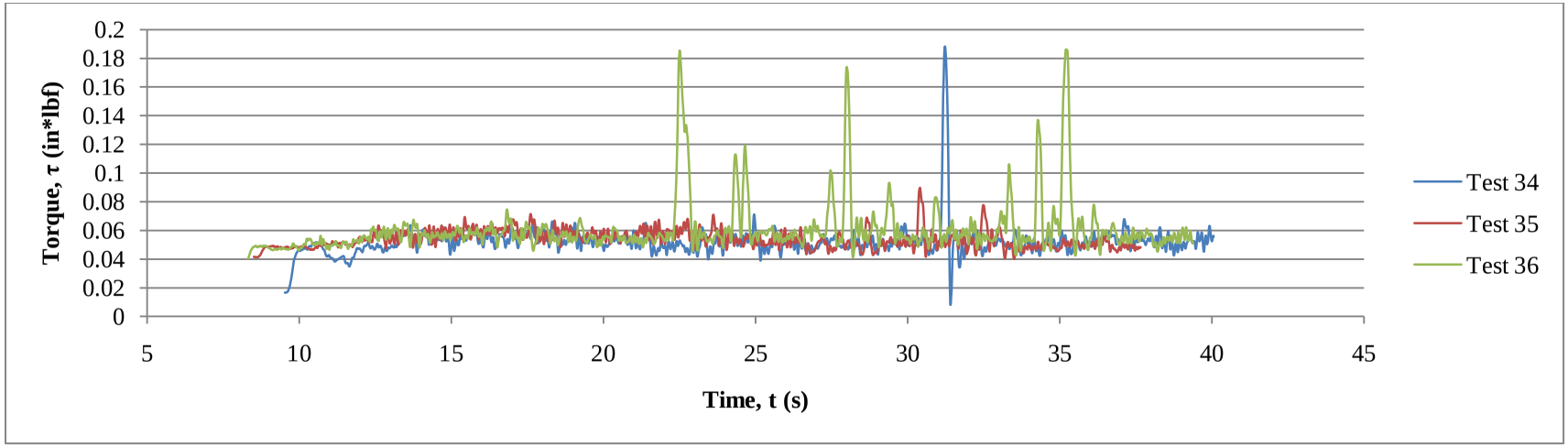

Figure 68: Processed Torque Data, Dynamometer Loaded With Molasses, 35° β

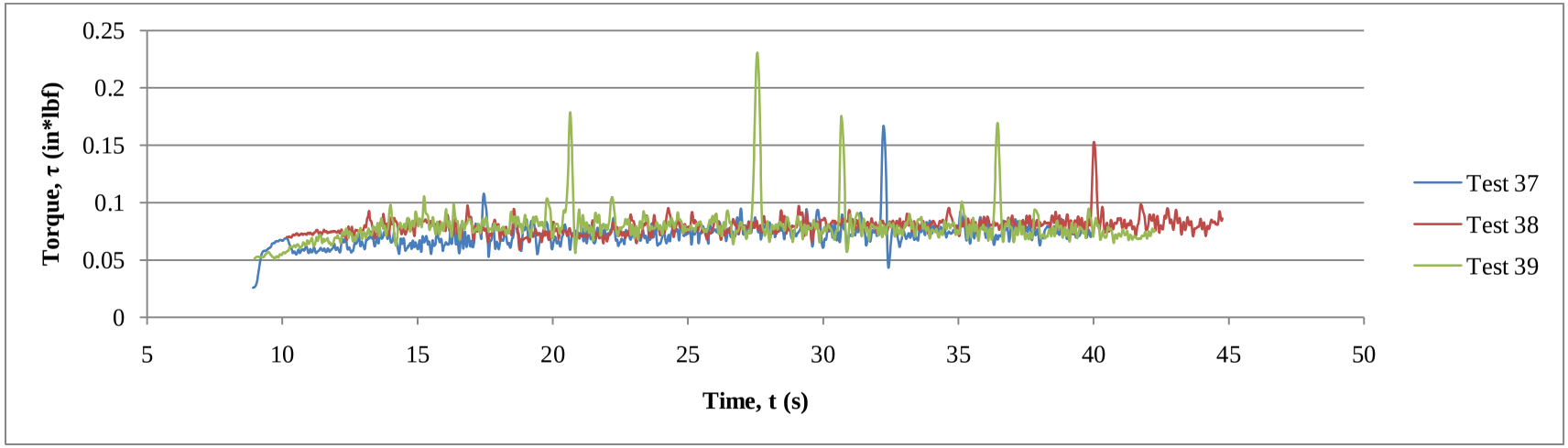

Figure 69: Processed Torque Data, Dynamometer Loaded With Molasses, 40° β

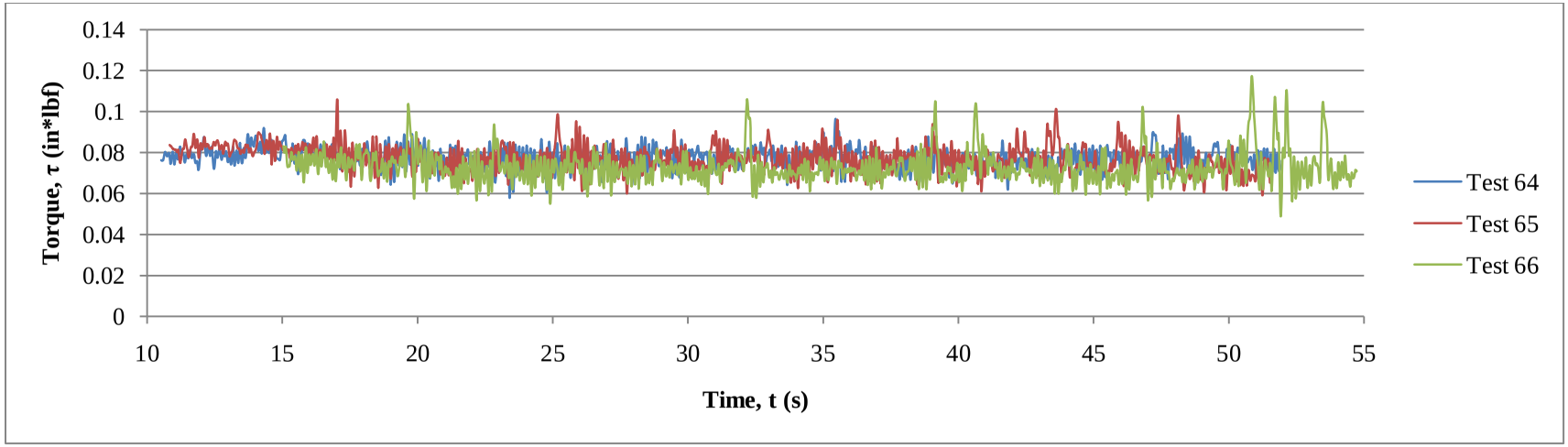

Figure 70: Processed Torque Data, Dynamometer Loaded With Molasses, 45° β

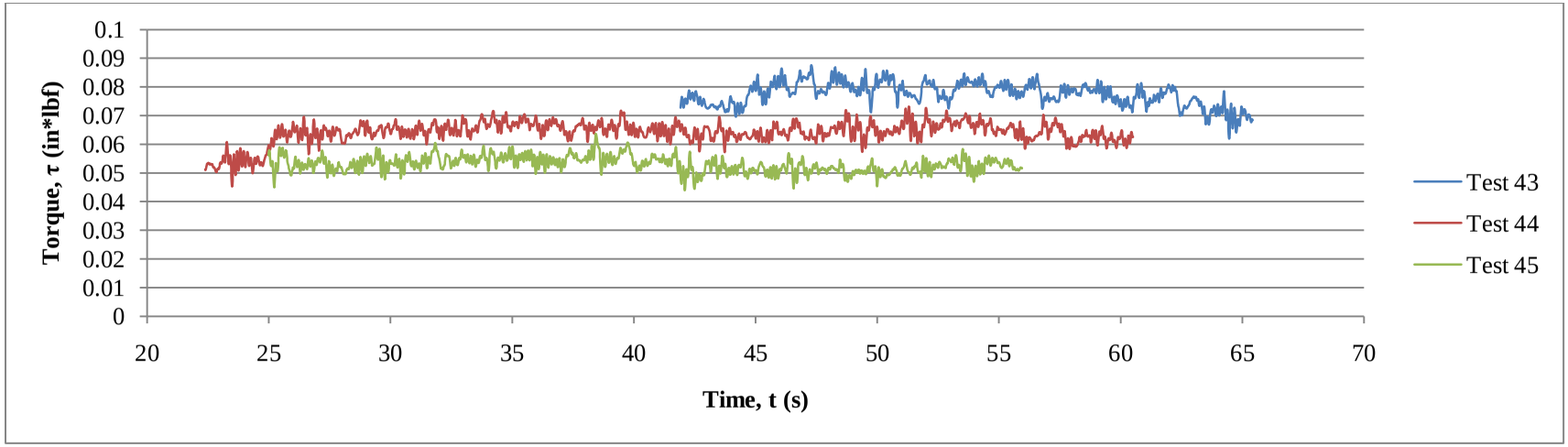

Figure 71: Processed Torque Data, Dynamometer Loaded With Resin, 15° β

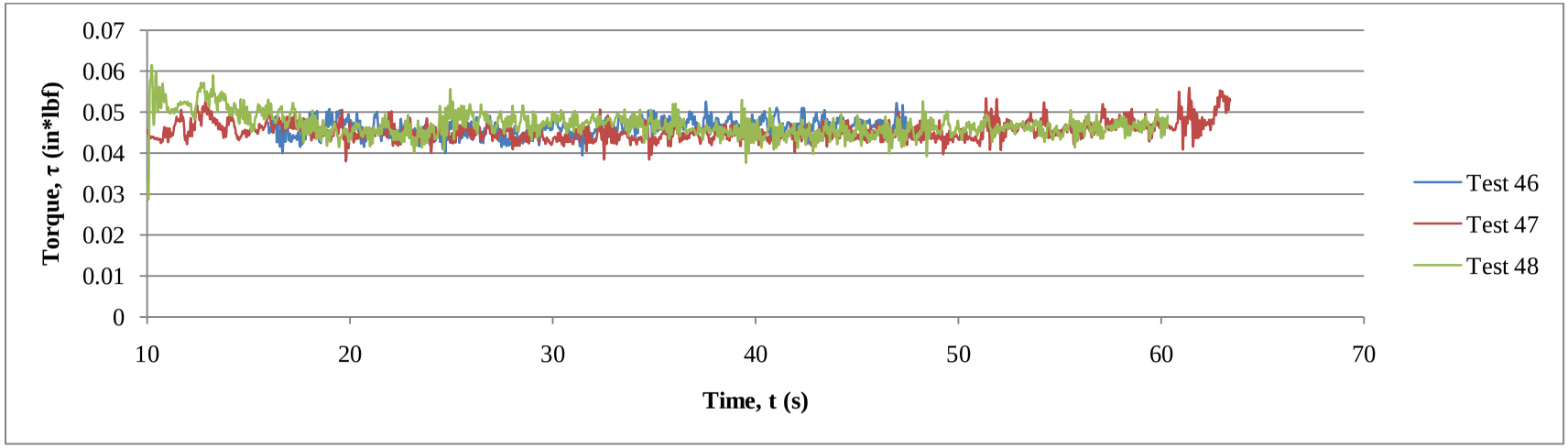

Figure 72: Processed Torque Data, Dynamometer Loaded With Resin, 20° β

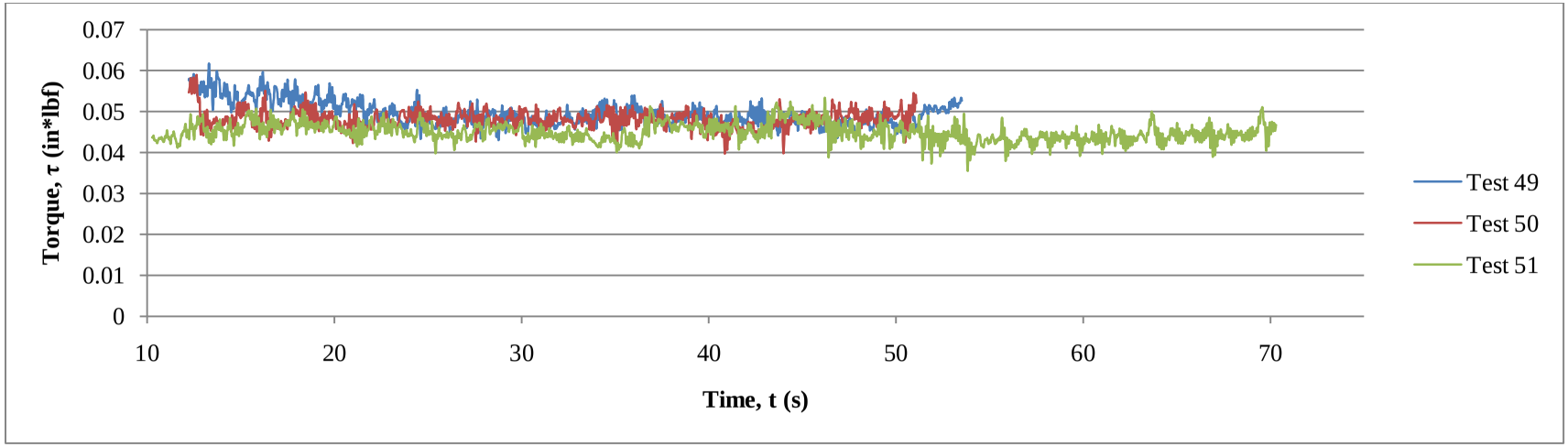

Figure 73: Processed Torque Data, Dynamometer Loaded With Resin, 25° β

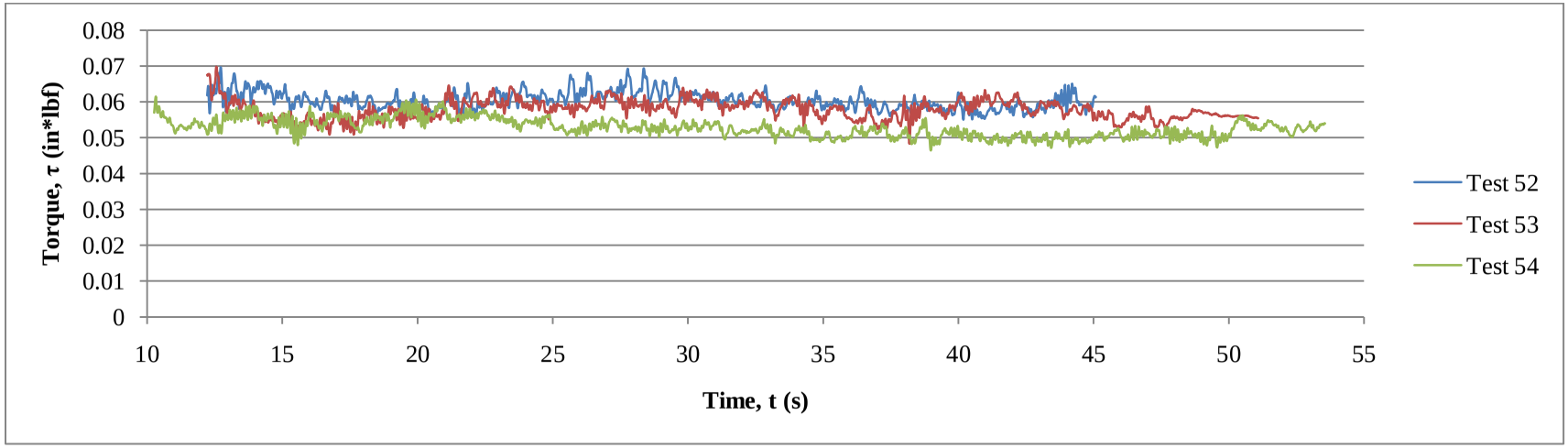

Figure 74: Processed Torque Data, Dynamometer Loaded With Resin, 30° β

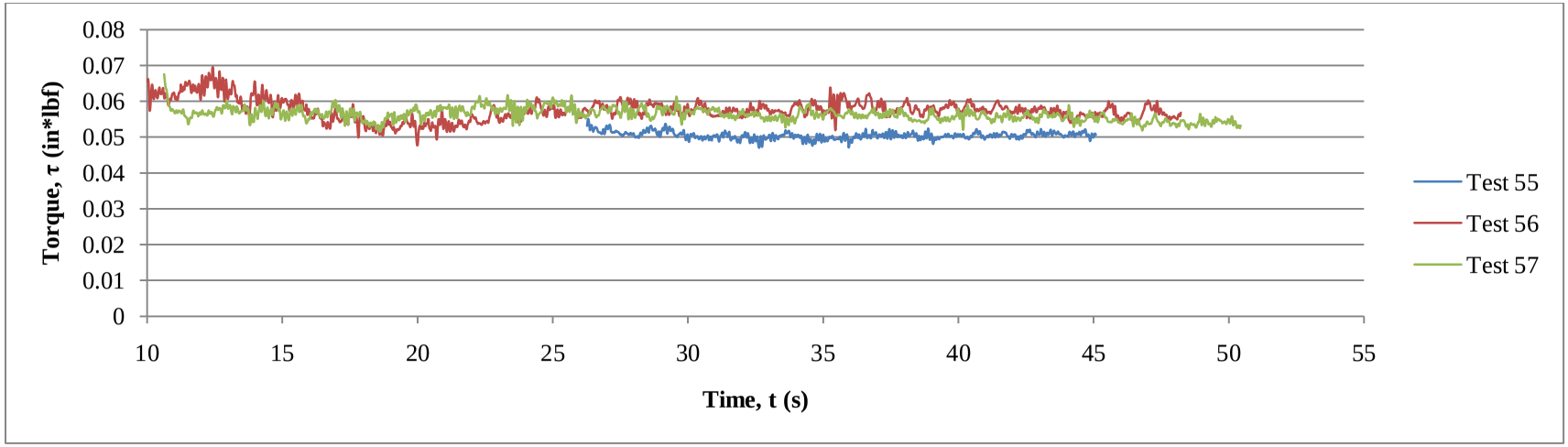

Figure 75: Processed Torque Data, Dynamometer Loaded With Resin, 35° β

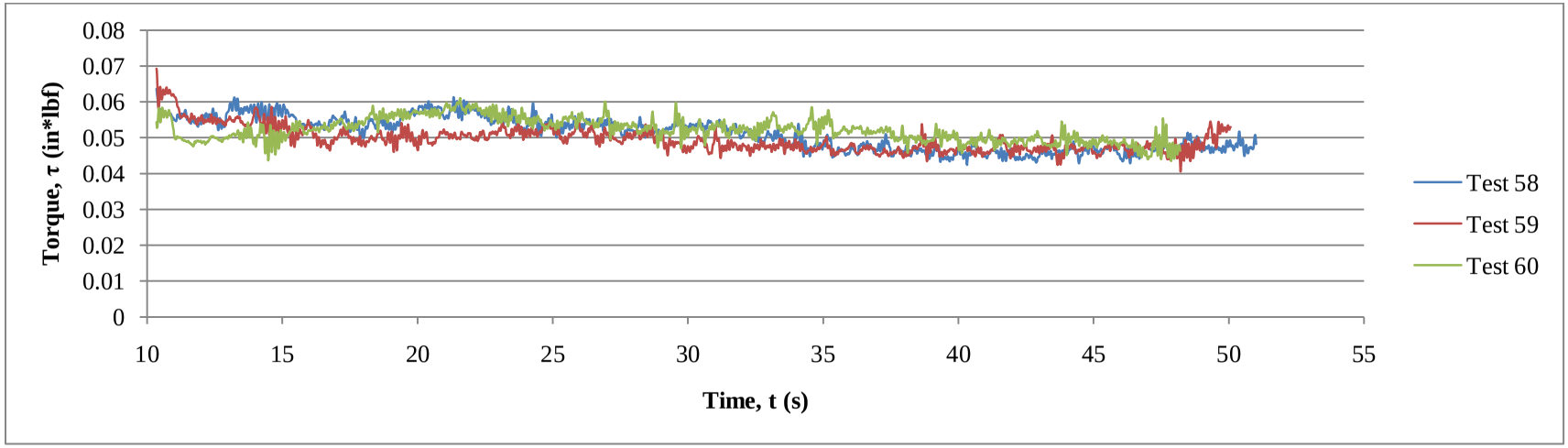

Figure 76: Processed Torque Data, Dynamometer Loaded With Resin, 40° β

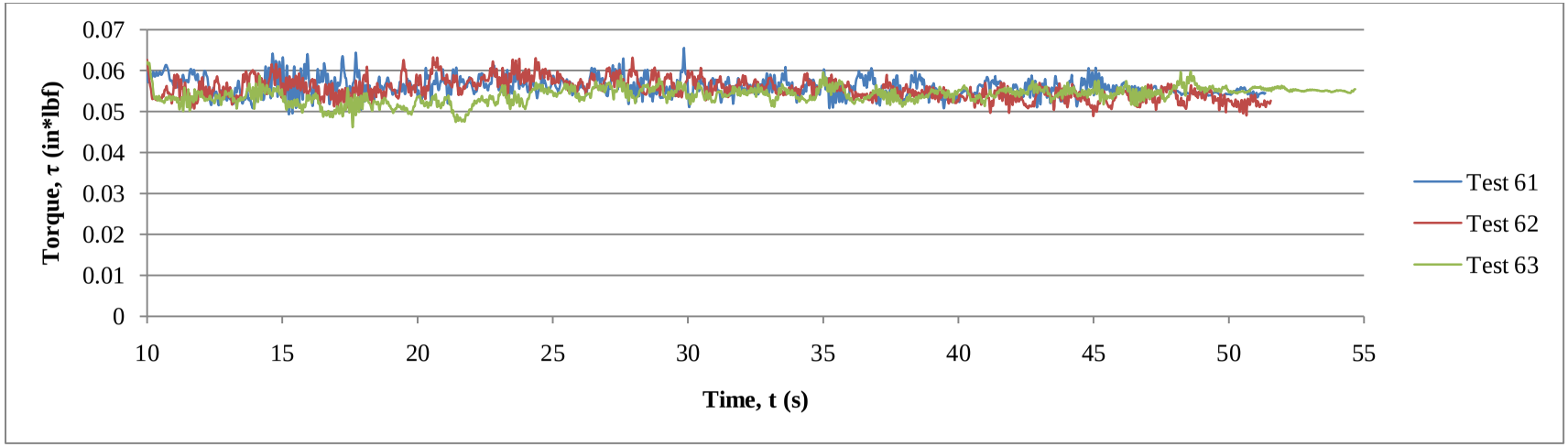

Figure 77: Processed Torque Data, Dynamometer Loaded With Resin, 45° β

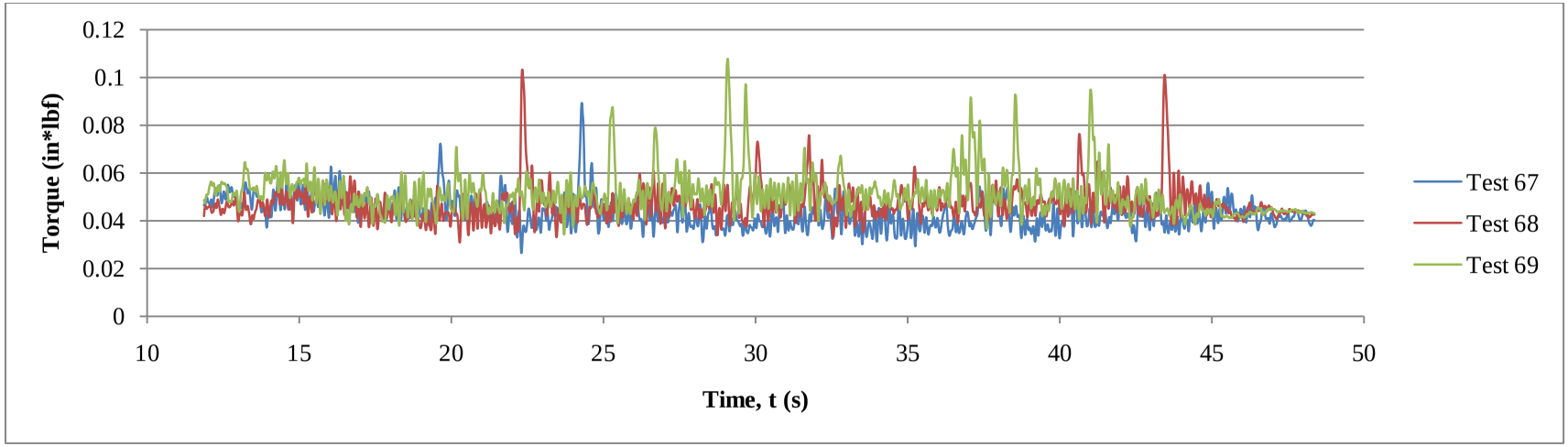

Figure 78: Processed Torque Data, Dynamometer Loaded With Molasses, 35° β, -1°Δ

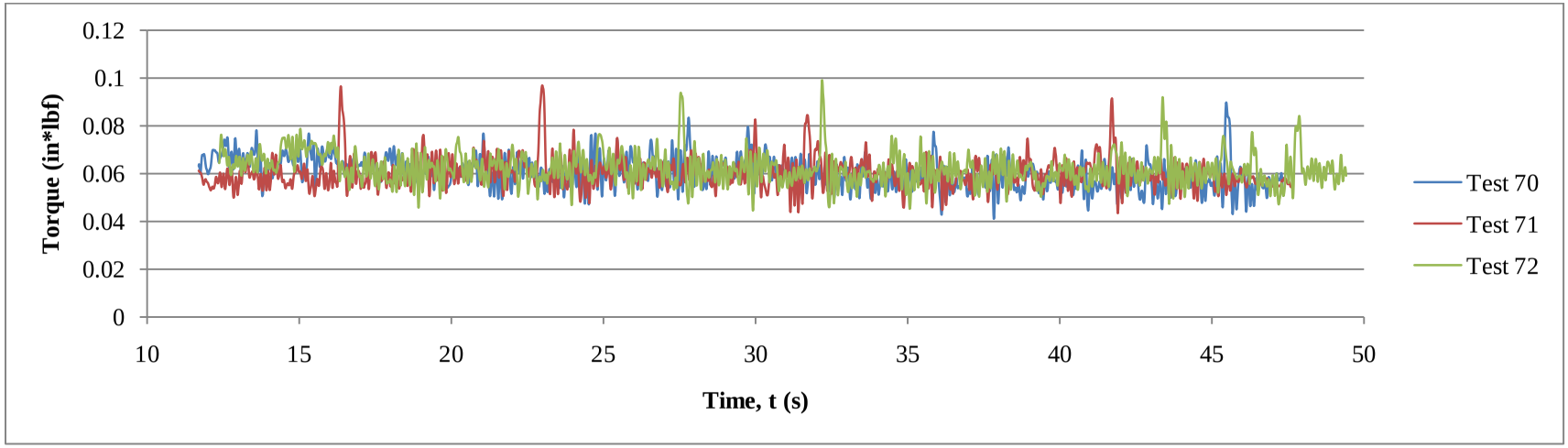

Figure 79: Processed Torque Data, Dynamometer Loaded With Molasses, 35° β, 0°Δ

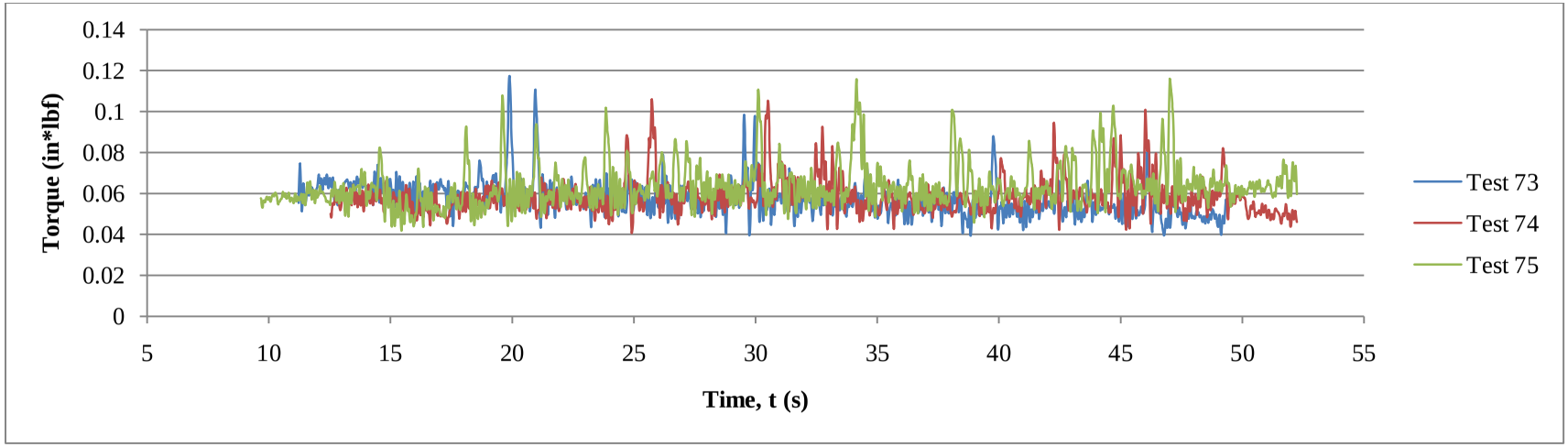

Figure 80: Processed Torque Data, Dynamometer Loaded With Molasses, 35° β, 1°Δ

Appendix B: Measured Data & Calculated Values

Table 6: Measured Data & Calculate Values, Dynamometer Loaded With Corn Syrup

Test #	β (deg)	p_o (psia)	RPM	Exit Mach #	T* (°R)	ρ* (lbm/ft^3)	a* (ft/s)	m-dot (slug/s)	$P_{air\ KE}$ (hp)	ω (rad/s)	Mid Bucket Mach #	τ_{Avg} ($in*lb_f$)	P_{Shaft} (hp)	η
1	15	79	27700	1.74	716	0.00489	1312	0.000547	0.855	2901	0.269	0.0568	0.0250	2.92
2	15	78	28000	1.73	714	0.00485	1309	0.000541	0.843	2932	0.272	0.0512	0.0227	2.70
3	15	78	27900	1.73	714	0.00485	1309	0.000541	0.843	2922	0.271	0.0542	0.0240	2.85
4	20	78	31500	1.73	714	0.00485	1309	0.000541	0.843	3299	0.306	0.0566	0.0283	3.36
5	20	79	31700	1.74	716	0.00489	1312	0.000547	0.855	3320	0.308	0.0610	0.0307	3.59
6	20	78	31900	1.73	714	0.00485	1309	0.000541	0.843	3341	0.310	0.0589	0.0298	3.54
7	25	80	32800	1.75	719	0.00493	1314	0.000553	0.867	3435	0.319	0.0578	0.0301	3.47
8	25	78	32700	1.73	714	0.00485	1309	0.000541	0.843	3424	0.318	0.0525	0.0272	3.23
9	25	80	33100	1.75	719	0.00493	1314	0.000553	0.867	3466	0.322	0.0511	0.0268	3.09
10	30	78	32600	1.73	714	0.00485	1309	0.000541	0.843	3414	0.317	0.0553	0.0286	3.39
11	30	79	33000	1.74	716	0.00489	1312	0.000547	0.855	3456	0.321	0.0550	0.0288	3.37
12	30	78	32600	1.73	714	0.00485	1309	0.000541	0.843	3414	0.317	0.0581	0.0300	3.56
13	35	80	32800	1.75	719	0.00493	1314	0.000553	0.867	3435	0.319	0.0624	0.0325	3.74
14	35	79	32500	1.74	716	0.00489	1312	0.000547	0.855	3403	0.316	0.0607	0.0313	3.66
15	35	79	32800	1.74	716	0.00489	1312	0.000547	0.855	3435	0.319	0.0590	0.0307	3.59
16	40	79	32200	1.74	716	0.00489	1312	0.000547	0.855	3372	0.313	0.0790	0.0404	4.72
17	40	78	31800	1.73	714	0.00485	1309	0.000541	0.843	3330	0.309	0.0643	0.0325	3.85
18	40	79	32200	1.74	716	0.00489	1312	0.000547	0.855	3372	0.313	0.0638	0.0326	3.81
19	45	79	31400	1.74	716	0.00489	1312	0.000547	0.855	3288	0.305	0.0555	0.0277	3.24
20	45	79	31300	1.74	716	0.00489	1312	0.000547	0.855	3278	0.304	0.0514	0.0255	2.99
21	45	79	31600	1.74	716	0.00489	1312	0.000547	0.855	3309	0.307	0.0538	0.0270	3.16

Table 7: Measured Data & Calculate Values, Dynamometer Loaded With Molasses

Test #	β (deg)	p_o (psia)	RPM	Exit Mach #	T* (°R)	ρ* (lbm/ft^3)	a* (ft/s)	m-dot (slug/s)	$P_{air\ KE}$ (hp)	ω (rad/s)	Mid Bucket Mach #	τ_{Avg} (in*lb_f)	P_{Shaft} (hp)	η
22	15	79	23000	1.74	716	0.00489	1312	0.000547	0.855	2409	0.224	0.0560	0.0204	2.39
23	15	79	24100	1.74	716	0.00489	1312	0.000547	0.855	2524	0.234	0.0473	0.0181	2.11
24	15	78	24200	1.73	714	0.00485	1309	0.000541	0.843	2534	0.235	0.0390	0.0150	1.78
25	20	79	30800	1.74	716	0.00489	1312	0.000547	0.855	3225	0.300	0.0516	0.0252	2.95
26	20	78	31300	1.73	714	0.00485	1309	0.000541	0.843	3278	0.304	0.0520	0.0258	3.06
27	20	78	31000	1.73	714	0.00485	1309	0.000541	0.843	3246	0.301	0.0671	0.0330	3.91
28	25	78	32700	1.73	714	0.00485	1309	0.000541	0.843	3424	0.318	0.0630	0.0327	3.88
29	25	78	32800	1.73	714	0.00485	1309	0.000541	0.843	3435	0.319	0.0553	0.0288	3.42
30	25	78	32600	1.73	714	0.00485	1309	0.000541	0.843	3414	0.317	0.0541	0.0280	3.32
31	30	78	32300	1.73	714	0.00485	1309	0.000541	0.843	3382	0.314	0.0554	0.0284	3.37
32	30	78	32400	1.73	714	0.00485	1309	0.000541	0.843	3393	0.315	0.0528	0.0271	3.22
33	30	79	32500	1.74	716	0.00489	1312	0.000547	0.855	3403	0.316	0.0593	0.0306	3.58
34	35	79	32000	1.74	716	0.00489	1312	0.000547	0.855	3351	0.311	0.0528	0.0268	3.13
35	35	78	32000	1.73	714	0.00485	1309	0.000541	0.843	3351	0.311	0.0546	0.0277	3.29
36	35	78	32000	1.73	714	0.00485	1309	0.000541	0.843	3351	0.311	0.0605	0.0307	3.65
37	40	79	32000	1.74	716	0.00489	1312	0.000547	0.855	3351	0.311	0.0726	0.0368	4.31
38	40	78	31700	1.73	714	0.00485	1309	0.000541	0.843	3320	0.308	0.0798	0.0402	4.77
39	40	78	31700	1.73	714	0.00485	1309	0.000541	0.843	3320	0.308	0.0786	0.0395	4.69
64	45	73	29700	1.69	700	0.00462	1297	0.000511	0.781	3110	0.289	0.0770	0.0363	4.65
65	45	73	29700	1.69	700	0.00462	1297	0.000511	0.781	3110	0.289	0.0761	0.0358	4.59
66	45	73	29700	1.69	700	0.00462	1297	0.000511	0.781	3110	0.289	0.0730	0.0344	4.40

Table 8: Measured Data & Calculate Values, Dynamometer Loaded With Resin

Test #	β (deg)	p_o (psia)	RPM	Exit Mach #	T* (°R)	ρ* (lbm/ft^3)	a* (ft/s)	m-dot (slug/s)	$P_{air\ KE}$ (hp)	ω (rad/s)	Mid Bucket Mach #	τ_{Avg} (in*lb_f)	P_{Shaft} (hp)	η
43	15	79	29500	1.74	716	0.00489	1312	0.000547	0.855	3089	0.287	0.0775	0.0363	4.24
44	15	78	30100	1.73	714	0.00485	1309	0.000541	0.843	3152	0.293	0.0639	0.0305	3.62
45	15	78	29700	1.73	714	0.00485	1309	0.000541	0.843	3110	0.289	0.0533	0.0251	2.98
46	20	80	31700	1.75	719	0.00493	1314	0.000553	0.867	3320	0.308	0.0462	0.0232	2.68
47	20	78	31900	1.73	714	0.00485	1309	0.000541	0.843	3341	0.310	0.0454	0.0230	2.73
48	20	78	31900	1.73	714	0.00485	1309	0.000541	0.843	3341	0.310	0.0471	0.0238	2.83
49	25	79	32100	1.74	716	0.00489	1312	0.000547	0.855	3362	0.312	0.0510	0.0260	3.04
50	25	79	32300	1.74	716	0.00489	1312	0.000547	0.855	3382	0.314	0.0482	0.0247	2.89
51	25	78	32500	1.73	714	0.00485	1309	0.000541	0.843	3403	0.316	0.0451	0.0233	2.76
52	30	80	31400	1.75	719	0.00493	1314	0.000553	0.867	3288	0.305	0.0604	0.0301	3.47
53	30	78	31400	1.73	714	0.00485	1309	0.000541	0.843	3288	0.305	0.0579	0.0288	3.42
54	30	79	31600	1.74	716	0.00489	1312	0.000547	0.855	3309	0.307	0.0536	0.0269	3.14
55	35	78	31200	1.73	714	0.00485	1309	0.000541	0.843	3267	0.303	0.0504	0.0250	2.96
56	35	78	31300	1.73	714	0.00485	1309	0.000541	0.843	3278	0.304	0.0574	0.0285	3.39
57	35	78	31500	1.73	714	0.00485	1309	0.000541	0.843	3299	0.306	0.0564	0.0282	3.34
58	40	80	31100	1.75	719	0.00493	1314	0.000553	0.867	3257	0.302	0.0520	0.0257	2.96
59	40	78	31300	1.73	714	0.00485	1309	0.000541	0.843	3278	0.304	0.0499	0.0248	2.94
60	40	78	31000	1.73	714	0.00485	1309	0.000541	0.843	3246	0.301	0.0535	0.0263	3.12
61	45	80	29500	1.75	719	0.00493	1314	0.000553	0.867	3089	0.287	0.0560	0.0262	3.02
62	45	78	29900	1.73	714	0.00485	1309	0.000541	0.843	3131	0.291	0.0555	0.0263	3.13
63	45	78	29700	1.73	714	0.00485	1309	0.000541	0.843	3110	0.289	0.0539	0.0254	3.02

Table 9: Measured Data & Calculate Values, Dynamometer Loaded With Molasses, 35° β

Test #	Δ (deg)	p_o (psia)	RPM	Exit Mach #	T* (°R)	ρ* (lbm/ft^3)	a* (ft/s)	m-dot (slug/s)	$P_{air\ KE}$ (hp)	ω (rad/s)	Mid Bucket Mach #	τ_{Avg} (in*lb_f)	P_{Shaft} (hp)	η
70	-1°	73	29200	1.69	700	0.00462	1297	0.000511	0.781	3058	0.284	0.0440	0.0204	2.61
71	-1°	73	30000	1.69	700	0.00462	1297	0.000511	0.781	3142	0.292	0.0472	0.0225	2.88
72	-1°	74	30000	1.70	703	0.00467	1300	0.000517	0.793	3142	0.292	0.0518	0.0247	3.11
73	0°	74	30300	1.70	703	0.00467	1300	0.000517	0.793	3173	0.295	0.0595	0.0286	3.60
74	0°	73	30400	1.69	700	0.00462	1297	0.000511	0.781	3183	0.296	0.0602	0.0290	3.72
75	0°	73	30500	1.69	700	0.00462	1297	0.000511	0.781	3194	0.297	0.0628	0.0304	3.89
76	1°	74	31000	1.70	703	0.00467	1300	0.000517	0.793	3246	0.301	0.0586	0.0288	3.63
77	1°	74	30600	1.70	703	0.00467	1300	0.000517	0.793	3204	0.298	0.0585	0.0284	3.58
78	1°	73	30700	1.69	700	0.00462	1297	0.000511	0.781	3215	0.299	0.0631	0.0307	3.93

Appendix C: Data Plots With 15° β

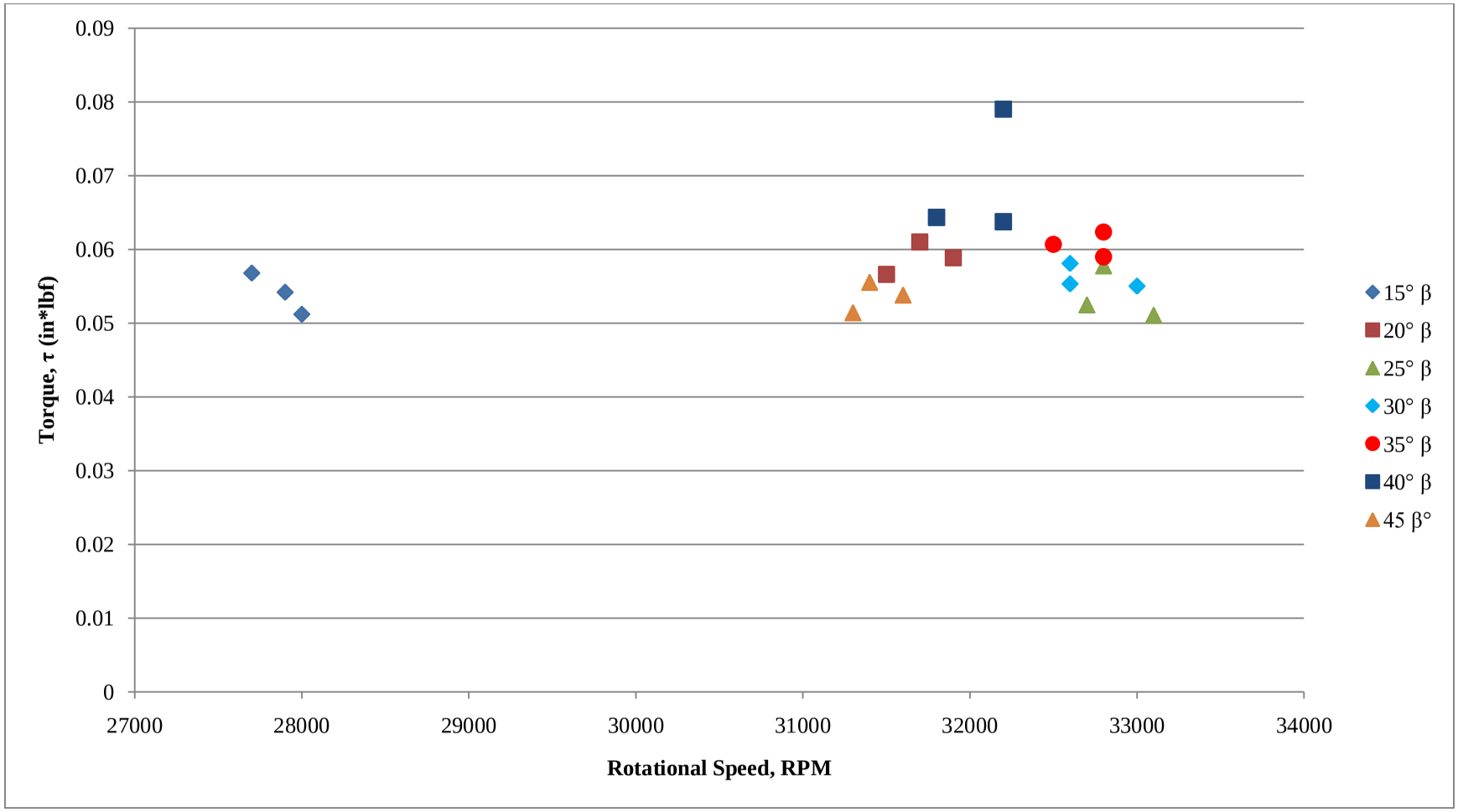

Figure 81: Torque Vs. Rotational Speed, Dynamometer Loaded With Corn Syrup

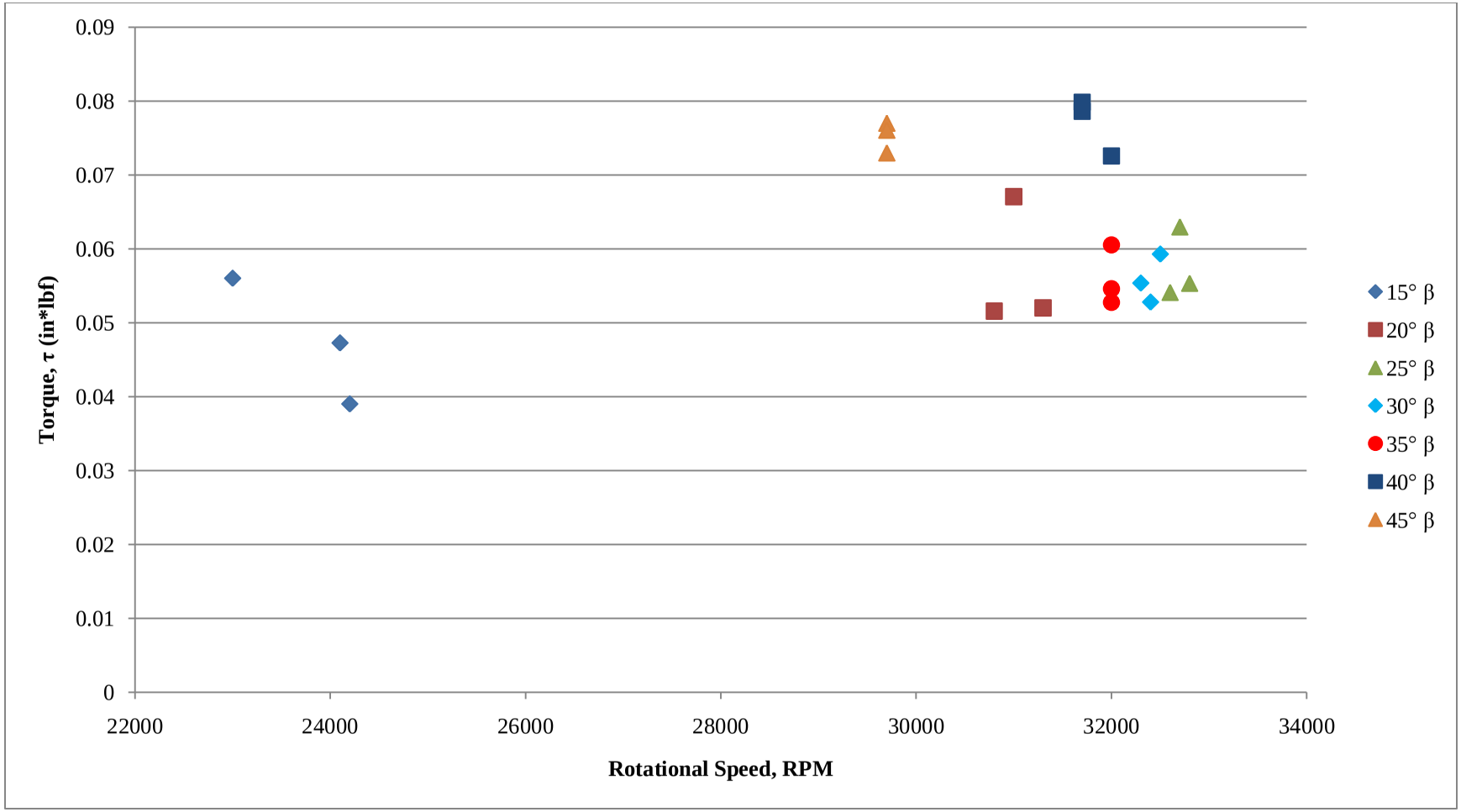

Figure 82: Torque Vs. Rotational Speed, Dynamometer Loaded With Molasses

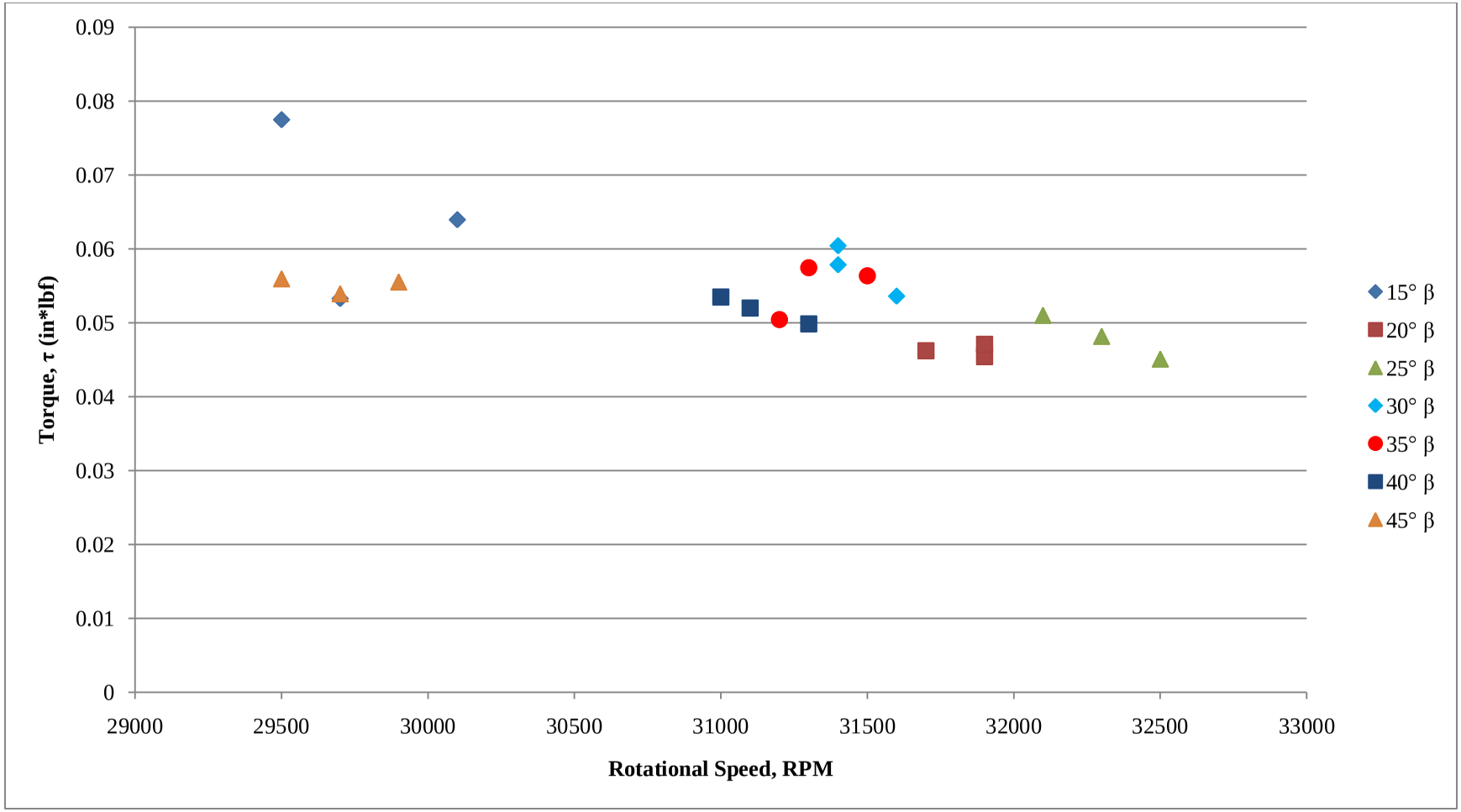

Figure 83: Torque Vs. Rotational Speed, Dynamometer Loaded With Resin

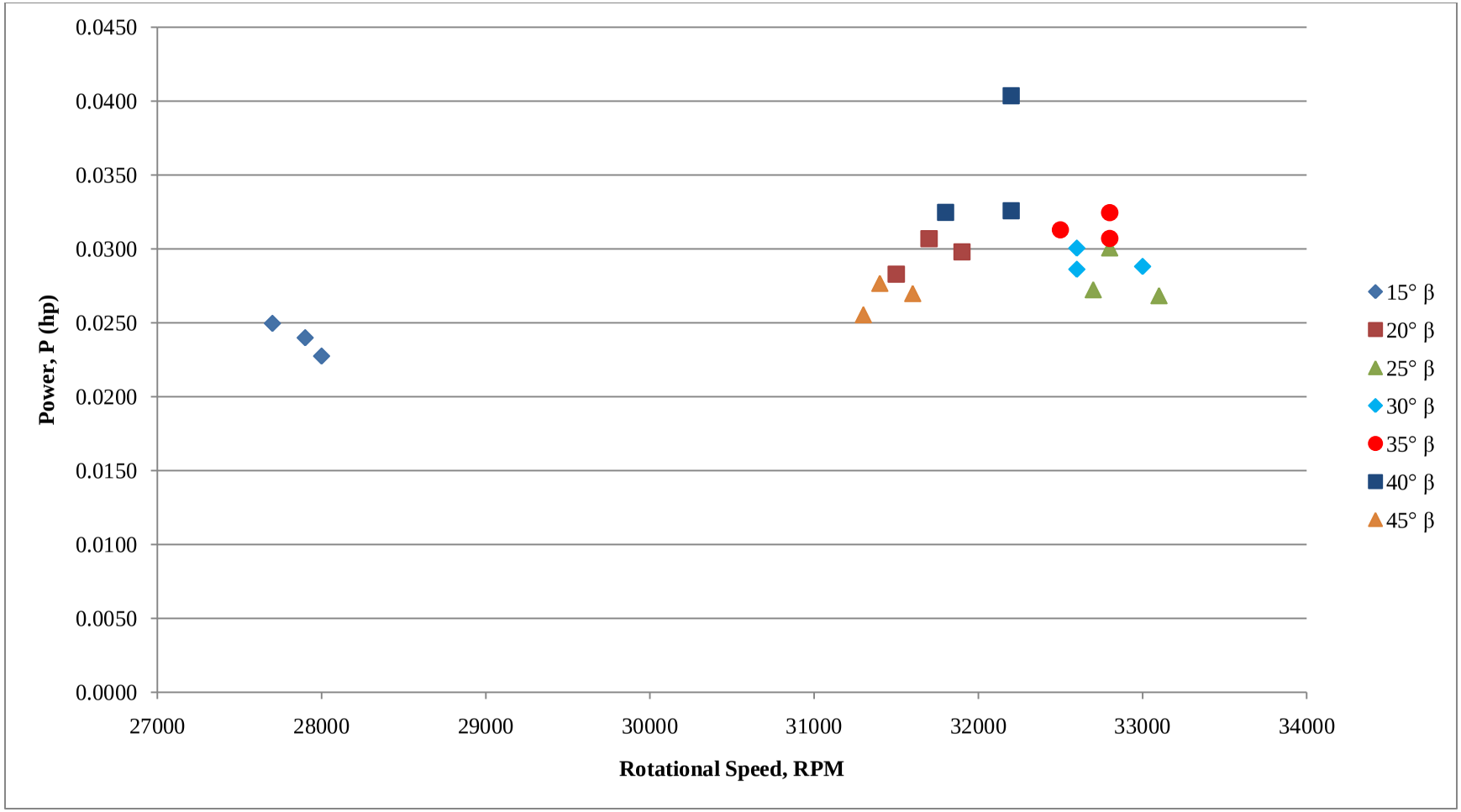

Figure 84: Power Vs. Rotational Speed, Dynamometer Loaded With Corn Syrup

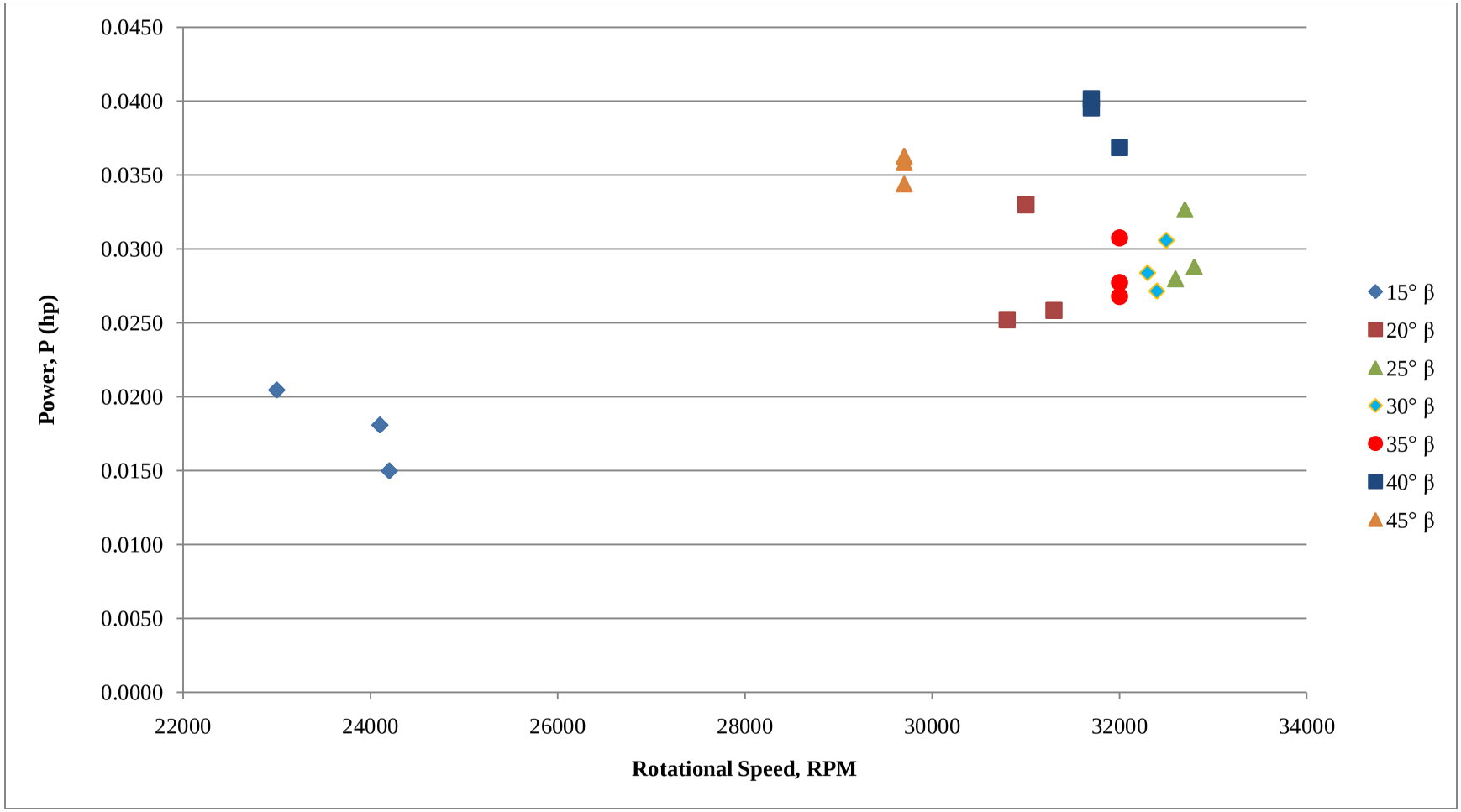

Figure 85: Power Vs. Rotational Speed, Dynamometer Loaded With Molasses

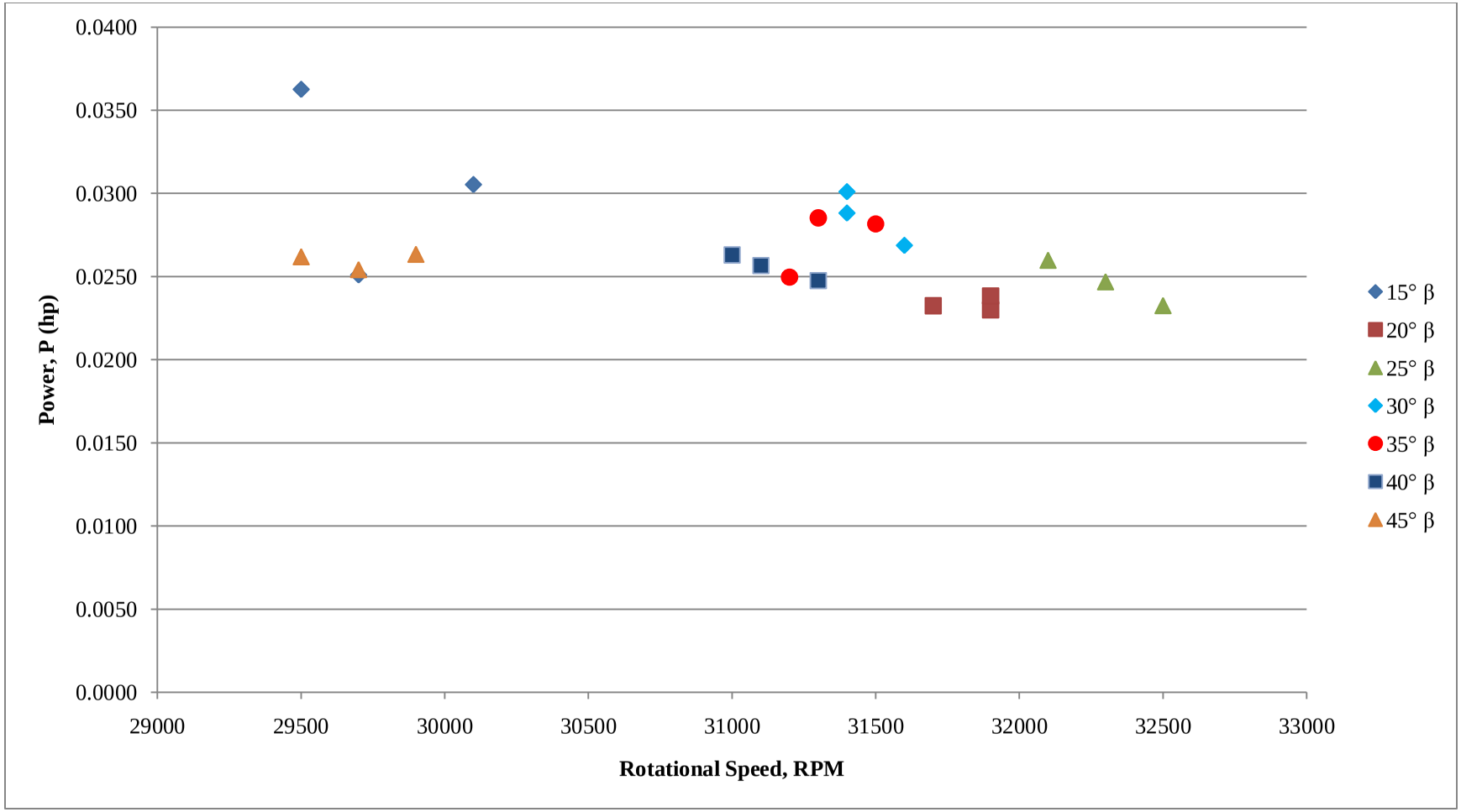

Figure 86: Power Vs. Rotational Speed, Dynamometer Loaded With Resin

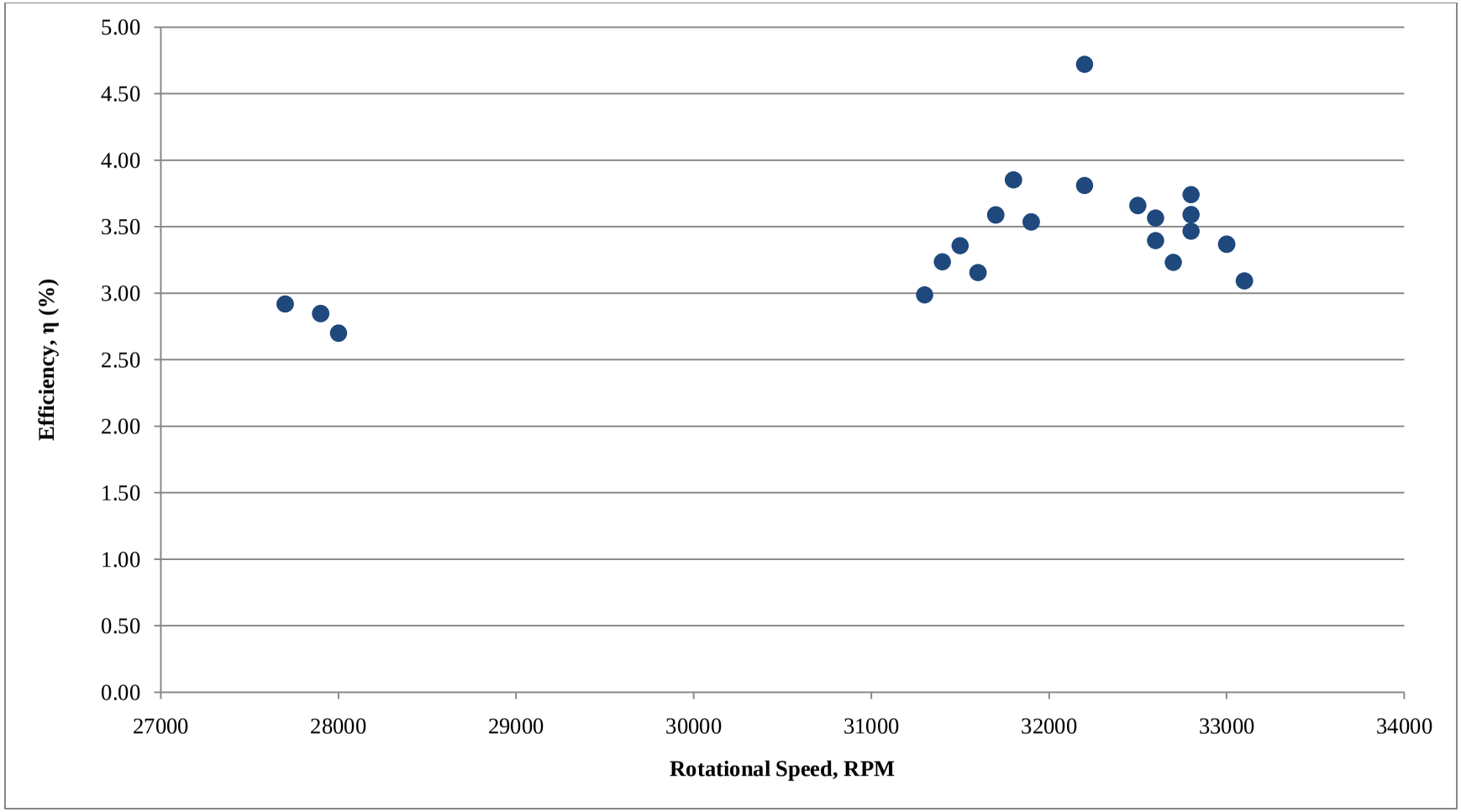

Figure 87: Efficiency Vs. Rotational Speed, Dynamometer Loaded With Corn Syrup

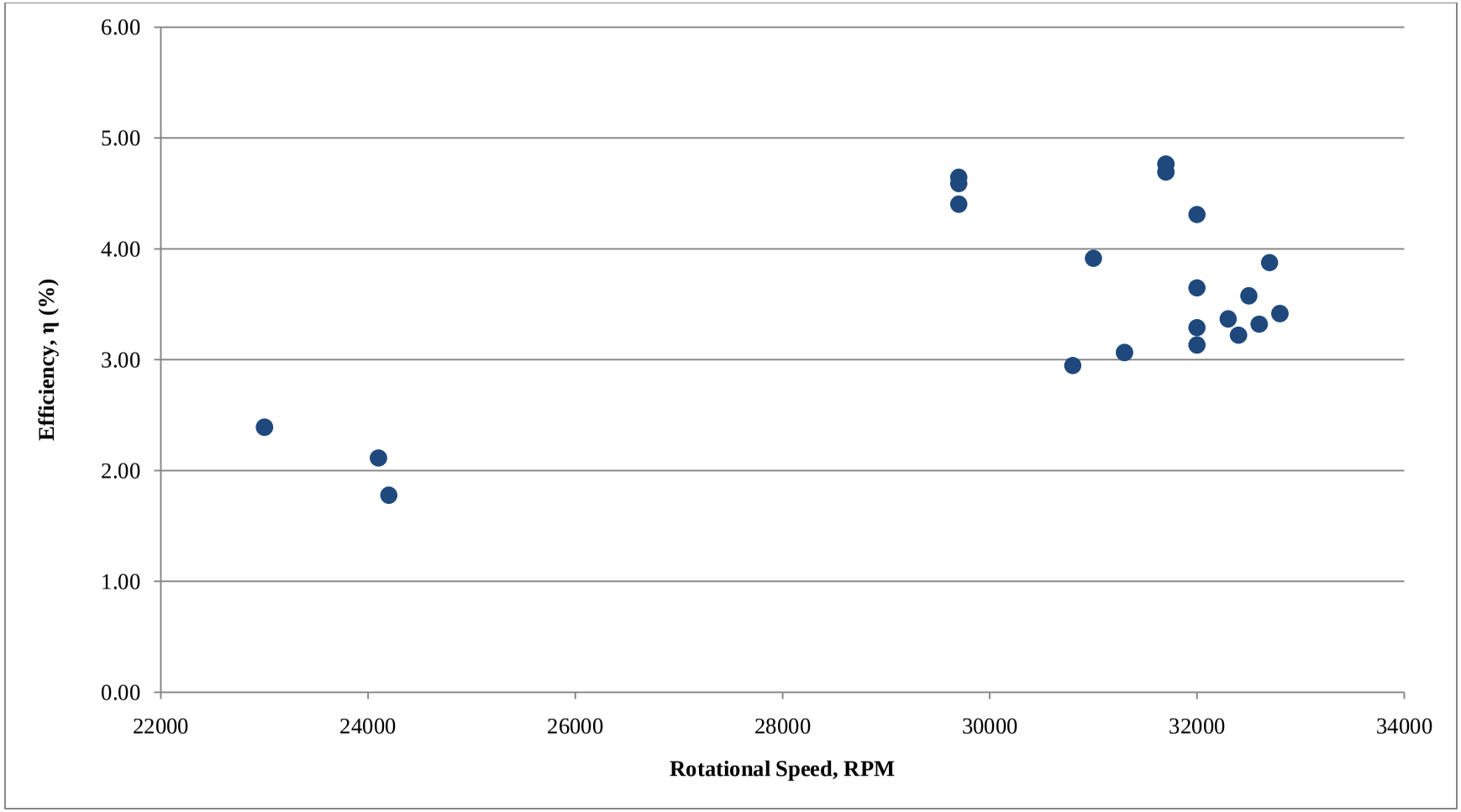

Figure 88: Efficiency Vs. Rotational Speed, Dynamometer Loaded With Molasses

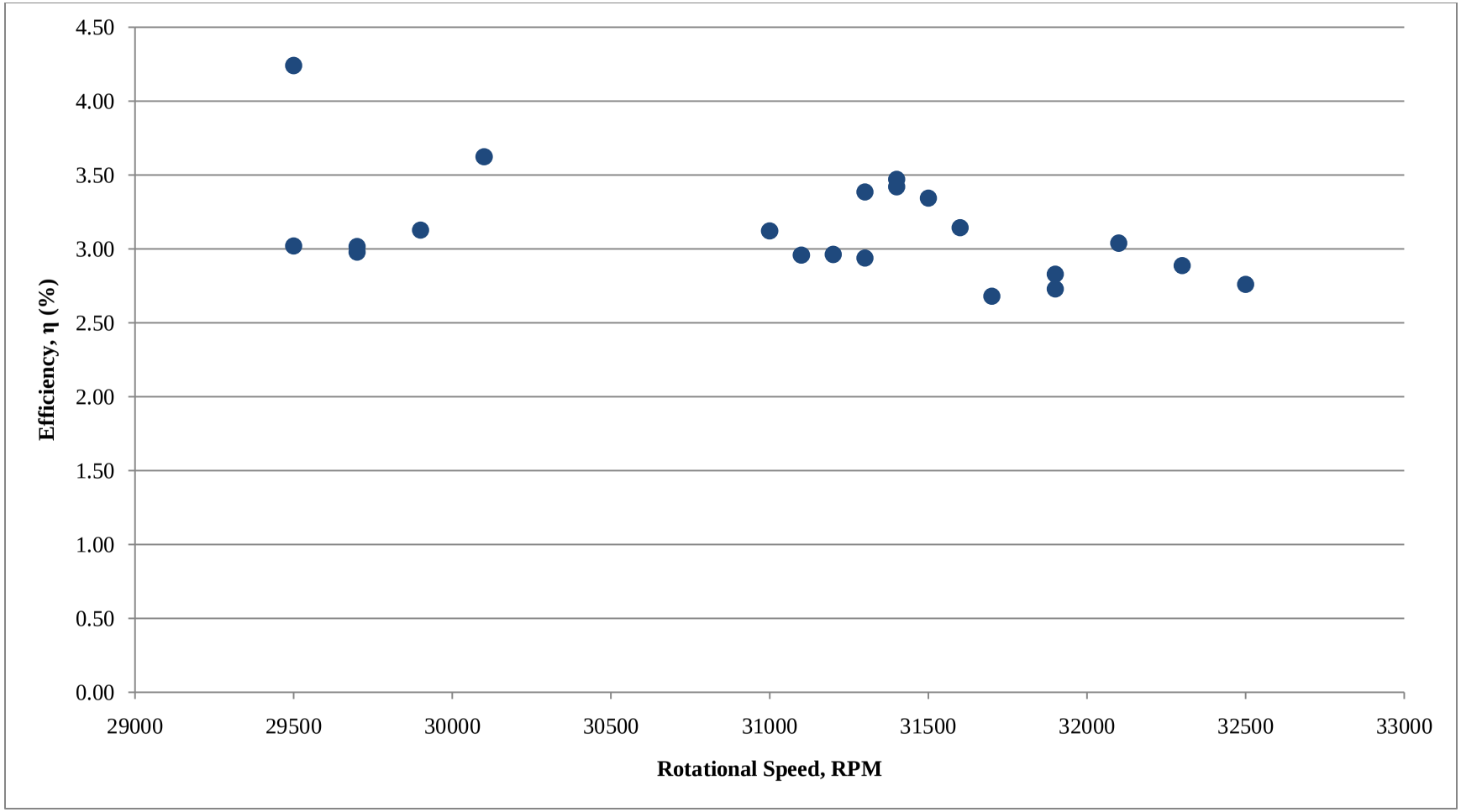

Figure 89: Efficiency Vs. Rotational Speed, Dynamometer Loaded With Resin